الجمهورية الجزائرية الديمقراطية الشعبية
République Algérienne démocratique Algérienne démocratique et Populaire
وزارة التعليم العالي و البحث العلمي
Ministère de l'Enseignement Supérieur et de la Recherche Scientifique
جـامـعـة الشهيد – حمه لخضر - الـوادي
Université Elchahid Hamma Lakher d'ElOued

Faculté de la technologie
Département de Génie Electrique
Réf:………

كلية التكنولوجيا
قسم الهندسة الكهربائية
المرجع:.............

THÈSE

Présentée pour l'obtention du diplôme de

DOCTORAT EN LMD

Domaine : Sciences et Technologie

Filière : Electrotechnique

Intitulé

Contribution à l'étude du filtre actif parallèle associé à la source renouvelable

Présentée par:

KRAMA Abdelbasset

Soutenue publiquement le........................

Devant le jury composé de:

SRAIRI Kamel	Prof	Université de Biskra	Président
ZELLOUMA Laid	Prof	Université d'El Oued	Rapporteur
RABHI Boualaga	Prof	Université de Biskra	Co- Rapporteur
BENCHOUIA Med Toufik	Prof	Université de Biskra	Examinateur
BEN ATTOUS Djilani	Prof	Université d'El Oued	Examinateur
BEKAKRA Youcef	MCA	Université d'El Oued	Examinateur
BEN AYSSA Omar	MCA	Université de Djelfa	Examinateur

الجمهورية الجزائرية الديمقراطية الشعبية
Popular and Democratic Republic of Algeria
وزارة التعليم العالي و البحث العلمي
Ministry of Higher Education and Scientific Research
جـامـعـة الشهيد – حمه لخضر - الـوادي
University of Elchahid Hamma Lakher ElOued

Faculty of technology
Departement of Electrical Engineering
Ref:………

كلية التكنولوجيا
قسم الهندسة الكهربائية
المرجع:.............

Thesis

A thesis submitted for the degree of

DOCTOR OF PHILOSOPHY

Field: Science and Technology

Electrotechnics

Entitled

Contribution to the study of the shunt active filter associated with renewable energy source

Presented by :

KRAMA Abdelbasset

Publicly defended On.........................

In front of the committee composed of:

SRAIRI Kamel	Prof	University of Biskra	President
ZELLOUMA Laid	MCA	University of El Oued	Supervisor
RABHI Boualaga	Prof	University of Biskra	Co- supervisor
BENCHOUIA M^{ed} Toufik	Prof	University of Biskra	Examiner
BEN ATTOUS Djilani	Prof	University of El Oued	Examiner
BEKAKRA Youcef	MCA	University of El Oued	Examiner
BEN AYSSA Omar	MCA	University of Djelfa	Examiner

بسم الله الرحمان الرحيم

Acknowledgement

*In the name of **ALLAH**, the Most Gracious and the Most Merciful. Thanks to **ALLAH** who is the source of all the knowledge in this world, for the strengths and guidance in completing this thesis.*

*I express my deep sense of gratitude and heart-felt thanks to my supervisor, **Dr.Zellouma Laid**, for his invaluable guidance, patience, kindness and consistent encouragement throughout the duration of the work. Many Thanks to my Co-supervisor, **Prof. Rabhi Boualaga** for his valuable supervision and useful guidance and assistant.*

*I would like to express my appreciation to my thesis committee members: **Prof. SRAIRI Kamel** , **Prof . BENCHOUIA Mohamed Toufik, Prof. BEN ATTOUS Djilani, Dr. BEKAKRA Youcef** and **Dr. BEN AYSSA Omar**, for their discussions, suggestions, and feedbacks to improve my thesis.*

I cannot forget to mention all my Colleagues and professors at El-Oued University. Many thanks to the director of LVRES laboratory at El-Oued University, LMSE laboratory at Biskra University and SGC at Texas A&M University at Qatar.

I have not enough words to thank my ever first teachers in this life, my parents, who have been inspiring me and pushing me forward all the way. Their prayers and blessings were no doubt the true reason behind any success I have realized in my life.

Finally, I am grateful to all my family members for their kind support, endurance and encouragements, which have given me the energy to carry on and to motivate myself towards crossing the finish line.

Krama Abdelbasset

Abstract

This study is concerned with the power quality issues in the distribution network. One of the major problems facing power electronics technology nowadays is protecting the power distribution system from the harmful effects of current harmonics generated by nonlinear loads connected to the grid. On the other hand, the use of renewable energies is more than necessary; it is a global strategic issue and it would be a tool against global warming.

This research proposes a high-performance control scheme for a double function grid-tied double stage PV system. It is based on predictive direct power control with space vector modulation (P-DPC-SVM). This strategy uses a discrete model of the system based on time domain to generate the average voltage vector, at each sampling period, with the aim of canceling the errors between the estimated active and reactive power values and their references. Also, it imposes the sinusoidal waveform of the current at the grid side, which allows active power filtering without harmonic currents identification phase. The latter attempts to reduce the size and the cost of the system as well as providing better performance. In addition, it can be implemented in a low-cost control platform due to its simplicity. The performance of P-DPC-SVM is compared with Direct power control and Finite-control-set Model predictive control.

A double stage PV system is selected due to its flexibility in control, unlike the single-stage strategy. Sliding mode control based particle swarm optimization (PSO) is used to track the maximum power of the PV system. It offers high accuracy and good robustness. Concerning the DC bus voltage of the inverter, the anti-windup PI controller is tuned offline using a particle swarm optimization algorithm to deliver optimal performance in DC bus voltage regulation. All the studied control approaches are investigated in simulation using Matlab/Simulink and validated in an experimental test bench based on dSPACE 1104.

Keywords: Shunt Active Power Filter, Photovoltaic, Sliding Mode, Particle Swarm Optimization, Predictive.

Résumé

Cette étude concerne les problèmes de qualité de l’énergie dans le réseau de distribution. L’un des problèmes majeurs auxquels l’électronique de puissance est actuellement confrontée est la protection du système de distribution d’énergie contre les effets néfastes des harmoniques de courant générés par des charges non linéaires connectées au réseau. D'autre part, l'utilisation des énergies renouvelables est plus que nécessaire ; il s’agit d’un enjeu stratégique global et d’un outil de lutte contre le réchauffement climatique.

Cette recherche propose un schéma de commande hautes performances pour un système photovoltaïque à double étage connecté au réseau. Il repose sur le contrôle prédictif de la puissance directe avec modulation de largeur d’impulsion vectoriel (P-DPC-SVM). Cette stratégie utilise un modèle discret du système basé sur le domaine temporel pour générer le vecteur de tension moyenne, à chaque période d'échantillonnage, dans le but d'annuler les erreurs entre les valeurs de puissance active et réactive estimées et leurs références. De plus, il impose la forme d'onde sinusoïdale du courant côté réseau, ce qui permet un filtrage de puissance active sans phase d'identification des courants harmoniques. Ce dernier tente de réduire la taille et le coût du système tout en améliorant les performances. De plus, il peut être implémenté dans une plate-forme de contrôle à faible coût en raison de sa simplicité. Les performances de P-DPC-SVM sont comparées à celles du contrôle direct de la puissance et du contrôle prédictif par modèle fini.

Un système photovoltaïque à double étage est sélectionné en raison de sa flexibilité de contrôle, contrairement à la stratégie à un étage. L’algorithme de mode glissant basée sur l'optimisation de l'essaim de particules (PSO) est utilisée pour suivre la puissance maximale du système photovoltaïque. Il offre une grande précision et une bonne robustesse. En ce qui concerne la tension de bus continu du l’onduleur, le régulateur PI avec anti-emballement est réglé hors ligne à l’aide d’un algorithme d’optimisation de l’essaim de particules afin d’optimiser le performance de régulation de la tension du bus continu. Toutes les approches de contrôle sont vérifiées en simulation avec Matlab / Simulink et validées sur un banc d’essai expérimental basé sur dSPACE 1104.

Mots clés : Filtre active parallèle de puissance, Photovoltaïque, Mode glissant, Optimisation des essaims de particules, Prédictif.

ملخص

تهتم هذه الدراسة بقضايا جودة الطاقة في شبكة التوزيع. تتمثل إحدى المشكلات الرئيسية التي تواجه تكنولوجيا إلكترونيات الطاقة في الوقت الحاضر في حماية نظام توزيع الطاقة من الآثار الضارة للتوافقيات الناتجة عن الأحمال غير الخطية المتصلة بالشبكة. من ناحية أخرى ، فإن استخدام الطاقات المتجددة أصبح مطلب جد ملح ؛ إنها قضية إستراتيجية عالمية وستكون أداة فعالة للتقبيل من الاحتباس الحراري.

يقترح هذا البحث نظام تحكم عالي الأداء لمصفاة فعالة تفرعية مرتبط بمصدر طاقة ضوئية. يعتمد على التحكم المباشر في الطاقة باستعمال القدرة التنبؤية. تستخدم هذه الاستراتيجية نموذجًا مفصلاً للنظام استنادًا إلى المجال الزمني لتوليد متجه الجهد المتوسط بهدف إلغاء الأخطاء بين قيم القدرة النشطة والمتفاعلة والقيم المرجعية. وكذلك يفرض الشكل الجيبي لتيار الشبكة الرئيسية والذي يسمح بتحسين معامل القدرة. تسمح تقنية التحكم المقترحة من التقليل في حجم وكلفة النظام. ذلك، أنه يمكن تنفيذه في منصة تحكم منخفضة التكلفة بسبب بساطته. يتم القيام بدراسة مقارنة بين جميع أساليب التحكم المدروسة في الأطروحة.

يتم اختيار نظام تحكم مرن ودقيق وعالي الأداء للتحكم في طاقة الألواح الشمسية وتتبع الطاقة القصوى لنظام الطاقة الضوئية. كما يتم إستعمال خوارزمية للحصول على أداء أمثل للنظام. يتم فحص جميع أنظمة التحكم المدروسة في المحاكاة باستخدام برنامج ماطلاب والتحقق من صحتها في اختبار تجريبي.

الكلمات الرئيسية: معامل القدرة، الطاقة الضوئية ، وضع انزلاق، التنبؤية، المصفاة الفعالة التفرعية.

List of publications

INTERNATIONAL PUBLICATIONS

- ✓ **A. Krama**, L. Zellouma, B. Rabhi, 'Anti-Windup Proportional Integral Strategy for Shunt Active Power Filter Interfaced by Photovoltaic System using Technique of Direct Power Control', Rev. Roum. Sci. Techn.– Électrotechn. Énerg. 62 (2017) 252–257.
- ✓ L. Zellouma, B. Rabhi, **A. Krama**, A. Benaissa, M.F. Benkhoris, 'Simulation And Real Time Implementation of Three Phase Four Wire Shunt Active Power Filter Based on Sliding Mode Controller', Rev. Roum. Sci. Techn.– Électrotechn. Énerg. 63(2018) 77–82.
- ✓ **A. Krama**, L. Zellouma, A. Benaissa, et al, 'Design and Experimental Investigation of Predictive Direct Power Control of Three-Phase Shunt Active Filter with Space Vector Modulation using Anti-windup PI Controller Optimized by PSO', Arab J Sci Eng (2018), https://doi.org/10.1007/s13369-018-3611-6.
- ✓ **A, Krama**, L, Zellouma, B, Rabhi, S.S, Refaat, M, Bouzidi, M. 'Real-Time Implementation of High Performance control Scheme for Grid-Tied PV System for Power Quality Enhancement Based on MPPC-SVM Optimized by PSO Algorithm', Energies 2018, 11, 3516. https://doi.org/10.3390/en11123516.

INTERNATIONAL COMMUNICATIONS

- ✓ M.R. Rezoug, **A. Krama**, 'Control Device for Automatic Orientation of a Solar Panel Based on a Microcontroller (Pic16f628a)', 16th international conference TMREES16, 15-18 April 2016, Beirut-Lebanon .
- ✓ **A. Krama**, L. Zellouma, B. Rabhi, 'Improved Control of Shunt Active Power Filter Connected to a Photovoltaic System Using Technique of Direct Power Control', 8th international conference ICMIC, 15-17 November 2016, University of Média, Algeria.
- ✓ **A. Krama**, L. Zellouma, B. Rabhi, 'Improvement of power quality using direct power control of shunt active power filter', 3nd international conference ICESD, 07-08 February 2017, Adrar university, Algeria.

- ✓ **A. Krama**, L. Zellouma, B. Rabhi, ‘Improved direct power control of shunt active power filter using fuzzy logic approach’, the 3nd international conference ICPEA, 16-17 September 2017, University of Djelfa, Algeria.
- ✓ B. Kahia, A. Bouafia, A. Chaoui, M. Abdelrahem, **A. Krama** and R. Kennel, ‘An Improved Look-up Table-Direct Power Control strategy for Three Level NPC Rectifier’, 2nd international conference ICAAID, 16-17 September 2017, University of Djelfa, Algeria.
- ✓ **A. Krama**, L. Zellouma, B. Rabhi, A. Laib, ‘Fuzzy logic controller for improving DC side of PV connected shunt active filter based on MPPT sliding mode control’, 1st international conference IC-AIRES 2017, ESC-Koléa, Tipaza, 22-24 October 2017 Algeria.
- ✓ B. Kahia, A. Bouafia, A. Chaoui, M. Abdelrahem, **A. Krama** and R. Kennel, ‘A Predictive Direct Power Control Strategy for Three-Level NPC Rectifier’, 5th international conference ICEE 2017, University of Boumerdes, 29-31 October 2017, Algeria.
- ✓ B. Kahia, A. Bouafia, A. Chaoui, M. Abdelrahem, **A. Krama** and R. Kennel, ‘Multi Level Hysteresis Direct Power Control Strategy for Three-Level NPC Rectifier’, 5th international conference ICEE, University of Boumerdes, 15-18 April 2017, Algeria.

NATIONAL COMMUNICATIONS

- ✓ **A. Krama**, L. Zellouma,’Experimental investigation of an effective solution for harmonic elimination and reactive power compensation using SAPF’, 11st Journée technique de Sonatrach JST11, 16-19 April 2018, Oran, Algeria.
- ✓ **A. Krama**, L. Zellouma, B. Rabhi, ‘Comparative study of different control strategies for double function grid tied PV system’ 1st summer university at USTHB 8-14 July 2018, Algeria.

Table of Contents

List of Figures

List of Tables

List of Abbreviations and Symbols

Abbreviations

AC	Alternating Current
DC	Direct Current
VFD	Variable frequency drive
MMF	Magnetomotive forces
THD	Total Harmonic Distortion
IEEE	Institute of Electrical and Electronics Engineers
IEC	International Electrotechnical Commission
EMC	Electromechanical Commission
PCC	Point of common coupling
rms	Root mean square
CSI	Current Source Inverter
VSI	Voltage Source Inverter
UPQC	Unified Power Quality Conditioner
DPC	Direct power control
SAPF	Shunt active power filter
PLL	Phase locked loop
PWM	Pulse with modulation
EMD	Empirical decomposition
ASD	Adjustable speed drive
FFT	Fast Fourier transform
IGBT	Insulated-gate bipolar transistor
FCS-MPC	Finite control-set model predictive control
VSF	Variable Switching Frequency
CSF	Constant Switching Frequency
PSO	Particle swarm optimization
PV	Photovoltaic
P-DPC	Predictive direct power control
MPPT	Maximum power point tracking
STC	Standard test condition

VOC	Voltage oriented control
DTC	Direct torque control
SVM	Space vector modulation
VF	Virtual Flux
PD	Phase detector
LF	Low pass filter
VCO	Voltage controlled oscillator
STF	Self-tuning filter
P&O	Perturb and Observe
IC	Incremental Conductance
ITAE	Integral time absolute error
IAE	Integral absolute error
ISE	Integral square error

Symbols

I_{SC}	Maximum short-circuit current
I_L	Maximum demand load
S	Apparent power
v	The rms value of voltage
i	The rms value of current
D	Distortion power
Q	Reactive power
P	Active power
PF	Power factor
L	Inductor
C	Capacitor
φ	Phase angle
i_{sa}, i_{sb}, i_{sc}	Source current
i_{la}, i_{lb}, i_{lc}	Load current
i_{fa}, i_{fb}, i_{fc}	Filter current
S_a, S_b, S_c,….	Switching pulses
v_{dc}	DC bus voltage
L_f	Filtering inductor
C_{dc}	DC link capacitor
Θ	Voltage vector position
Hp and Hq	hysteresis bands
Sp and Sq	digitized variables
k_{stf}	Tuning parameter
ω_n	Natural frequency
ξ	Frequency of damping
G_a	Anti-windup gain
Ts	Sampling time
k_p	Proportional controller
K_i	Integral controller

Ps,, Psref	Source active power
qs, qsref	Source reactive power, reference reactive power
λp, λq	Weighting factors
Cf	Cost function
Vsc	Short-circuit voltage
Ioc	Open-circuit current
Isc	Short-circuit current
Voc	Open-circuit voltage
Isc	Photo-current generated by PV cell.
I0	Saturation current of the diode
Vt	Thermal voltage of PV cell.
Rp	The equivalent parallel resistance.
Rs	The equivalent series resistance.
α	Diode ideality factor.
Icell	Current generated by PV cell.
Vcell	Voltage at the output of PV cell
G_{best}	Global best
P_{best}	Personel best
i	Number of particle.
k	Current number of iteration.
c_1, c_2	Acceleration coefficients.
	Inertia coefficient

General Introduction

The widespread use of nonlinear loads in manufacturing activities as well as for domestic reason has caused an undesirable impact on the quality of electric power systems. These nonlinear loads draw non-sinusoidal currents from utility grid that causes harmonic currents which introduce many problems such as increasing of line losses, saturation of distribution transformers and poor power factor. However, the demand of good power quality is increasing due to the growth of using sensitive devices that require smooth sinusoidal waveforms. As a result, power quality enhancement has become the necessity of the day and it has attracted the interest of many researchers.

Traditionally, passive filters have been used to suppress current harmonics and to mitigate the power pollution in grid for a long time. Although, this kind of filters offer numerous shortcomings such as huge size, heavy, and sensitivity to parameters variation that may lead to resonance problems. The abovementioned problems have been effectually relieved by using active filters that was recognized nearly in 1970s. Shunt active power filter (SAPF) is a flexible solution for harmonic currents mitigation as well as power factor correction. Moreover, it has a perfect ability to adapt with different type of loads. The combination of SAPF is based on voltage /current source inverter that is connected in parallel with nonlinear loads. It generates the needed harmonic components to suppress harmonic currents drawn by nonlinear loads, therefore it makes the main current sinusoidal and in phase with supply voltage[1].

Today, in the so-called advanced countries, electric power has become more than necessary as natural water, because it allows operating the equipment at any time for everyone. The most kinds of equipment around us (heating devices, lighting tools, information technology devices, communication, cooking tools ...) need electric power to operate. Obviously, this ease of use should not hide the major problem of the creation of this energy from its alternative form, which is by far the most used, it does not exist naturally. That is, a primary source of energy is needed to make electricity. Each year, more electricity is generated from renewable energy than in the previous year. Hydropower still accounted for some 60% of renewable electricity production in 2018, followed by wind power (21%), solar PV (9%) and bio-power (8%). Overall, the installed renewable power capacity at year's end was enough to supply around 26.2% of global electricity production[2].

Among all renewable energies, photovoltaic energy presents itself as a solution for the future because it offers a multitude of advantages;

- Photovoltaic energy is exploitable everywhere, in a mountain, in a remote village than in the center of a big city, because the sunlight is available almost everywhere.
- Photovoltaic electricity can be produced as close as possible to its place of consumption in a decentralized way, directly to the user, which makes it accessible to a large part of the world's population.
- The photovoltaic is a clean energy since the production of this electricity does not emit greenhouse gases, but the environmental impact of the manufacturing of the system must be reduced.

The presented theses has been written in four main chapters, which can be summarized as follows:

The first chapter presents the main kinds of disturbance affecting the voltage and current of the electrical network. The issue of harmonics, their origins and consequences are well explained. In addition, the international standards for current and voltage distortion limits for general distribution systems are given. Then, the different traditional and modern solutions of filtering are presented such as passive filters, series and shunt active filter as well as hybrid filter.

In chapter two, overview of shunt active power filter is presented; different configuration and control strategies for SAPF are discussed and the mathematical model of SAPF is given. The second part is dedicated to Direct power control strategy, presenting its state of art, working principle and discussing simulation and experimental results.

The third chapter is dedicated to the investigation of predictive control strategies applied on shunt active power filter using three-phase two-level inverters. Two control strategies are presented, Finite-control set model predictive control (FCS-MPC), then predictive direct power control with space vector modulation (PDPC-SVM). Simulation and experimental results are presented and discussed. Lastly, a comparative study of the three control strategies studied in this thesis is given.

In the fourth chapter, overview of photovoltaic energy is given; presenting the modelling of PV module, different configuration of PV system and some maximum power point tracking algorithm (MPPT) are discussed, The concept of Sliding mode based MPPT is given. In addition, the working principle of a powerful optimization algorithm named particle swarm (PSO) is presented and its mathematical model is given.

In the second part, the association of shunt active power filter with double stage PV system is described. The optimization of PI controller parameters and sliding mode MPPT parameter are explained; showing the adopted objective functions. Simulation and experimental results are presented for two different modes of operations.

Finally, the last part presents the general conclusion of the thesis as well as the perspectives of the current study.

Chapter I: Power Quality Issues, Standards, and Solutions

I.1. Introduction

Power systems apparatuses are designed to supply an alternating voltage and current, which are purely sinusoidal. From terminological point of view, the purely sine waveform which the system is designed and is expected to operate is known as fundamental wave. The corresponding frequency is called fundamental frequency[3].

The quality of the electric power depends on the voltage at the points of common coupling. However, this voltage usually undergoes disturbances during its transport until its arrival at the end user. The causes of these disturbances are numerous; in addition to incidents relating to the nature of the equipment of distribution networks or transmission lines.

In this chapter, the main kind of disturbances affecting the voltage and current of the electrical network will be presented and discussed. We will discuss also the origin of harmonics and their effects. International standards on harmonic emissions will be shown.

Finally, we will expose traditional and modern solutions used to overcome problems related to harmonic disturbances.

I.2. Power Quality:

The quality of energy is a fairly broad concept which covers both the quality of the generated power, the quality of the voltage wave and the quality of the currents. The electrical energy is supplied as a three-phase sinusoidal voltage with the following characteristics[4]:

- The amplitude (or effective value) of the three voltages.
- The waveform that must be as close as possible to a sinusoid.
- Frequency (50 Hz or 60 Hz).
- The symmetry of the three-phase system, characterized by the equality of the amplitude of the three voltages and their relative phase shift.

Any physical phenomenon affecting one or more of these characteristics is considered a disturbance.

I.3. Electrical disturbances [5–8]

The quality of the voltage can be affected, either because of certain incidents inherent in the physical nature, or because of certain sensitive receptors (especially non-linear loads) which degrade the quality of the current in the network and the quality of the voltage, These disturbances affecting one or more of the four parameters previously defined. So the electrical disturbances can be classified as follows[5]:

I.3.1. Voltage sag

A voltage sag (also called a "dip") is a brief decrease in the rms line voltage of 10 to 90 percent of the nominal line-voltage.

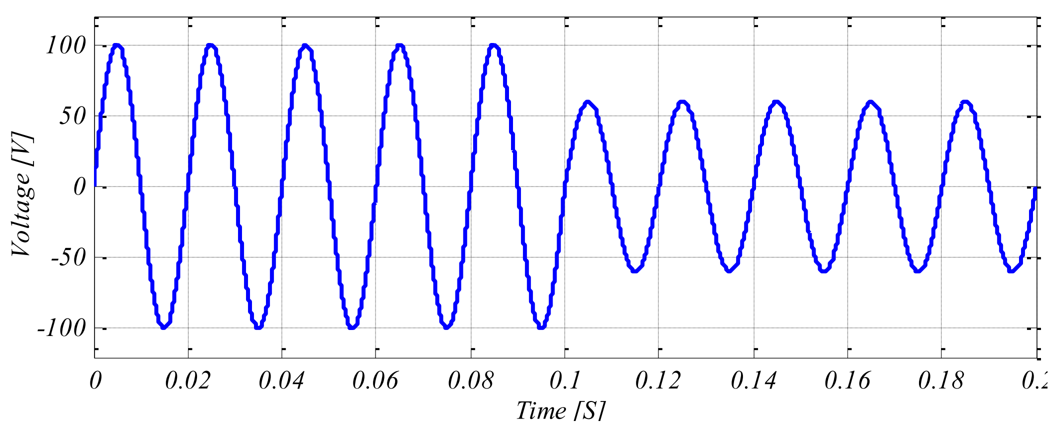

Figure I.1 : Voltage sag

The duration of a sag is 10 ms to 1 minute. Common sources of sags are the starting of large induction motors and utility faults.

I.3.2. Voltage swell

A voltage swell is the converse to the sag. A swell is a brief increase in the rms line-voltage of 10 to 90 percent of the nominal line-voltage for a duration of 10 ms to 1 minute. Sources of voltage swells are line faults and incorrect tap settings in tap changers in substations.

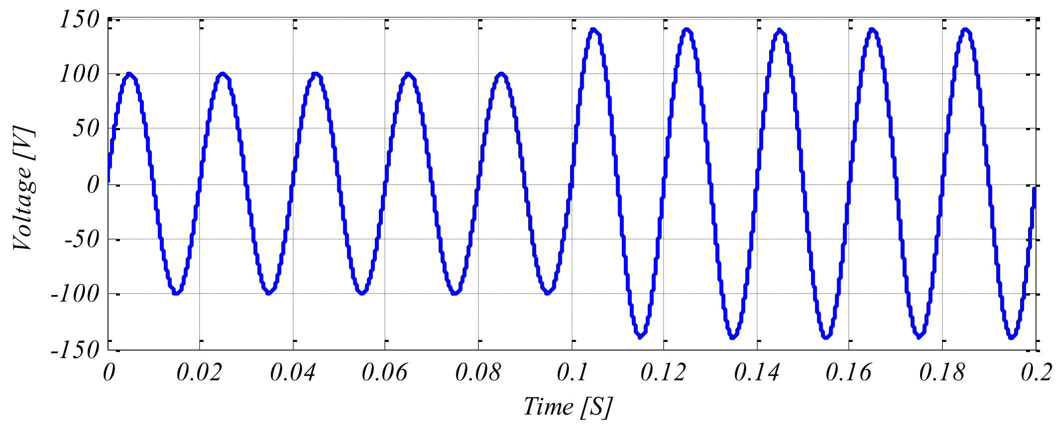

Figure I.2 : Voltage swell

I.3.3. Voltage fluctuations

Voltage fluctuations are relatively small (less than 5 percent) variations in the rms line-voltage. These variations can be caused by cycloconverters, arc furnaces, and other systems that draw current not in synchronization with the line frequency. Such fluctuations can result in variations in the lighting intensity due to an effect known as “flicker” which is visible to the end-user.

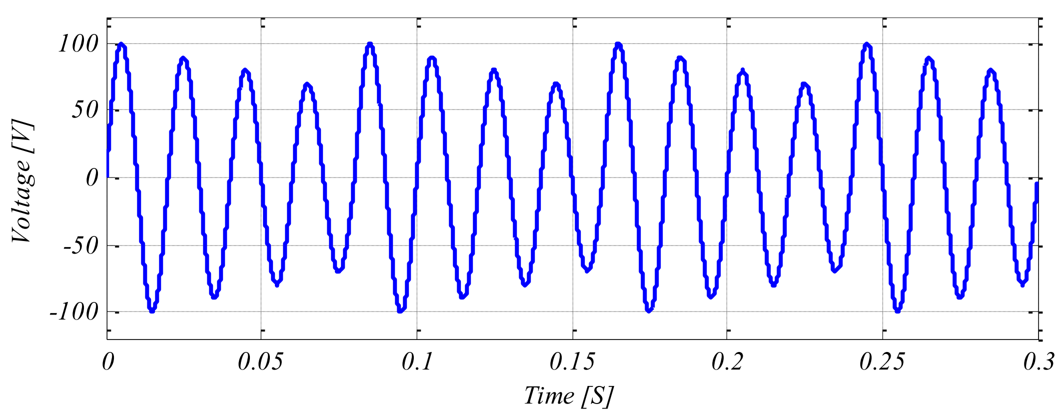

Figure I.3 : Voltage fluctuations

I.3.4. Voltage imbalance

A voltage imbalance is a variation in the amplitudes of three-phase voltages, relative to another one. Figure I.4 shows a three-phase voltage waveform where the phases a, b, and c have different amplitudes. imbalance can be caused by different loads on the phases, resulting in different voltage drops through the phase-line impedances. Generally, the difference between the highest and the lowest voltages should not exceed 4% of the lowest voltage. Greater imbalances may cause overheating of components and result in intermittent shutdown of motor controllers. A voltage imbalance can cause a reverse-rotating air gap field in induction machines, increasing heat loss and temperature rise.

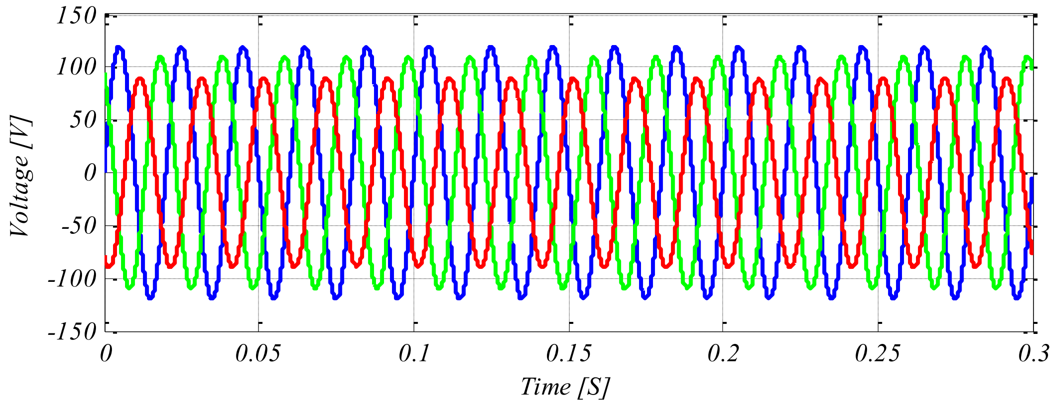

Figure I.4 : Voltage imbalance

I.3.5. Frequency variation

The frequency-related power quality problems are frequency variation above or below the desired base value. These affect the performance of a number of loads and other equipment such as transformers in the distribution system.[8]. In normal operating conditions, the average value of the fundamental frequency variation must be within the range of 1%[6].

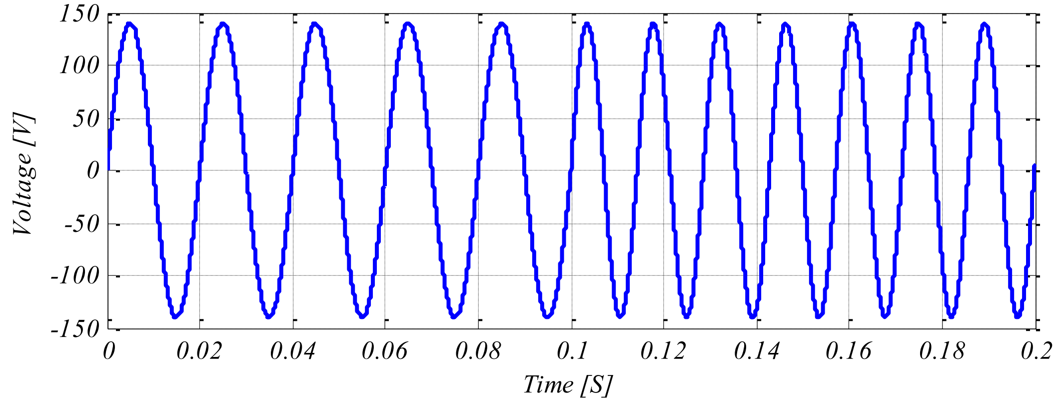

Figure I.5 : Voltage frequency

I.3.6. Harmonics

Harmonics, the term "harmonics" was originated in the field of acoustics, where it was related to the vibration of a string or an air column at a frequency that is a multiple of the base frequency. A harmonic component in an AC power system is defined as a sinusoidal component of a periodic waveform that has a frequency equal to an integer multiple of the fundamental frequency of the system. Harmonics in voltage or current waveforms can then be conceived as perfectly sinusoidal components of frequencies multiple of the fundamental frequency.[7]

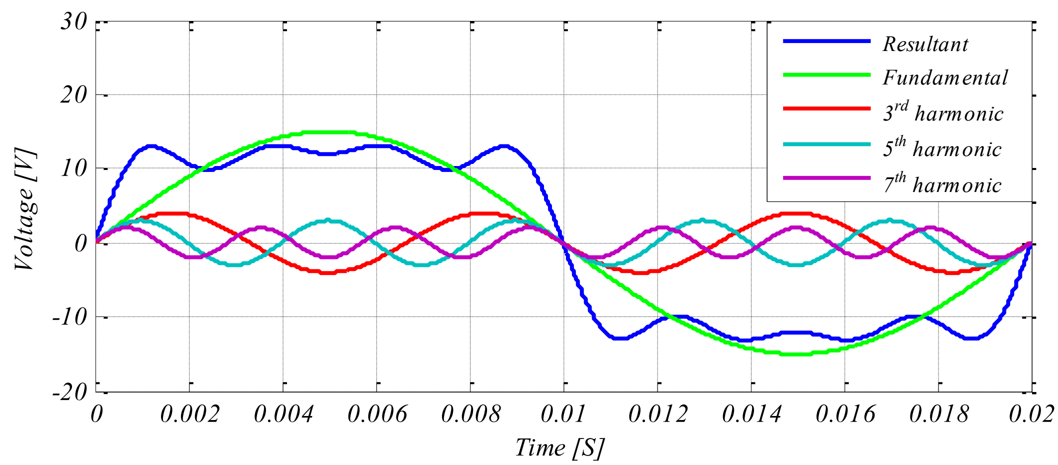

Figure I.6 : Voltage harmonics

I.4. Harmonics sources, effects and standards

There are many nonlinear loads drawing non-sinusoidal currents from electrical power systems. These non-sinusoidal currents pass through different impedances in the power systems and produce voltage harmonics. These voltage harmonics propagate in power systems and affect all of the power system components.[9].

I.4.1. Harmonics sources

The harmonic sources are classified as follows.[7]

I.4.1.1. Power converters

The increasing use of the power conditioners in which parameters like voltage and frequency are varied to adapt to specific industrial and commercial processes has made power converters the most widespread source of harmonics in distribution systems. Electronic switching helps the task to rectify 50/60 Hz AC into DC power. In DC applications, the voltage is varied through adjusting the firing angle of the electronic switching device. Basically, in the rectifying process, current is allowed to pass through semiconductor devices during only a fraction of the fundamental frequency cycle, for which power converters are often regarded as energy-saving devices. If energy is to be used as AC but at a different frequency, the DC output from the converter is passed through an electronic switching inverter that brings the DC power back to AC. Converters can be grouped into the following categories:

- Large power converters like those used in the metal smelter industry and in HVDC transmission systems.
- Medium-size power converters like those used in the manufacturing industry for motor speed control and in the railway industry.
- Small power rectifiers used in residential entertaining devices, including TV sets and personal computers. Battery chargers are another example of small power converters.

I.4.1.2. Variable frequency drive

VFDs are, in reality, power converters. The reason to further address them under a separate section is because, by themselves, VFDs constitute a broad area of application used in diverse and multiple industrial processes. In a very general context, two types of VFDs can be distinguished: those that rectify AC power and convert it back into AC power at variable frequency and those that rectify AC power and directly feed it to DC motors in a number of industrial applications.

I.4.1.3. Fluorescent lamps

Fluorescent tubes are highly nonlinear in their operation and give rise to odd harmonic currents of important magnitude. As a brief portrayal of the fluorescent lamp operation, we can state that magnetic core inductors or chokes contained inside the start ballasts function to limit the current to the tube. Likewise, they use a capacitor to increase the efficiency of the ballast by increasing its power factor. Electronic ballasts operate at higher frequency, which permits the use of smaller reactors and capacitors. The use of higher frequencies allows them to create more light for the same power input. This is advantageously used to reduce the input power.

I.4.1.4. Electric furnaces

The melting process in industrial electric furnaces is known to produce substantial amounts of harmonic distortion. The introduction of fundamental frequency harmonics develops from a combination of the delay in the ignition of the electric arc along with its highly nonlinear voltage-current character. Additionally, voltage changes caused by the random variations of the arc give rise to a series of frequency variations in the range 0.1 to 30 kHz; each has its associated harmonics. This effect is more evident in the melting phase during the interaction of the electromagnetic forces among the arcs.

I.4.2. Effect of harmonics on power system

For more Than 100 years, harmonics have been reported to cause operational problems to the power systems. Some of the major effects are cited below[10]:

I.4.2.1. Thermal effects on transformers

Modern industrial and commercial networks are increasingly influenced by significant amounts of harmonic currents produced by a variety of nonlinear.

In general, harmonics losses occur from increased heat dissipation in the windings and skin effect; both are a function of the square of the rms current, as well as from eddy currents and core losses. This extra heat can have a significant impact in reducing the operating life of the transformer insulation. Transformers are a particular case of power equipment that has experienced an evolution that allows them to operate in electrical environments with considerable harmonic distortion. In industry applications in which transformers are primarily loaded with nonlinear loads, continuous operation at or above rated power can impose a high operating temperature, which can have a significant impact on their lifetime[7].

I.4.2.2. Effects on Rotating Machines

Similar to transformers, rotating machines are exposed to thermal effects from harmonics. Because the effective resistance of a conductor goes up as frequency rises, a current wave rich in harmonics may cause greater heating on winding conductors than a sine wave of the same rms value. The overall effect can lead to a decreased transformer lifetime.

Additionally, magnetomotive forces (mmf) induced by positive and negative sequence harmonics interact with the nominal frequency mmf force creating torque components of different frequencies as described in [7]. This may lead to problems on the shaft of rotating machines subject to the influence of harmonic torsional pairs including: (equipment fatigue, increased vibration and bearing wear out).[7]

I.4.2.3. Communication interference

Passing harmonic currents through the transmission lines causes interference with the communication circuits and sensitive devices near the transmission lines and may cause a malfunction malfunction or performance degradation of these circuits and sensitive devices[9].

I.4.2.4. Neutral Conductor Overloading

The presence of current harmonics in electrical power systems increases neutral currents. In this case, the most important part of the neutral current is the third harmonic. Liew’s experimental results [11] show that in fluorescent lamp circuits, the neutral current is 30% of the line current. In other nonlinear loads such as adjustable speed drives, this percentage is higher[9].

I.4.3. Total harmonic distortion

The term THD (Total Harmonic Distortion) represents the ratio between the rms value of the harmonics and the rms value of the fundamental. The harmonic distortion rate is a concept widely used to define the importance of the content harmonic of an alternative signal.

The current harmonics is expressed as follows:

$$THD_i = \sqrt{\sum_{i=2}^{\infty} (\mathrm{i}_i^2 / \mathrm{i}_1^2)} = \sqrt{\sum_{i=2}^{\infty} (\mathrm{i}_i^2 / \mathrm{i}_1)} \qquad \text{(I.1)}$$

The voltage harmonics is expressed as follows:

$$THD_v = \sqrt{\sum_{i=2}^{\infty} (\mathrm{v}_i^2 / \mathrm{v}_1^2)} = \sqrt{\sum_{i=2}^{\infty} (\mathrm{v}_i^2 / \mathrm{v}_1)} \qquad \text{(I.2)}$$

Where i_i and v_i represent the harmonic component of rank i. i_1 and v_1 represents the fundamental component.

I.4.4. Harmonic standards

Restrictions on current and voltage harmonics maintained in many countries through IEEE(Institute of Electrical and Electronics Engineers) 519-1992 in the USA and IEC (International Electrotechnical Commission) IEC 61000-3-2/ 61000-3-4/ 61000-3-3 in Europe standards, are associated with the popular idea of "clean power".[12]. The main difference between the IEEE 519 standard and Electromagnetic compatibility standard from the International Electromechanical Commission EMC IEC 61000 is the fact that the latter is aimed to limit the harmonic contribution of electrical equipment as oppose to merely electrical system recommendations that mitigates the impact of current harmonics. In that regards, it explicitly applies to electrical manufactures while IEEE 519 means to give recommendations to users on the application of power electronics converters.[13]

IEEE 519-1992, recommended practices and requirements for harmonic control in electric power systems, established limits on harmonic currents and voltages at the point of common coupling (PCC). Tables I.1–I.3 show some important limits on voltages and currents in these standards.

Table I.1: IEEE Standard 519-1992: Current distortion limits for general distribution systems (120–69 000 V) [14].

Maximum harmonic current distortion (in percent of I_L)						
Individual harmonic order (odd harmonics)						
I_{SC}/I_L	h<11	11≤h≤17	17≤h≤23	23≤h≤35	35≤h	THD(%)
<20*	4.0	2.0	1.5	0.6	0.3	5.0
20 to <50	10.0	3.5	2.5	1.0	0.5	8.0
50 to <100	12.0	4.5	4.0	1.5	0.7	12.0
100 to <1000	15.0	5.5	5.0	2.0	1.0	15.0
>1000		7.0	6.0	2.5	1.4	20.0
Maximum harmonic current distortion (in percent of I_L)						
Individual harmonic order (odd harmonics)						
I_{SC}/I_L	h<11	11≤h≤17	17≤h≤23	23≤h≤35	35≤h	THD(%)
<50	2.0	1.0	0.75	0.3	0.15	2.5
	3.0	1.5	1.15	0.45	0.22	3.75
Bus voltage at PCC		**Individual voltage distortion(%)**		**Total voltage distortion (%)**		
69 KV and below		3.0		5.0		
69.001-161 kv		1.5		2.5		
161.001 kv and above		1.0		1.5		

- Even harmonics are limited to 25% of the odd harmonic limits above.
- *All power generation equipment is limited to these values of current distortion, regardless of actual I_{LSC}/I_L, where I_{SC}=maximum short-circuit current at PCC and I_L=maximum demand load current (fundamental frequency component) at PCC.

Table I.2: IEEE Standard 519-1992: Current distortion limits for general distribution systems (>161 kV), dispersed generation and cogeneration [14].

Maximum harmonic current distortion (in percent of I_L)						
Individual harmonic order (odd harmonics)						
Isc/I_L	h<11	11≤h<17	17≤h<23	23≤h<35	35≤h	THD(%)
<50	2.0	1.0	0.75	0.3	0.15	2.5
≥50	3.0	1.5	1.15	0.45	0.22	3.75

- Even harmonics are limited to 25% of the odd harmonic limits above.

Table I.3: IEEE Standard 519-1992: voltage distortion limits[14].

Bus voltage at PCC	**Individual voltage distortion (%)**	**Total voltage distortion (%)**
69 KV and below	3.0	5.0
69.001-161 KV	1.5	2.5
161.001 KV and above	1.0	1.5

I.5. Concepts of Power under Non-sinusoidal Conditions

I.5.1. Power Definitions by Budeanu

A set of power definitions established by Budeanu [15] in 1927 is still very important for the analysis of power systems in the frequency domain. He introduced definitions that are valid for generic waveforms of voltage and current. However, since they are defined in the frequency domain, they can be applied only in a steady-state analysis. In other words, they are limited to periodic waveforms of voltage and current.

If a single-phase ac circuit with a generic load and a source is in steady state, its voltage and current waveforms can be decomposed in Fourier series. Then, the corresponding phase for each harmonic component can be determined, and the following definitions of powers can be derived.[8]

I.5.2. Apparent power

Apparent power S is defined as:

$$S = v.i \qquad \text{(I.3)}$$

Where v and i are the rms values of generic, periodic voltage and current waveforms, which are calculated as:

$$v = \sqrt{\frac{1}{T}\int_0^T v^2(t)dt} = \sqrt{\sum_{n=1}^{\infty} v_n^2} \qquad \text{(I.4)}$$

$$i = \sqrt{\frac{1}{T}\int_0^T i^2(t)dt} = \sqrt{\sum_{n=1}^{\infty} i_n^2} \qquad \text{(I.5)}$$

Here, v_n and i_n correspond to the rms value of the n^{th} order harmonic components of the Fourier series, and T is the period of the fundamental component. No direct current (DC) component is being considered in this analysis.

I.5.3. Active power

The active power P of a signal with harmonics is the sum of the active powers due to voltages and currents of the same rank. The decomposition of voltage and current into their harmonic components yields:

$$P_n = \sum_{N=1}^{\infty} P_n = \sum_{N=1}^{\infty} v_n i_n \cos\varphi_n \qquad \text{(I.6)}$$

Where φ_n represents the phase angle of each pair of n^{th} order harmonic voltage and current components.

I.5.4. Reactive power

The reactive power is defined as follows:

$$Q_n = \sum_{N=1}^{\infty} Q_n = \sum_{N=1}^{\infty} v_n I_n \sin\varphi_n \quad (I.7)$$

I.5.5. Distortion power

The loss of power quality under nonsinusoidal conditions is better characterized by another power definition, the distortion power *D*, that was introduced by Budeanu. This distortion power complements the above set of power definitions as shown in the Fresnel diagram in Figure I.7.

Distortion power *D* is defined as

$$D^2 = S^2 - P^2 - Q^2 \quad (I.8)$$

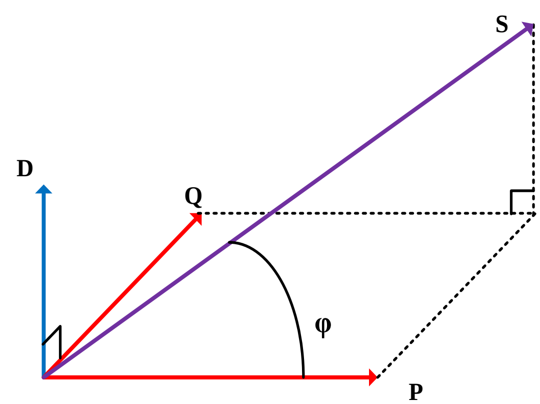

Figure I.7 : Fresnel diagram

I.5.6. Power factor

A low power factor value results in improper use of this equipment. This power factor is affected also by harmonics as follows :

$$PF = P / \sqrt{P^2 + Q^2 + D^2} \quad (I.9)$$

I.6. Harmonic elimination solutions

Harmonic elimination solutions can be classified into two main groups: traditional solutions (Passive filters) and modern solutions (Active filters).

I.6.1. Traditional solutions for harmonic elimination

The most common solution is to use passive filters. The underlying mechanism behind passive filters is to present low impedance for the harmonic to be eliminated. The impedance presented by the filter should be significantly lower than the equivalent impedance of the power source at the frequency to be filtered. Therefore, the current harmonic will circulate between filter and load and it will not propagate to the rest of the electrical system. In other words, the harmonic will be trapped in the filter; that is the reason why passive filters are often referred to as harmonic traps.[13] The passive filter is usually placed as shown in Figure I.8 to divert a selected portion of the harmonic currents produced by the nonlinear load. The passive filter consist of passive elements such as capacitors, inductors, and resistors. Among the most common filtering devices, there is the tuned passive filter and the damped or high-pass passive filter.

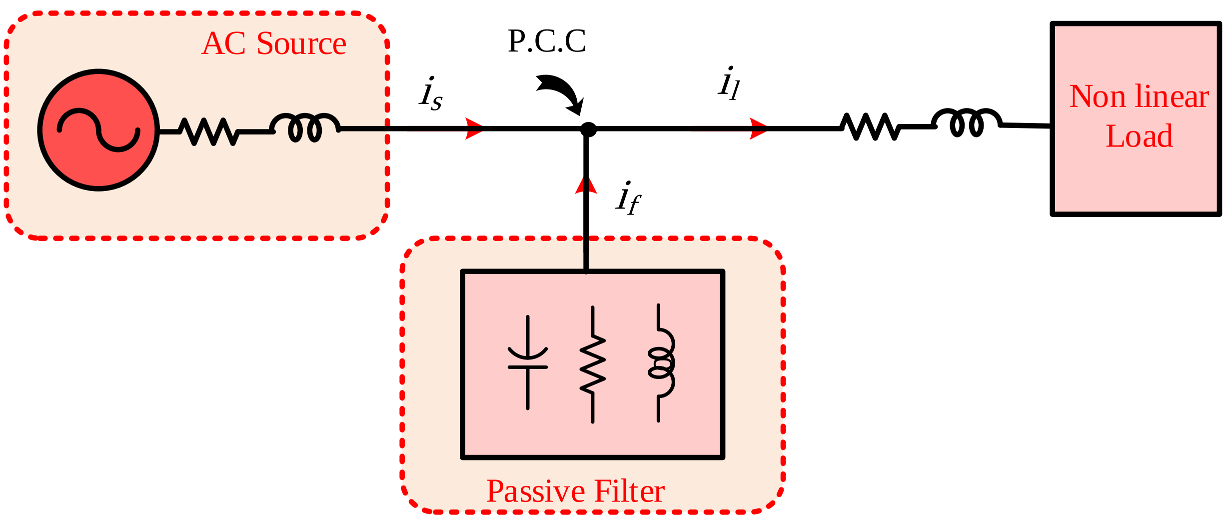

Figure I.8 : Single line diagram of grid-connected passive filter

I.6.1.1. Tuned passive filter

The tuned passive filters work based on the principle of providing and alternative branch that would trap the harmonic to be eliminated. The impedance of the filter has to be significantly lower than the source impedance. A tuned harmonic filter is typically composed of an inductor in series with a capacitor. The values of L and C are selected in a way such that the cut-off or resonance frequency of the circuit corresponds to the harmonic frequency to be mitigated[13].

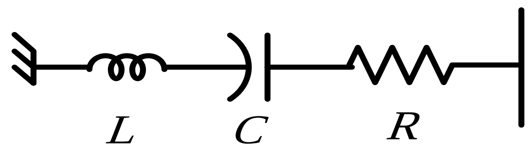

Figure I.9 : Tuned passive harmonic filter .

The main advantages of tuned passive filters are their simplicity and low cost. However, issues such as resonance, prone to overload, detuning, and the fact that they can only be designed to mitigate a single frequency are a big concern[13].

I.6.1.2. High pass filter.

A high pass filter presents low impedance for frequency above the resonant frequency. The objective is to mitigate more than one harmonic. However, they draw high current at fundamental frequency, which increases the resistive losses. The filter can be designed to more effectively mitigate a band of harmonics. The equivalent circuit of high-pass filter is shown in Figure. I.10.

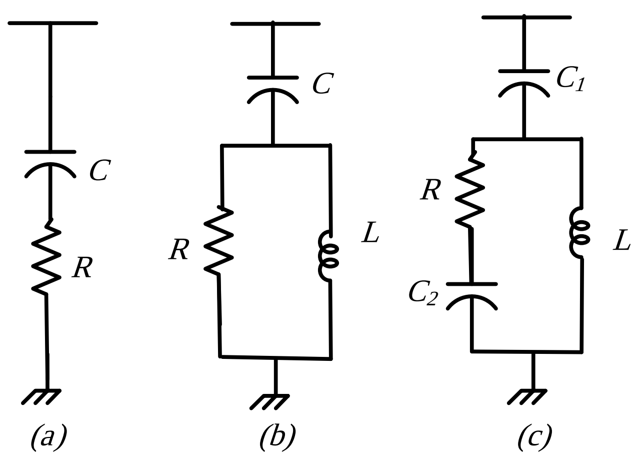

Figure I.10 : High-pass passive harmonic filter .

(a): First order high-pass filter

(b): Second order high-pass filter

(c): Third order high-pass filter

I.6.1.3. Disadvantages of passive filters

Passive are extensively used in many applications. However, they have many disadvantages such as[16]:

- The passive filters are not adaptable to varying system conditions and remain rigid once they are installed in an application. The size and tuned frequency cannot be altered easily.
- The change in operating conditions of the system may result in detuning of the filter and it may cause increased distortion. Such a change may happen undetected provided there is online detection or monitoring in the system.
- The design of the passive filter is reasonably affected by the source impedance. For an effective filter design, its impedance must be less than the source impedance. It may result in large size of the filter in a stiff system with low source impedance, which may result in overcompensation of the reactive power.
- In case of large filters, the power losses may be substantial because of resistive elements.
- The parallel resonance due to interaction between the source and the filter can cause amplification of some harmonics. Such problems enforce constraints on the designer in selecting tuned frequency for avoiding such resonances.
- The size of the damped filter becomes large in handling the fundamental and harmonic frequencies.
- The environmental effects such as aging, deterioration, and temperature change and detune the filters in a random manner.
- In some cases, even the presence of a small DC component and harmonic current may cause saturation of the reactors of the filter.

I.6.2. Modern solutions for harmonic elimination

The active filtering AF technology is now mature for providing compensation for harmonics, reactive power, and/or neutral current in ac grids. It has evolved in the past quarter of century of development with varying configurations, control strategies and solid-state devices. AFs are also used to eliminate voltage harmonics, to regulate terminal voltage, to suppress voltage flicker, and to improve voltage balance in three-phase systems. This wide range of application is achieved individually or in combination, depending upon the requirements and control strategy and configuration, which have to be selected approximately.[17]

Active filters are basically categorized into three types, namely, two-wire (single phase), three-wire, and four-wire three-phase configurations to meet the requirements of the three types of nonlinear loads on supply systems. Several configurations and control strategies to meet the needs of three-phase nonlinear loads have been reported. Configurations, such as the active series filter, active shunt filter, and combination of shunt and series filters have been developed and commercialized.[17]

Active filters can be classified based on converter type, topology, and number of phases. The converter type can be either Current Source Inverters (CSI) or Voltage Source Inverter (VSI). CSI-based active filters employ an inductor as the energy storage device. VSI-based active filters used a capacitor as the energy storage device. The topology can be shunt, series, or a combination of both. The third classification is based on the number of phases, such as two-wire (single-phase) and three- or four wire (three-phase) systems[18].

I.6.2.1. Shunt active filter

The basic idea of Shunt active filter is to inject to the line equal magnitudes of the current/voltage harmonics generated by the nonlinear load and with 180 degrees phase angle difference so they cancel each other.

Three-phase active filters are used for high-power nonlinear loads such as AC/DC converters. Active filters of many configurations have been introduced and improved. Shown in Figure. I.11, is the fundamental configuration of shunt active filter. Among all various configurations, the shunt active filter using the voltage source inverter topology accompanied by high performance current regulation methods is the most frequently employed type[18].

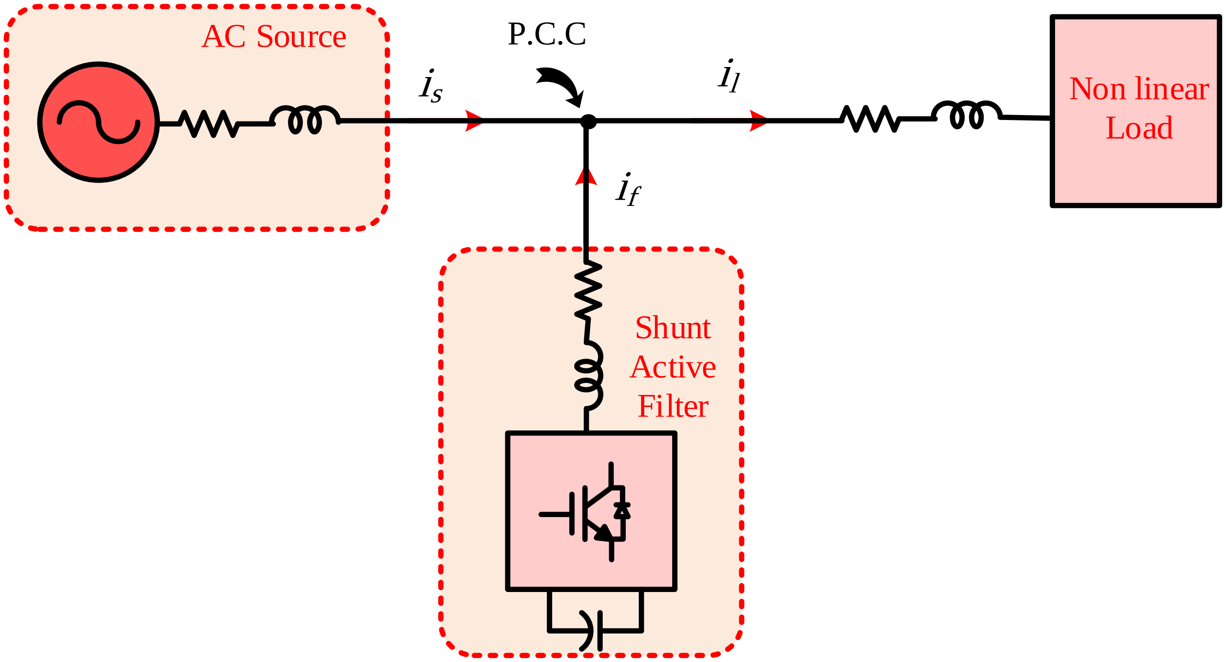

Figure I.11: Single line diagram of shunt active filter.

I.6.2.2. Series active filter

The filter in this configuration produces a Pulse with modulation (PWM) voltage waveform, which is to be added/substracted, on an instantaneous basis, to/from the supply voltage in order to apply a pure sinusoidal voltage waveform to the load. The main power circuit configuration is shown in Figure. I.12. The inverter configuration accompanying such a system is of the voltage source inverter. These series active filters are less common industrially than their rivals, the shunt active filters. This is because of the main drawback of series filters. Due to their position in the circuit, they have to withstand high values of rated load current, which increases their current rating considerably; especially the secondary side of the coupling transformer (increasing the copper losses and the physical size of the filter). Series filters have a main advantage over shunt ones in that they can be used much easier to eliminate voltage waveform harmonics, and to balance three phase voltages[19].

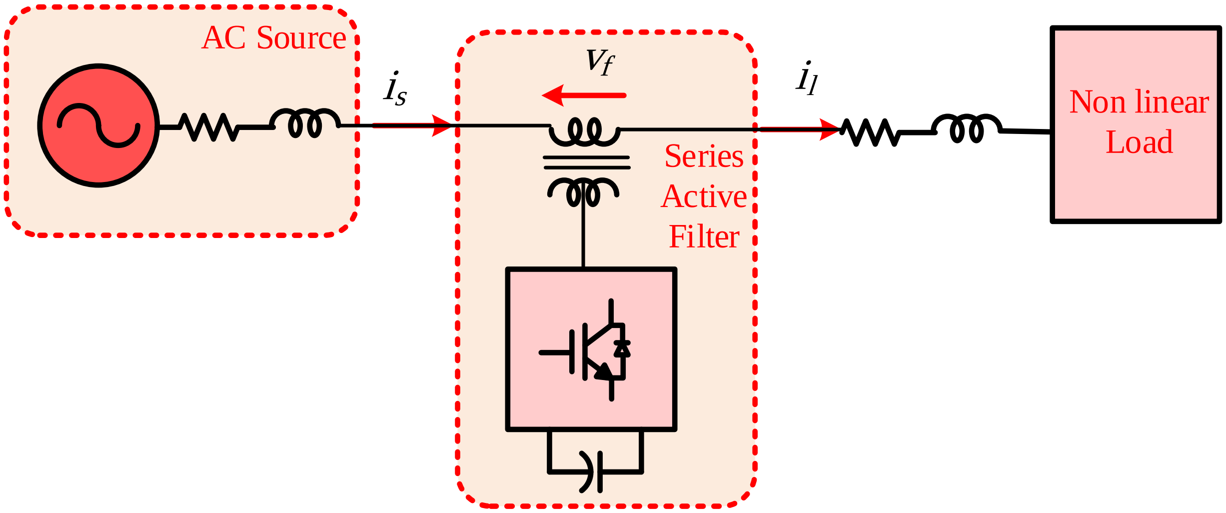

Figure I.12 : Single line diagram of series active filter.

I.6.2.3. Unified power quality conditioner

Combined series and shunt power quallity conditioners (UPFC) are formed by two power converters connected back-to-back through a common dc-link. Figure I.13 shows the basic configuration of a generic Unified Power Quality Conditioner. The ac output of one converter is inserted in series with the power system, whereas the ac output of the second one is connected in parallel. Although two current-source converters (CSCs) could be employed in the basic configuration shown in Fig. 6-1, it is common to use two voltage-source converters (VSCs) connected back-to-back through a common dc voltage link. VSC technology is widely used and dominates the market.[8] This universal compensator is able to perform reactive power compensation in addition to voltage and current harmonic compensation simultaneously.

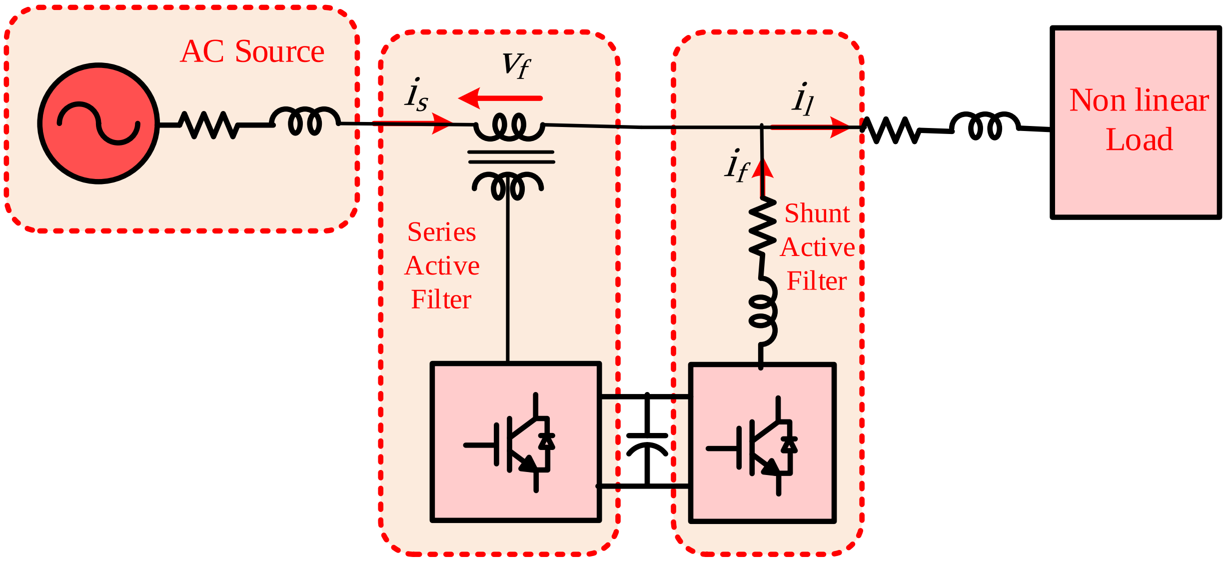

Figure I.13 : Single line diagram of series and shunt power conditioner .

I.6.2.4. Hybrid filter

It should be noted that there is several other combinations of active filters with passive filters. These structures are designed to optimize filtering performance of the system. There are mainly three configurations[20]:

- Series active filter with shunt passive filters.
- Series active filter connected in series with shunt passive filters.
- Shunt active filter with shunt passive filter.

I.6.2.5. Advantages and limitations of Active power filters

Active power filters have the following advantages [21]:

- Continuous measurement and cancellation of current and voltage harmonics.
- They do not consume any real power other than what is required to account for the internal losses of switches and inductor.
- They have fast response characteristics and sufficient bandwidth to cancel several harmonics appearing in the power system.

- They employ state-of-the-art power semiconductor devices and therefore are compact, light weight, and occupy little space.

However, active power filters have the following problems[21]:

- It is difficult to construct an APF with a high power rating and high frequency response and low loss.
- Total costs are high for low power ratings compared to passive filters.
- One of the important factors to be considered when evaluating the active power filters is the high price of the filter compared to passive filter.

I.7. Conclusion

In this chapter, we presented various disturbances affecting the electrical network. The harmonic disturbance problems were discussed in deep as well as their origins and effects.

International standards on harmonic emissions were presented. Then we showed the different solutions of harmonic filtering. Each filtering device has some positive points and disadvantages. Our study focuses on the three-phase three-wire shunt active filter as modern solution for current filtering. The next chapter will focus on the configuration of shunt active filter, modelling and direct power control strategy.

Chapter II: Direct Power Control Approach based Shunt Active Power Filter

I.1. Introduction

Due to the increase in nonlinear loads in electrical power systems, which produce current, the problem of harmonics has become serious, affecting power quality. There are many problems associated with the use of passive filters. Shunt Active filters are the emerging devices, which can perform the job of current harmonic cancellation properly[22]. Voltage source inverters (VSI) are frequently used in SAPF as a robust and highly efficient solution. However, the dynamic and static performance of SAPF depends strongly on adopted control algorithm. Therefore, control of SAPF has been well studied in literature and a number of control strategies has been proposed. On the other hand, Direct power control strategy is an appropriate control strategy because it offers faster transients and robust behavior with direct control of power.

In this chapter, an overview of shunt active filter is performed, the configuration of SAPF is modeled and analyzed. In the second part, state of the art of DPC is presented. DPC approach is evaluated by simulation and experimental results.

II.2. Overview of Shunt active power filter:

The shunt active filter is an inverter connected in parallel with the nonlinear loads and injects a harmonic current into the source to cancel the harmonics contained in the load current. There are two basic types of inverters used as a shunt APF:

- Voltage Source Inverter: In this type of filter, the DC source of inverter consists of a capacitor that resists sudden voltage changes.
- Current Source Inverter. In this type, the DC source consists of an inductor that resists sudden current changes.

The choice between these two types depends on the source of distortion at the specified bus, equipment cost, and the amount of correction desired. In both cases, the DC source plays an essential role as an energy element but it does not need any separate DC power supply as it receives its power from the AC power system through the switching action. Different types of shunt active power filters are explained in the following section[21].

II.2.1 Shunt active power filter types:

II.2.1.1 Single-Phase APF [21]

The basic configuration of a single phase shunt A P F with a capacitor as energy storage is shown in Figure II.1. A n inductor can also be used for shunt APF s (current source inverter type). In shunt APF, the filter controller senses the load current harmonics, and then injects equal anti-phase components into the utility. The result is that the utility provides only the load fundamental current component, and the active filter provides all the load harmonics.

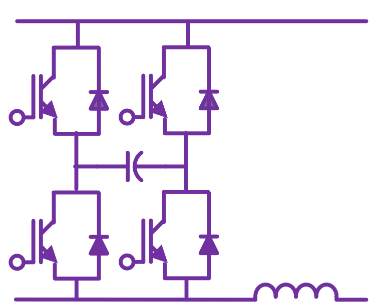

Figure II.1 : Single-phase Shunt APF

II.2.1.2 Three-Phase, Three-Wire Shunt APF[21]

In Three-Phase, Three-Wire Shunt APF the neutral conductor is not available for use. The absence of the neutral conductor in a balanced three-phase, three-wire system prevents the flow of triplen harmonic currents (i.e. 3rd, 9th, 15th , etc.). The primary purpose of any filtering in this type of distribution system is then the elimination of the 5th, 7th, 11th, 13th, etc. harmonic components.

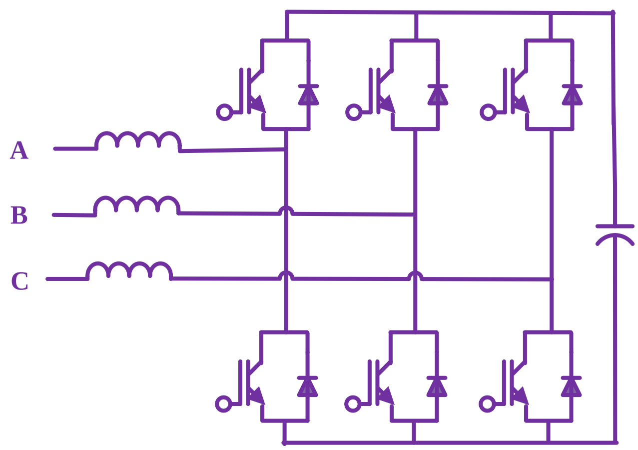

Figure II.2 : Three-phase, three-wire Shunt APF

The voltage source inverter type of three-phase three-wire Shunt APF is illustrated in Figure II.2. This type of APF inverter provides the harmonic currents required by the load (e.g. 5th, 7th, etc.). If the utility voltage is not distorted, the nonlinear load and filter combination can appear as a unity power factor load to the utility. Of course, the practical level of filtering is a function of many variables including source impedance, the inverter control loop, device component rating, and the current sensor's accuracy and phase shift. A current source inverter also has been used by some other authors[23]. Due to the higher efficiency of the voltage source inverter type, it is preferred by many authors[1]. For instance almost all shunt APFs which have been put into practical use in Japan are of the voltage source inverter type[24].

II.2.1.3. Three-phase four wire Active power filter[21]

In practical situations, power is distributed through a three-phase, four-wire system to domestic and commercial loads. Many of these applications uses single phase power and usually employ power electronics converters that draw excessive harmonic current of which a significant portion is the third harmonic component. Triplen harmonic currents are in phase in three-phase systems.

Therefore, they reinforce, rather than cancel, and the result is excessive neutral current. A survey revealed that 22.6% of the surveyed sites had neutral current more than 100% of the phase current[25]. This excessive neutral current creates some potential problems that are as follows [35]:

- Wiring failure due to improper sizing of the neutral conductor
- Overheating of the transformer due to harmonic currents, resulting in insulation damage and failure
- Excessive neutral-to-ground voltage due to a voltage drop caused by the neutral current.

Recently a number of shunt active power filters have been proposed that can be used for three-phase, four wire systems[20,26,27]. The active filter proposed by Enjeti[26]only removes the zero sequence from phase current. The other proposed APF can cancel all the harmonics when the neutral is returned to a fourth switch leg as shown in Figure II.3 (a) [27]. There is also another topology, called split-capacitor, in which system neutral is connected to the electrical midpoint the DC-bus through an optional inductor as shown in Figure II.3 (b). The analysis and simulation results of these topologies and three single phase APFs are summarised in [28].

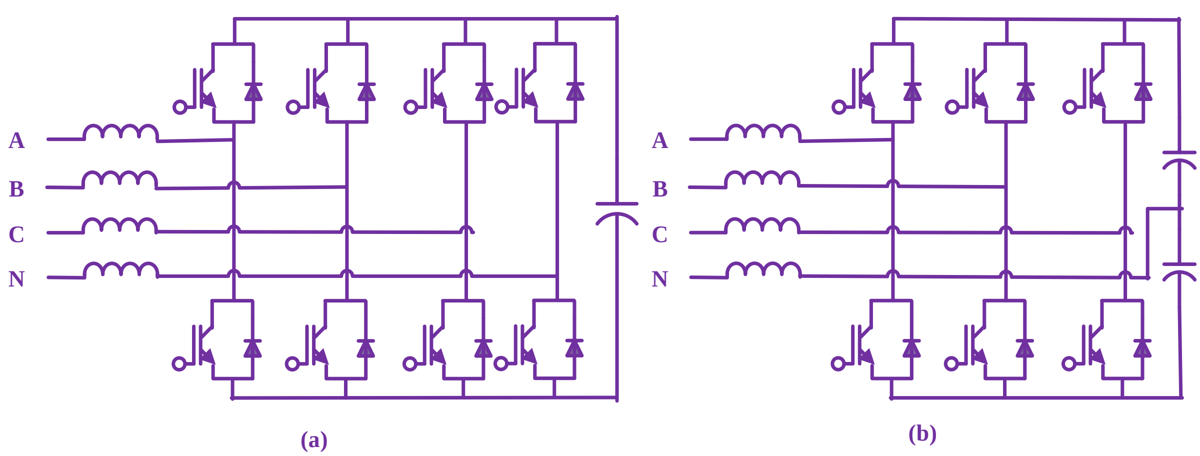

Figure II.3 : Four-wire*(a)*, Capacitor-midpoint topology *(b)* used as shunt APF

II.2.2. Control strategies

II.2.2.1. Time domain approaches[29]

Time-domain approaches are based on the principle of instantaneous compensation of current disturbances[30] [18, 37]. In this technique, the instantaneous error resulting from the deviation of current from its reference waveform is used to control the PWM voltage or current source inverters for injection of correcting component into the PCC . The shunt active power filter reference waveform includes the harmonic components of current as well as the reactive component.

A phase locked loop (PLL) tracks the fundamental frequency component and provides a timing reference for the controller. The main advantage of time-domain techniques is the fast response to changes in the load harmonic current. The computational burden of time-domain approaches are minimal[30] [18].

Many control strategies such as instantaneous reactive power theory (p_q theory) initially developed by Akagi et al. [31,32], synchronous frame d–q theory[33,34], synchronous detection method[35] , and notch filter method are used in the development of three-phase AF's.[22]

II.2.2.2. Frequency Domain Approaches[29]

In frequency domain approaches, the frequency components of the load current are identified using frequency analysis. such as Fast Fourier transform theory, Wavelet transformation theory, Empirical decomposition (EMD) transformation theory, Hilbert–Huang transformation theory[16]. These frequency components are used to determine the harmonic compensation reference waveform.

The frequency domain analysis of current distortion gives the flexibility using different configurations and circuits for each harmonic. For instance, to compensate the current harmonics of an AC adjustable speed drive (ASD) passive filters can be installed for the fifth harmonic which is the dominant harmonic component and a single active filter to compensate all the other harmonics and/or interharmonics.

The most commonly used tool for frequency domain analysis is the fast Fourier transform (FFT). The individual harmonic components in the load current are retrieved by performing a sliding FFT on the sampled load current waveform and then reproducing a compensating current waveform that has the exact harmonic components with the opposite phase angle.

However, these frequency domain algorithms are sluggish and slow, requiring heavy computation burden; therefore, these control methods are not too much preferred for real-time control of SAPF compared with time-domain control algorithms[16].

II.2.2.3 Shunt Active filter configuration[36]

The basic scheme of a SAPF with an L-type filter is shown in Figure. II.4. The structure of the converter consists of six switching cells based on switching devices such as IGBT, in such a way that eight possible configurations of the switches (S_a, S_b, S_c, S_a', S_b', S_c') are available, leading to seven possible voltage states at the output of the converter. Figure. II.5. shows the available configurations of one switching leg of the converter.

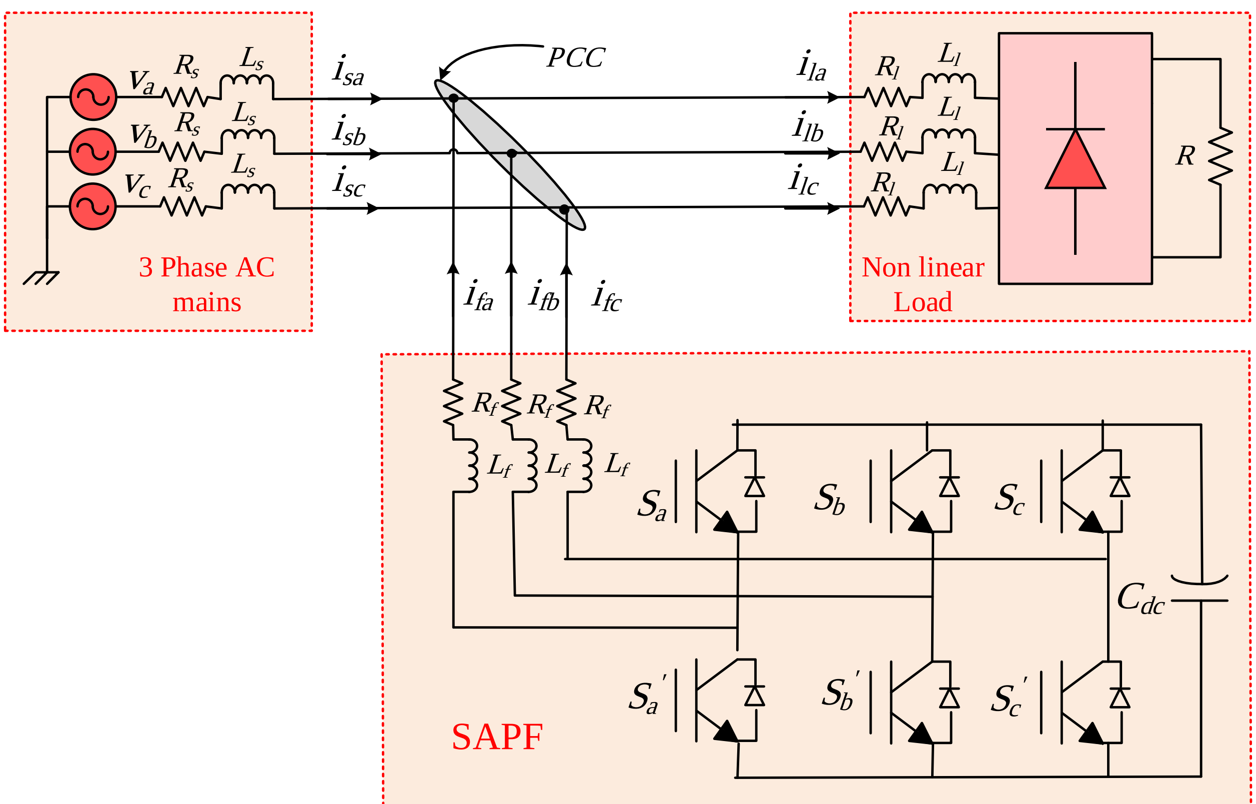

Figure II.4 : Basic configuration of Shunt APF

The output is connected to the negative (-) or positive (+) point of the DC-link when the state of the switch S is equal to '0' or '1', establishing a current way between the DC-side and AC-side. It should be noted that the switches (S_a, S_b, S_c) and (S_a', S_b', S_c') are operating in a complementary manner to avoid DC bus short-circuit.

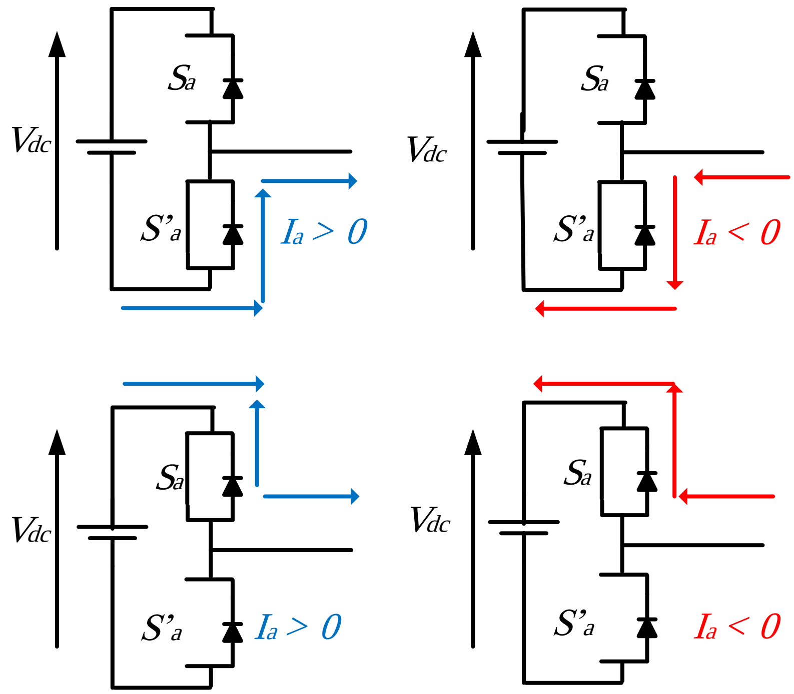

Figure II.5 : Availlable switching states in the converter's leg (a) of 2 level VSI

Equation (II.1) computes the available voltage vectors in the complex space. Six of them are classified as active vectors.

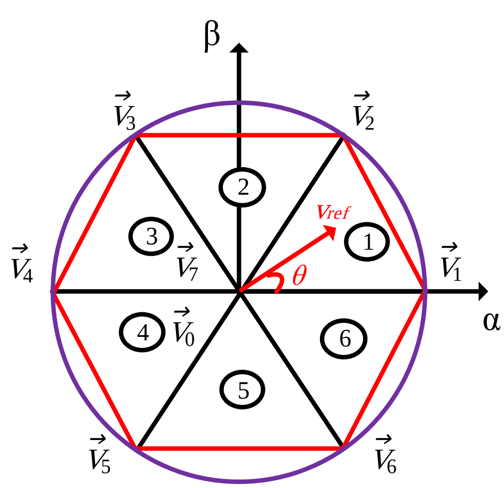

Figure II.6 : The voltage vectors of two-level inverter.

$$u_n = \begin{cases} \sqrt{\frac{2}{3}} v_{dc} e^{j(n-1)\frac{\pi}{3}} & n = 1...6 \\ 0 & n = 0,7 \end{cases}$$

(II.1)

Where v_{dc} is the DC voltage, n is a number of voltage vector, u_n is the value of voltage vector at the output of VSI.

The output voltages of the eight possible switching states of the inverter are illustrated in Table II.1.

Table II.1: Output voltages of different switching states of two-level inverter.

STATE	S_a	S_b	S_c	v_a	v_b	v_c	v_α	v_β	v_i
1	0	0	0	0	0	0	0	0	v_0
2	1	0	0	$-2\,v_{dc}/3$	$v_{dc}/3$	$v_{dc}/3$	$v_{dc}\sqrt{2/3}$	0	v_1
3	1	1	0	$v_{dc}/3$	$v_{dc}/3$	$-2\,v_{dc}/3$	$v_{dc}/\sqrt{6}$	$v_{dc}/\sqrt{2}$	v_2
4	0	1	0	$-\,v_{dc}/3$	$2\,v_{dc}/3$	$-\,v_{dc}/3$	$-v_{dc}/\sqrt{6}$	$v_{dc}/\sqrt{2}$	v_3
5	0	1	1	$-\,v_{dc}/3$	$-\,v_{dc}/3$	$-\,v_{dc}/3$	$-v_{dc}/\sqrt{2/3}$	0	v_4
6	0	0	1	$-\,v_{dc}/3$	$-\,v_{dc}/3$	$2v_{dc}/3$	$-v_{dc}/\sqrt{6}$	$-v_{dc}\sqrt{2}$	v_5
7	1	0	1	$v_{dc}/3$	$-2\,v_{dc}/3$	$v_{dc}/3$	$v_{dc}/\sqrt{6}$	$-v_{dc}/\sqrt{2}$	v_6
8	1	1	1	0	0	0	0	0	v_7

Therefore, and assuming that the grid is a balanced three-phase power system, the following converter's per-phase equations related to the neutral point (n) of grid can be derived.

The instantaneous voltage of three phase balanced and sinusoidal system is based on the following expression:

$$v_{sa}(t) = \sqrt{2}v_s \cos(\omega t)$$
$$v_{sb}(t) = \sqrt{2}v_s \cos(\omega t - 2\frac{\pi}{3}) \quad \text{(II.2)}$$
$$v_{sc}(t) = \sqrt{2}v_s \cos(\omega t + 2\frac{\pi}{3})$$

Applying Kirchoff's laws on the circuit of Figure II.4 the per-phase dynamic behavior of the proposed power system SAPF is presented in Equation (II.3)

$$L_f \frac{di_{fx}}{dt} + R_f i_{fx} = u_{fx} - v_{sx}, \text{ x=a, b, c} \quad \text{(II.3)}$$

Where: v_s is the source voltage measured at PCC,

u_f is the volage at the output of the inverter

The equations are then given by:

$$L_f \begin{bmatrix} \frac{di_{fa}}{dt} \\ \frac{di_{fb}}{dt} \\ \frac{di_{fc}}{dt} \end{bmatrix} = -R_f \begin{bmatrix} i_{fa} \\ i_{fb} \\ i_{fc} \end{bmatrix} + \begin{bmatrix} u_{fa} \\ u_{fb} \\ u_{fc} \end{bmatrix} - \begin{bmatrix} v_{sa} \\ v_{sb} \\ v_{sc} \end{bmatrix} \quad \text{(II.4)}$$

Also, the behavior of the DC-link voltage can be expressed based on the converter's switching pattern and AC side currents.

$$C_{dc} \frac{dV_{dc}}{dt} = S_a i_{fa} + S_b i_{fb} + S_c i_{fc} \quad \text{(II.5)}$$

Then, it is possible to present the model of the SAPF in the three-phase coordinates abc as follows:

$$\begin{cases} L_f \dfrac{di_{fa}}{dt} = -R_f\, i_{fa} + u_{fa} - v_{sa} \\ L_f \dfrac{di_{fb}}{dt} = -R_f\, i_{fb} + u_{fa} - v_{sa} \\ L_f \dfrac{di_{fc}}{dt} = -R_f\, i_{fc} + u_{fa} - v_{sa} \\ C_{dc} \dfrac{dV_{dc}}{dt} = S_a i_{fa} + S_b i_{fb} + S_c i_{fc} \end{cases} \tag{II.6}$$

In many applications it is useful to present the system model in static α-β or rotating d-q reference frame, using the well-known Park's or Clark's transformations (See Appendix). Equations (II.7)and (II.8) show the system behavior under the α-β and d-q coordinates respectively.

$$\begin{cases} L_f \dfrac{di_{f\alpha}}{dt} = -R_f\, i_{f\alpha} + u_{f\alpha} - v_{s\alpha} \\ L_f \dfrac{di_{f\beta}}{dt} = -R_f\, i_{f\beta} + u_{f\beta} - v_{s\beta} \\ C_{dc} \dfrac{dV_{dc}}{dt} = -\dfrac{3}{2}(S_\alpha i_{f\alpha} + S_\beta i_{f\beta}) \end{cases} \tag{II.7}$$

$$\begin{cases} L_f \dfrac{di_{fd}}{dt} = -R_f\, i_{fd} - \omega i_q + u_{fd} - v_{sq} \\ L_f \dfrac{di_{fq}}{dt} = -R_f\, i_{fq} - \omega i_d + u_{fq} - v_{sd} \\ C_{dc} \dfrac{dV_{dc}}{dt} = -(S_d i_{fd} + S_q i_{fq}) \end{cases} \tag{II.8}$$

Where the appropriate switching states are expressed as:

$$f_\alpha = \frac{2S_a - (S_b + S_c)}{3} \tag{II.9}$$

$$f_\beta = \frac{1}{\sqrt{3}}(S_b + S_c)\,\text{(II.3)} \tag{II.10}$$

With

$$f_d = f_\alpha \cos(\omega t) + f_\beta \sin(\omega t) \tag{II.11}$$

$$f_q = f_\beta \cos(\omega t) - f_\alpha \sin(\omega t) \tag{II.12}$$

II.3. Direct power control strategy (DPC)

II.3.1 State of the Art of DPC approach[37–39]

Various control strategies on grid-converters have been proposed in previous works. A voltage oriented control (VOC) is well-known indirect active and reactive power control which is based on current vector orientation with respect to the line voltage vector (Voltage Oriented Control - VOC) [38]. VOC guarantees high dynamics and static performance via an internal current control loops. However, the final configuration and performance of the VOC system largely depends on the quality of the applied current control strategy[37]. A Direct Power Control (DPC) strategy based on direct control of instantaneous active and reactive power is firstly proposed by Ohnishi et al[40]. This technique is derived from the first and original Direct Torque Control (DTC) of AC machines[41]. In each sampling time it evaluates which one of the instantaneous voltage vectors (available at the output of the converter) is best suited in order to push the state of the system towards the reference value. As this evaluation is continuously carried out, direct control technique does not require any modulator and it is able to get the maximum dynamic capability available in the system. Moreover, it does not require any internal control loop or any coordinate transformation, avoiding coupling effects between transformed variables. In the DPC case, instantaneous active and reactive power control loops are based on hysteresis regulators that select the appropriate voltage vector from a look-up table (switching table), [36]

The hysteresis width and the nonlinearity of the system inherently introduce variable switching frequency, which can lead to resonance problems in some applications and generate a spread spectral content. This leads to the need for bulky and expensive filters. Some modifications have been proposed to control the switching frequency in DPC approach. A linear proportional–integral (PI) controller with a modulation have been replaced a look-up table, this control strategy is called DPC-SVM [42,43].

The linear control scheme with a modulation stage often requires additional coordinate transformations. In addition, the fact that a linear control is applied to a nonlinear system can lead to uneven performance throughout the dynamic range. Among these new control schemes, predictive control appears to be a very interesting alternative for the control of power converters. Predictive control comprises a very wide family of controllers with very different approaches[44–47]. The common ideas behind all predictive control are the use of a model of the system for calculating predictions of the future behavior of the controlled variables, and the use of an optimization criterion for selecting the proper actuation. [39]. The predictive control is the subject of this thesis and two different predictive control strategies will be investigated. The Virtual Flux (VF) is a promising concept. The virtual flux estimation technique is used to extract the grid voltage information from the converter switching states, line currents and DC bus output voltage[48]. One of the main advantages of this new approach is that it is less sensitive to line-voltage variations than other approaches[36].

II.3.2 Principle of DPC

Direct power control strategy is focused on using instantaneous active and reactive power as control variables instead of instantaneous three-phase currents as illustrated in Figure II.7.

DPC does not focus on current control loop or PWM modulation block, because this method selects the most appropriate control vector of the inverter from a predefined look-up table (switching table) based on the errors of active and reactive power, as well as the vector position of source voltage.

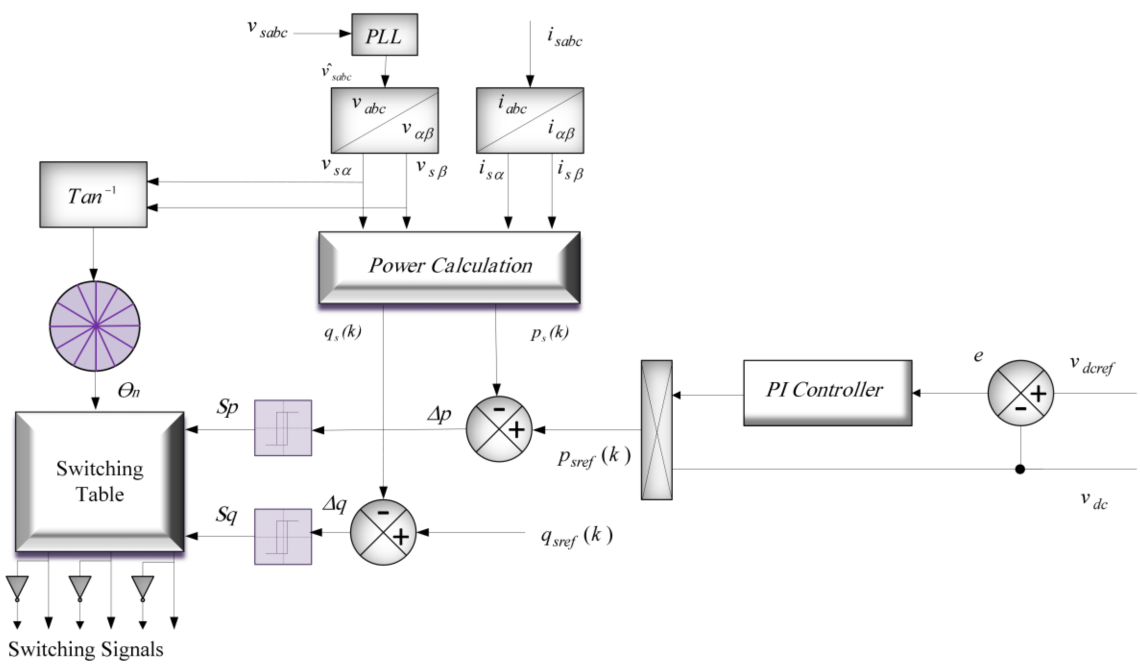

Figure II.7 : Control scheme of DPC based SAPF

Thus the choice of the optimum switching state is performed; so that, the error of active power can be limited within a hysteresis band width and the same for the error of reactive power. Referenced active power is delivered from outer DC-link controller. However, referenced reactive power is set to zero for unity power factor. The general control scheme of DPC.

II.3.2.1 Power Calculation

The most frequently referred power theory for three-phase three-wire system are:

- **The Takahashi power definition**

Takahashi define the instantaneous active power *p* as scalar product between the three phase voltages and currents and instantaneous reactive power *q* as vector product between them[49]:

$$p = \underline{u}_{abc} \cdot \underline{i}_{abc} \tag{II.13}$$

$$q = \underline{u}_{abc} \times \underline{i}_{abc} \tag{II.14}$$

By taking the advantages of an instantaneous complex power *p(t)* in the Cartesian plane:

$$\underline{p}(t) = \underline{u}(t) \times \underline{i}(t) = \mathrm{Re}\left\{\underline{p}(t)\right\} + \mathrm{Im}\left\{\underline{p}(t)\right\} = p(t) + jq(t) =$$

$$= u_a i_a + u_b i_b + u_c i_c + j\,\frac{1}{\sqrt{3}}\left[(u_b - u_c)\mathrm{i}_a + (u_c - u_a)\mathrm{i}_b + (u_a - u_b)\mathrm{i}_c\right] \tag{II.15}$$

- **Akagi power definition:**

The definition of instantaneous power has been proposed by Akagi[50] when the three-phase voltages and currents are transformed into α-β coordinates, and therefore, instantaneous active and reactive power on the three-phase circuit can be defined as follows

$$p = \underline{u}_{\alpha}\underline{i}_{\alpha} + \underline{u}_{\beta}\underline{i}_{\beta} \tag{II.16}$$

$$q = \underline{u}_{\alpha} \times \underline{i}_{\beta} + \underline{u}_{\beta} \times \underline{i}_{\alpha} \tag{II.17}$$

II.3.2.2 Sectors selection

The influence of each output vector that is provided by the inverter on active and reactive power is very dependent on the real position of the voltage vector of the source. To increase the accuracy and also to avoid the problems encountered at the borders of each control vector, The region of the voltage vector position is divided into 12 sectors of 30° for each one (Figure II.8), where the first sector is defined in Equation (II.18).

$$-\frac{\pi}{3} < \theta_1 < 0 \quad \text{(II.18)}$$

The sectors can be obtained by numerical expression as Equation (II.19).:

$$(n-2) < \frac{\pi}{6} < \theta_n \leq (n-1)\frac{\pi}{6} \quad \text{(II.19)}$$

Where n= 1, 2, 3 …..12

The angle is obtained using the inverse tangent function, which is based on the components of the voltage vector on stationary coordinates (α, β), indicated by Equation (II.20):

$$\theta = \arctan \frac{V_\alpha}{V_\beta} \quad \text{(II.20)}$$

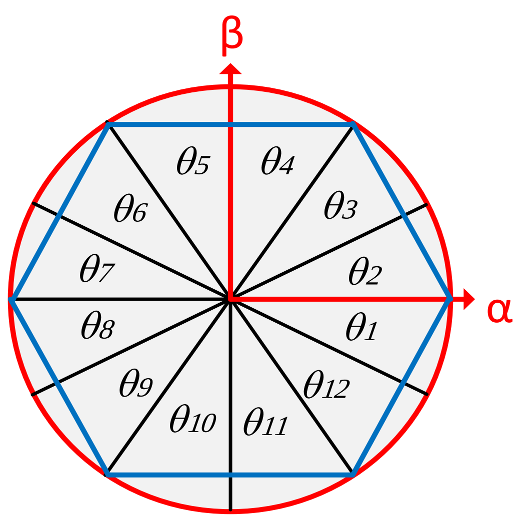

Figure II.8 : Sectors on stationary coordinates (α, β).

II.3.2.3 Switching Table

The idea of switching table based direct power control was firstly proposed in [40]. It is based on the concept that two-level inverter generates seven voltage vectors for eight different combinations; the calculation of each control vector is based on the respective switching state *Sa, Sb, Sc* and the DC bus voltage. The optimum control vector of the inverter, in each sampling time, is sellected based on the combination of the digital signals *Sp, Sq* and source voltage vector position Thus, different switching tables for DPC were proposed. Table. II.2 is adopted in this work.

Table. II.2: Switching table

S_P	S_Q	θ_1	θ_2	θ_3	θ_4	θ_5	θ_6	θ_7	θ_8	θ_9	θ_{10}	θ_{11}	θ_{12}
1	0	V_6	V_7	V_1	V_0	V_2	V_7	V_3	V_0	V_4	V_7	V_5	V_0
1	1	V_2	V_7	V_3	V_0	V_4	V_7	V_5	V_0	V_6	V_7	V_1	V_0
0	0	V_6	V_1	V_1	V_2	V_2	V_3	V_3	V_4	V_4	V_5	V_5	V_6
0	1	V_1	V_2	V_2	V_3	V_3	V_4	V_4	V_5	V_5	V_6	V_6	V_1

V_0=(000), V_1=(100), V_2=(110), V_3=(010), V_4=(011), V_5=(001), V_6=(101), V_7=(111).

II.3.2.4 Hysteresis controllers

The wide of hysteresis band for the controlled variables (the instantaneous active and reactive power) have a relevant effect on the converter performance. In particular, the harmonic current distortion, the average converter switching frequency, the power pulsation and the losses are strongly affected by the hysteresis wide. Two-level comparators for instantaneous active and reactive power hysteresis controllers can be described as:

$$S_p = \begin{cases} 1 \; for \; P_s < P_{sref} - H_p \\ 0 \; for \; P_s > P_{sref} + H_p \end{cases} \tag{II.21}$$

$$S_q = \begin{cases} 1 \; for \; q_s < q_{sref} - HQ \\ 0 \; for \; q_s > q_{sref} + HQ \end{cases} \tag{II.22}$$

where: *Hp* and *Hq* are hysteresis bands and *Sp* and *Sq* are the digitized variables.

II.3.2.5 Phase Locked Loop

P.L.L is an interesting component control of power electronics converter in grid-connected application . It is used as a means to retrieve phase and frequency information, which allows controlling the utility phase angle. The basic form of P.L.L is shown in Figure II.9, including a phase detector PD, low pass filter LF and a voltage controlled oscillator VCO.

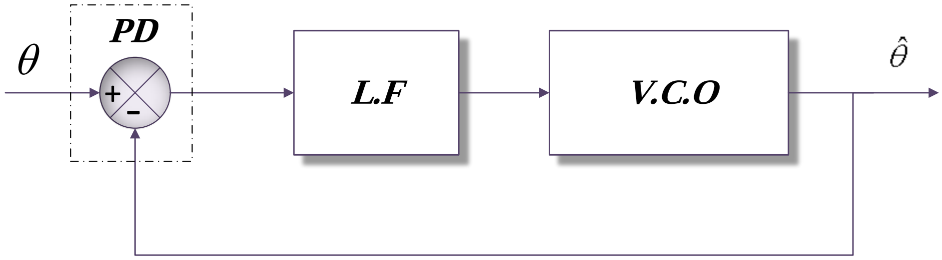

Figure II.9 : Conventional PLL

A robust PLL algorithm is presented in [51]. It is based on the basic concept of PLL with introducing a multivariable filter named self-tuning filter (STF) to extract the direct component of source voltage during distorted conditions.

The STF is presented by the following Equations II.(23-24).:

$$\hat{V}_{\alpha}(s)=\frac{k_{stf}}{s}\left[V_{\alpha}(s)-\hat{V}_{\alpha}(s)\right]-\frac{w_{stf}}{s}\hat{V}_{\alpha}(s) \tag{II.23}$$

$$\hat{V}_{\beta}(s)=\frac{k_{stf}}{s}\left[V_{\beta}(s)-\hat{V}_{\beta}(s)\right]+\frac{w_{stf}}{s}\hat{V}_{\beta}(s) \tag{II.24}$$

Wherer

w_{stf} is the cut-off frequency of STF.

k_{stf} tuning parameter

$V_{\alpha}(s), V_{\beta}(s)$ and $\hat{V}_{\alpha}(s), \hat{V}_{\beta}(s)$ are voltage signals, before and after filtering respectively.

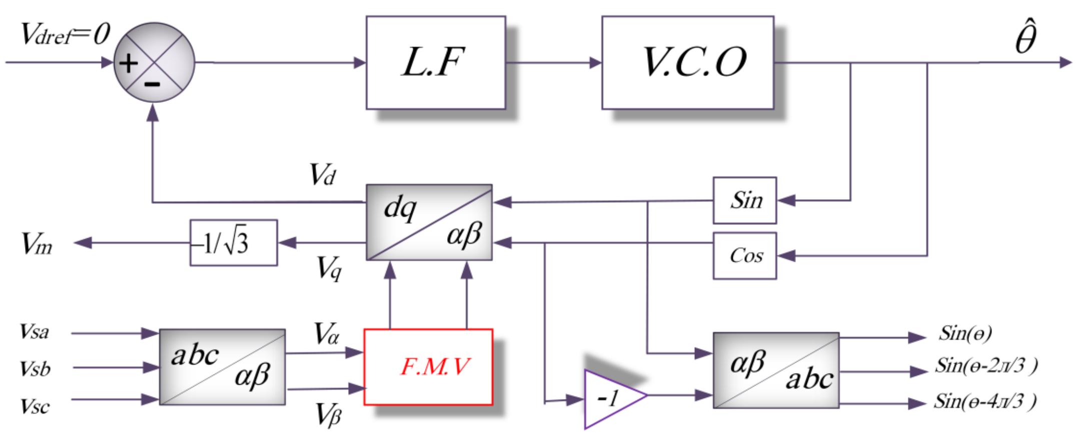

Figure II.10: Robust PLL

II.3.2.6 DC bus voltage controller

The control of the DC voltage of SAPF is an essential stage to ensure a good operation of the whole system. DC side control loop is necessary to make the voltage constant and to perform good operation in steady state. It relies on the concept of the equilibrium of energy stored in the capacitor according to reference voltage of DC side (v_{dcref}).

$$E_{dc} = \frac{1}{2} C_{dc} v^2_{dcref} \tag{II.25}$$

The development of voltage regulation loop is achieved using the transfer function that links the output value of the DC bus voltage v_{dc} with the amplitude of the active fundamental current is that is required to ensure the equilibrium of the active powers. It can be deduced based on the concept of Equation (II.25):

$$\frac{v_{dc}}{i_s} = \frac{3v_s}{\sqrt{2} v_{dcref} C_{dc} s} \tag{II.26}$$

Where: S is Laplace operator

Proportional integral controller has been proposed for correcting the oscillation of DC bus voltage and assuring the stability of the system. Figure II.11 illustrates the closed control loop that is adopted for DC bus voltage regulation.

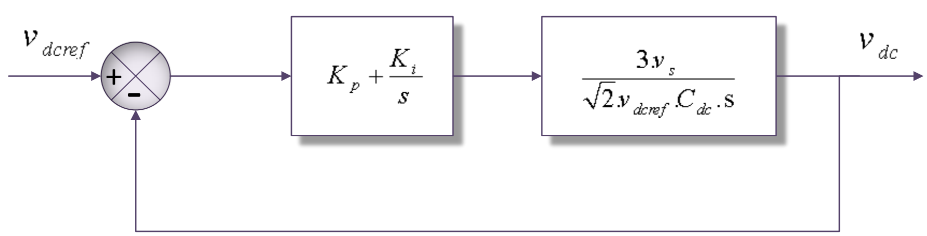

Figure II.11 : Control loop of DC bus voltage

The closed loop transfer function that is illustrated in Figure II.11 is a second order equation.

$$\frac{v_{dcref}}{v_{dc}} = \frac{\frac{K_p}{K_{dc}}\left(s + \frac{K_i}{K_p}\right)}{s^2 + \frac{K_p}{K_{dc}}.s + \frac{K_i}{K_{dc}}} \tag{II.27}$$

Where

$$K_{dc} = \frac{\sqrt{2}.C_{dc}.v_{dcref}}{3v_s} \tag{II.28}$$

The general form of second order trasfer function is defined by:

$$F(s) = \frac{2\xi\omega_n s + \omega^2}{s^2 + 2\xi\omega_n s + \omega_n^2} \tag{II.29}$$

The PI controller parameters are obtained by identification as follows :

$$K_P = 2.\xi.k_{dc}.\omega_n \tag{II.30}$$

$$K_i = \omega_n^2.k_{dc} \tag{II.31}$$

Where ω_n represents the natural frequency whereas ξ is the frequency of damping which is equal to 0.707 for optimal operation.

Although, high performance cannot be achieved by this type of controllers, in transient time, because of the large error that is caused by the saturation of controller. High gain of anti-windup has been introduced to PI controller *Ga* as depicted in Figure II.12 , in the aim of solving saturation problem and obtaining smooth operation in transient state[52].

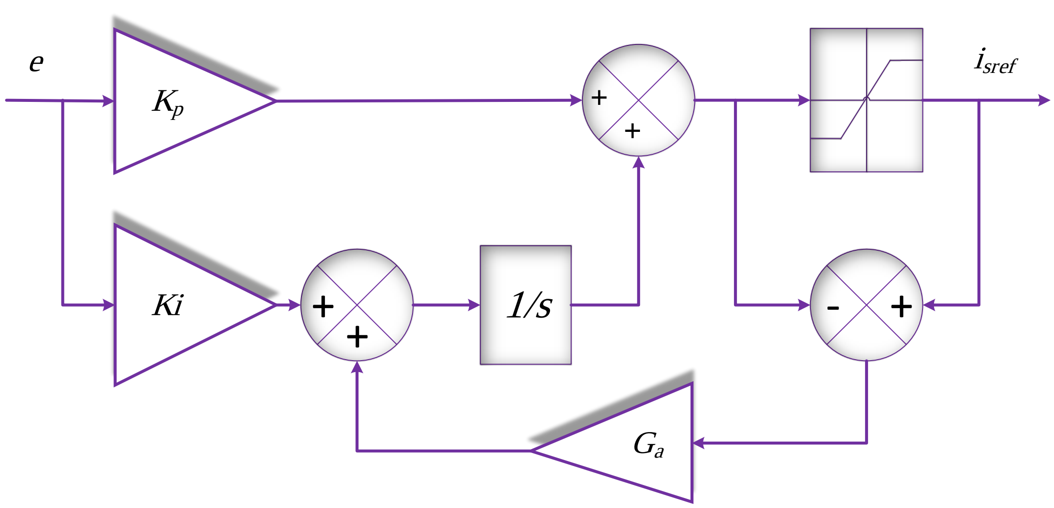

Figure II.12 : Anti-windup PI controller

II.4. Simulation results

In order to evaluate the performance of direct power control approach applied to SAPF, we developed a model under Matlab \ Simulink environment and several simulations have been carried out. DPC has been tested under steady state and transient conditions. The simulation parameters have been carefully defined to ensure convergence and good operation of the system. The basic simulation parameters are listed in Table. A.2 (See appendix).

Firstly, the source voltage has been investigated in Figure II.(13-14). It is interesting noting that the source voltage after the PLL shown in Figure II.13 (b) has better quality waveform than that measured from the source, which demonstrate the capability of the PLL to extract the direct component of source voltage. In addition, a good estimation of source voltage angular position θ is achieved.

Figure II.(14-15) show the response of the system during the operation of SAPF. Before, connecting the filter, the source current has non-sinusoidal waveform, no current is provided from the SAPF. The DC bus capacitor is charged to the peak of the input phase-to-phase voltage (*100V*) through the IGBTs' body diodes. According to Figure II.15 ,, the source provides active and reactive power simultaneously to the load. Once the filter is connected at *t=0.16s*, The APF takes approximately 3 to 4 line cycles to stabilize and fully compensate since the DC bus voltage experience a transient. As a result, the source current become sinusoidal, DC bus voltage stabilized at its reference value *160V*, the SAPF provides the required current harmonic components to make the source provide the fundamental component only. The source active power follows its reference. However, the source reactive power is almost zero to operate with unity power factor.

The quality of filtering has been evaluated by spectral analysis of the source current as shown in Figure II.16 (a-b). The current waveform was highly distorted before inserting the filter where THDis=24.24 %. However, the current total harmonic distortion has been reduced to THDis=1.20 % after filtering.

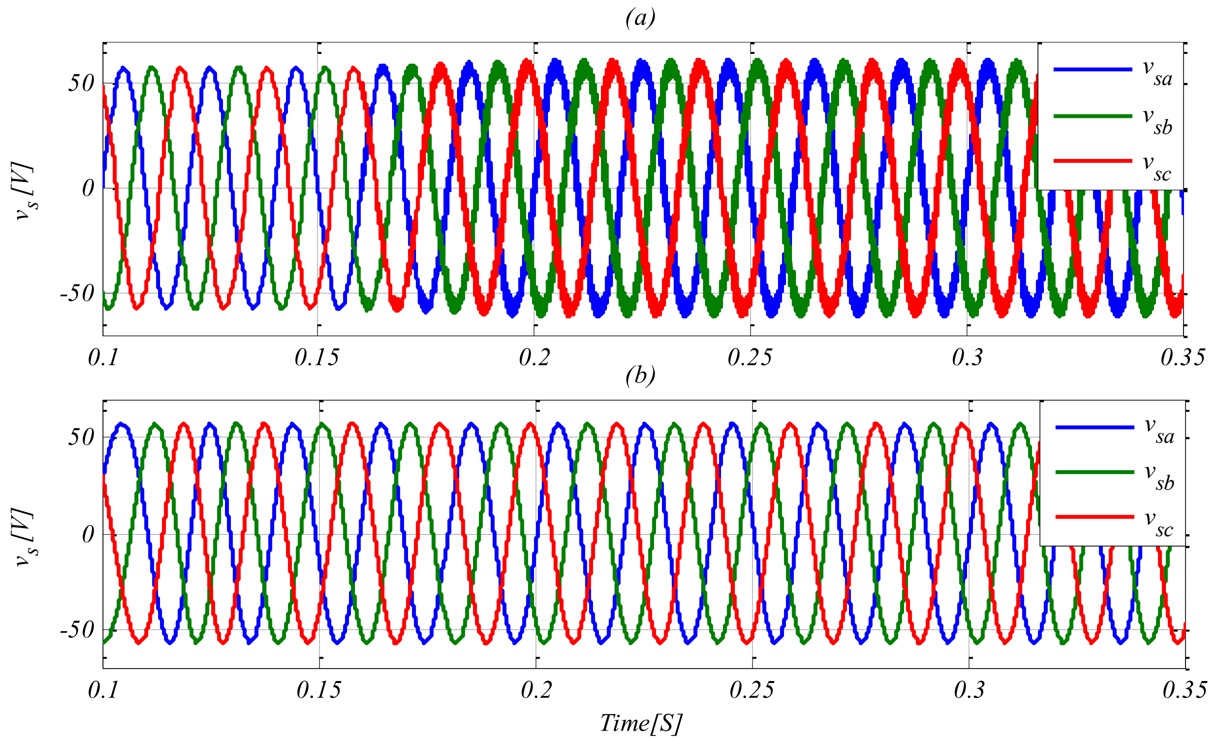

Figure II.13 : Source voltage *(a)* Before PLL, *(b)* After PLL, *SAPF is operated at t=0.16s.*

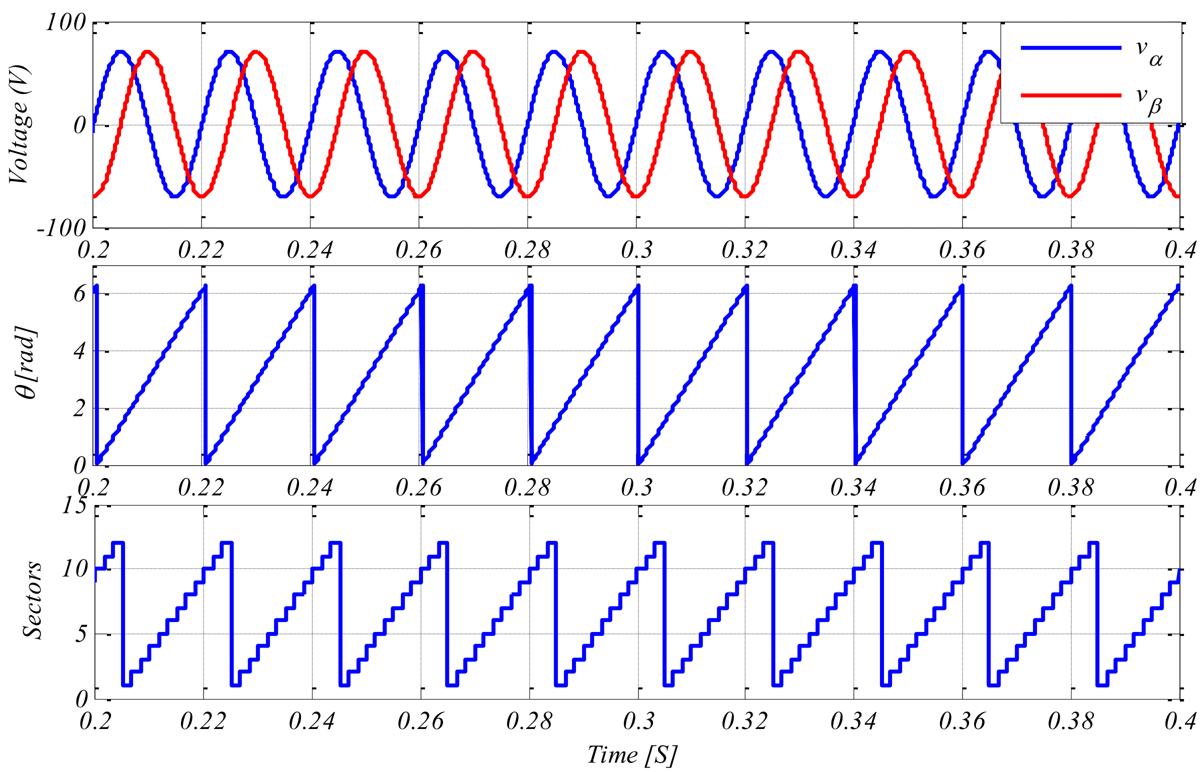

Figure II.14 : Simulation results of source voltage on stationary coordinates (v_α, v_β), phase angle and sectors.

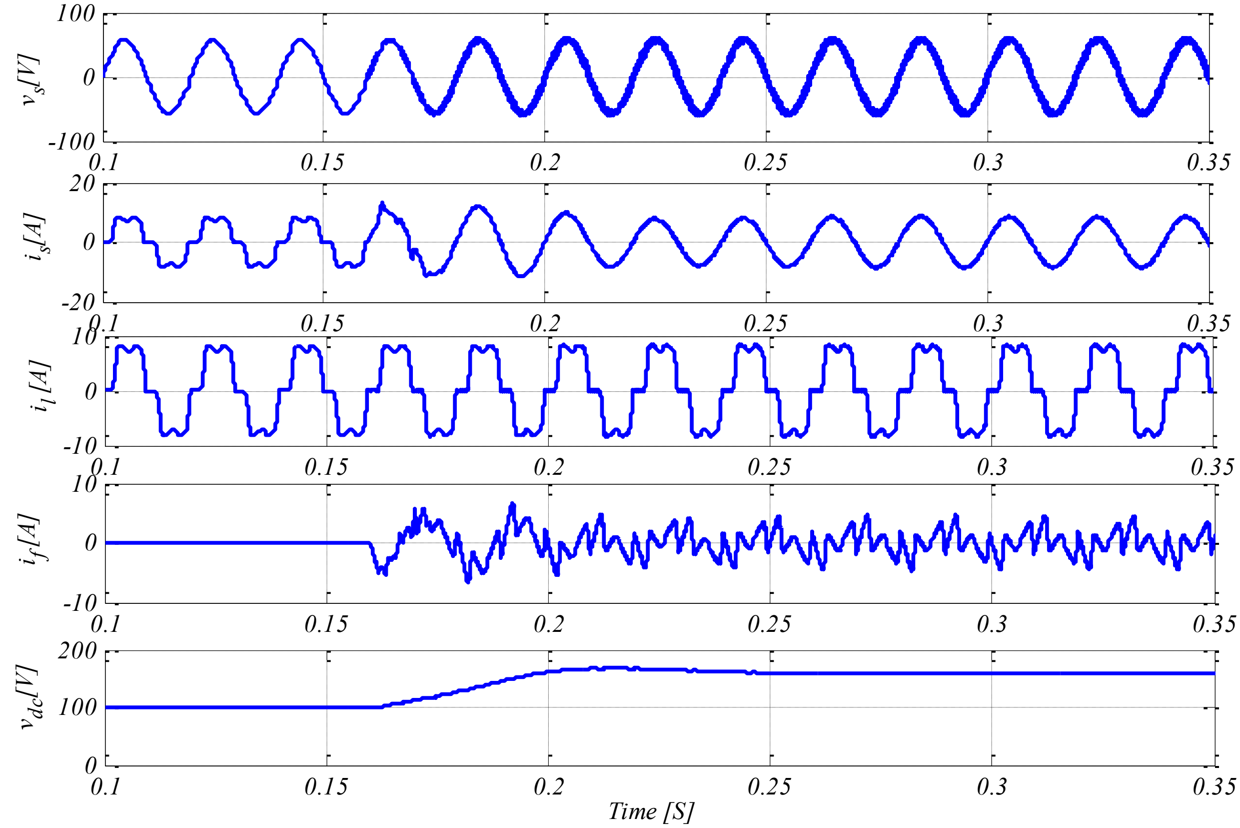

Figure II.15 : Simulation results of source voltage *(v_s)*, source current *(i_s)*,load current*(i_l)*, filter current*(i_f)*, DC bus voltage waveforms *(v_{dc})*, SAPF is operated at *t=0.16s*

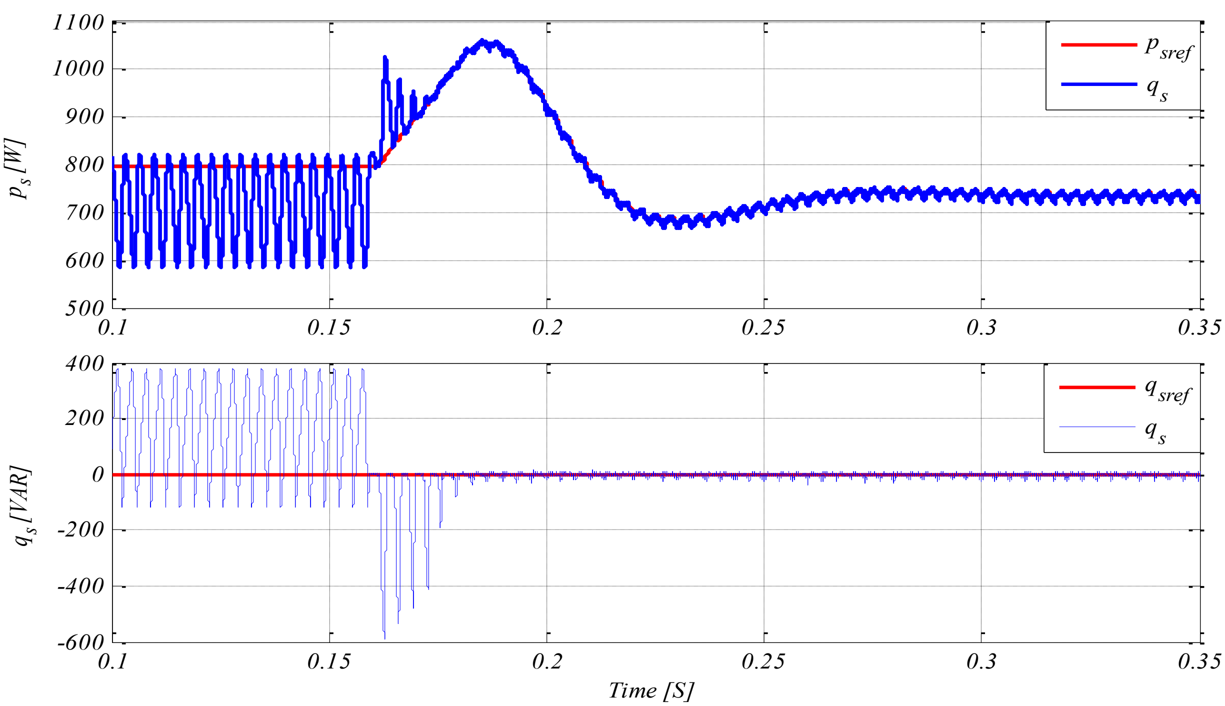

Figure II.16 : Simulation results of source active and reactive power *(ps , qs)* with their references *(psref , qsref)*, SAPF is operated at *t=0.16s.*

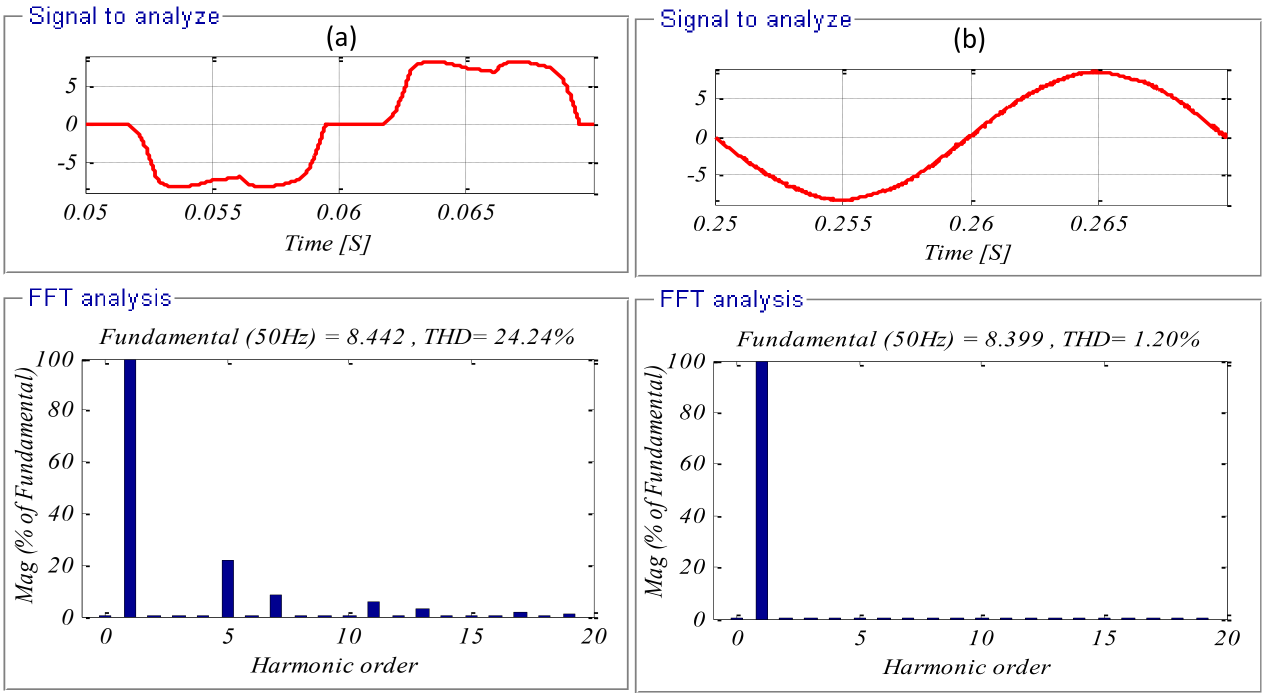

Figure II.17 : Simulation results of FFT analysis of source current before filtering *(a)* and after filtering *(b).*

Moreover, to show the performance during dynamic condition, the load current is increased at *t=0.2s* by decreasing the resistance value of the load from *22.66* Ω to *11.33* Ω (step variation of 50%).

Figure II.18 shows the response of SAPF during load variation. Small voltage dip is noticed in DC bus voltage when the load current is increased. However, the steady state is reached within 4 line cycles and DC bus voltage stabilized at its reference voltage $v_{dcref}=160V$. On the other hand, load currents undergo a sudden increase while that of the source maintain its dynamic and its sinusoidal form thanks to controller. It worthy to know that this load variation does not cause any disturbance in the voltage of the source.

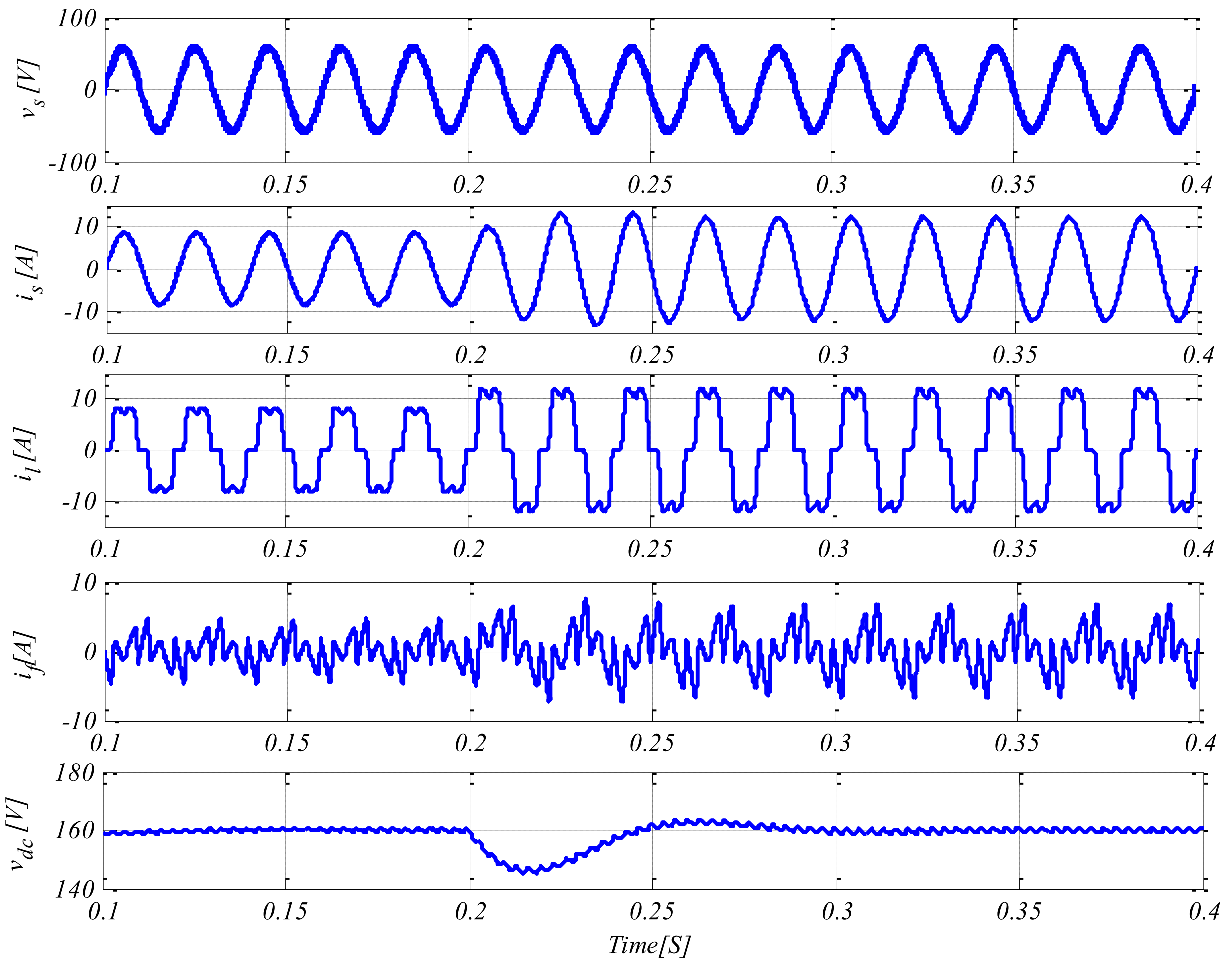

Figure II.18 : Simulation results of source voltage *(v_s)*, source current *(i_s)*,load current*(i_l)*, filter current*(i_f)*, DC bus voltage waveforms *(v_{dc})*, step increase of the load at *t=0.2s.*

Similarly, Figure II.19 shows the evolution of active and reactive power with their references during step increase of power. A necessary active power is delivered by the source starting from *t=0.2s*. Whereas, the reactive power stays equal to zero to ensure reactive power compensation.

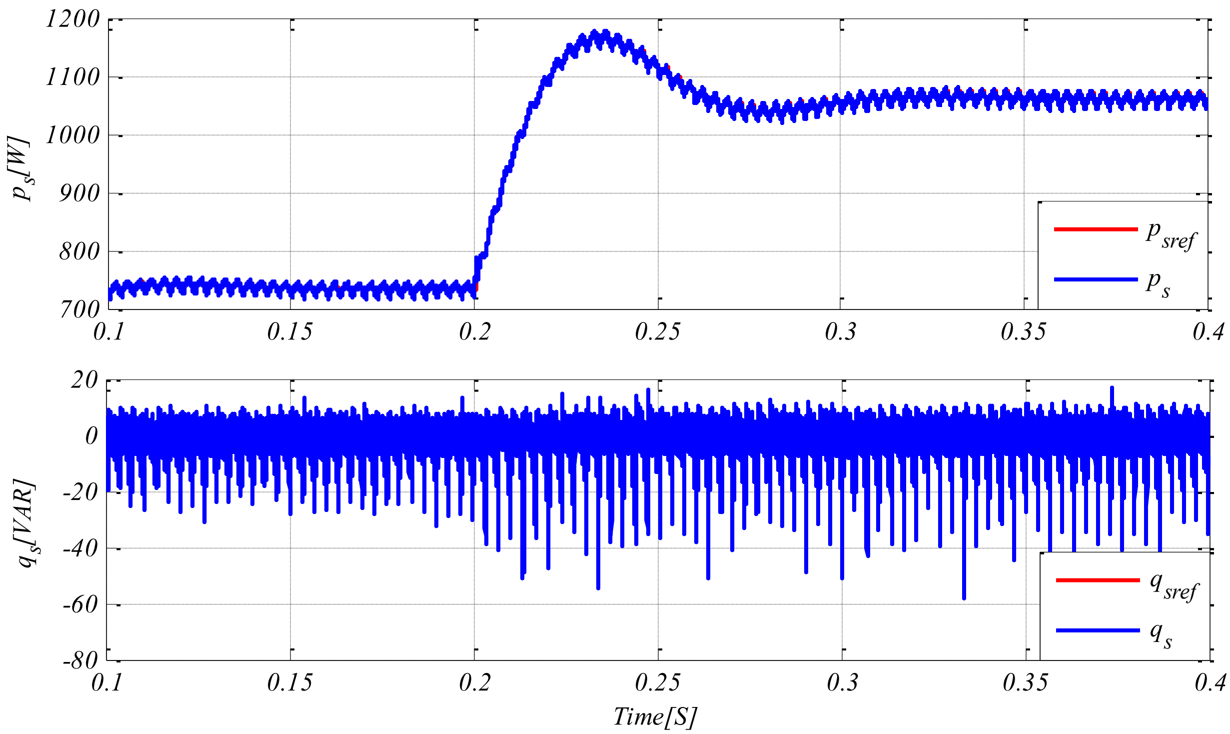

Figure II.19 : Simulation results of source active and reactive power *(p_s , q_s)* with their references *(p_{sref} , q_{sref})*, step increase of the load at *t=0.2s*.

II.5. Experimental results

The obtained results have been validated in experimental test bench developed in laboratory as shown in Figure II.20. The experimental pattern is designed for low voltage rate due to the available equipment found in the laboratory. It consists mainly of the following:

- Three phase power supply based on three-phase autotransformer.
- Two-level inverter is used to perform the compensation; it is made of 6 SEMIKRON IGBTs (SKM 50 GB 123D) joined with a common capacitor.
- Hall-effect current sensors LEM PR30 are used in current measurement signals ensuring isolation between power and control circuits.
- Voltage transducer (HAMEG HZ64) are also used in voltage measurement.
- The proposed algorithms are implemented using dSPACE 1104, where the generated control signals are adapted to 0–15 V range by means of a driver circuit to be suitable with IGBT modules.
- The experimental results are recorded through four-channel Oscilloscope (100 MHz, 2 GSa/s Agilent MSOX2014A).

The detailed system parameters are given in Table A.1 (see Appendix).

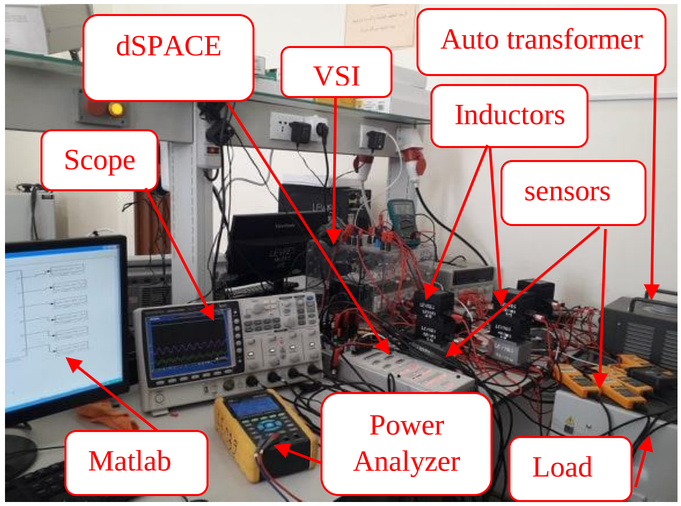

Figure II.20 : Experimental test bench in LEVRES laboratory.

In order to obtain experimental results comparable to those of the simulation, the experimental tests are conducted under the same operating conditions with simulation tests except the sampling time that was set at $Ts=5\mu s$ which is the lowest possible sampling time can be achieved by dSPACE 1104. The obtained results are illustrated in Figures II.(21-26).

Figure II.21 shows good performance of PLL in estimation of source voltage in stationary reference frame (α, β) , phase angle and sectors.

Initially, the SAPF in Figure II.22 is out of service, the DC bus voltage has reached its initial value $v_{dc}=100\ V$, the source current is non-sinusoidal. After, three line cycles, the filter is connected, the DC bus voltage then undergoes a transient then converges towards its reference 160V. the source current become sinusoidal.

Similarly, the active and reactive power are following their references, where the reactive power compensation is well performed.

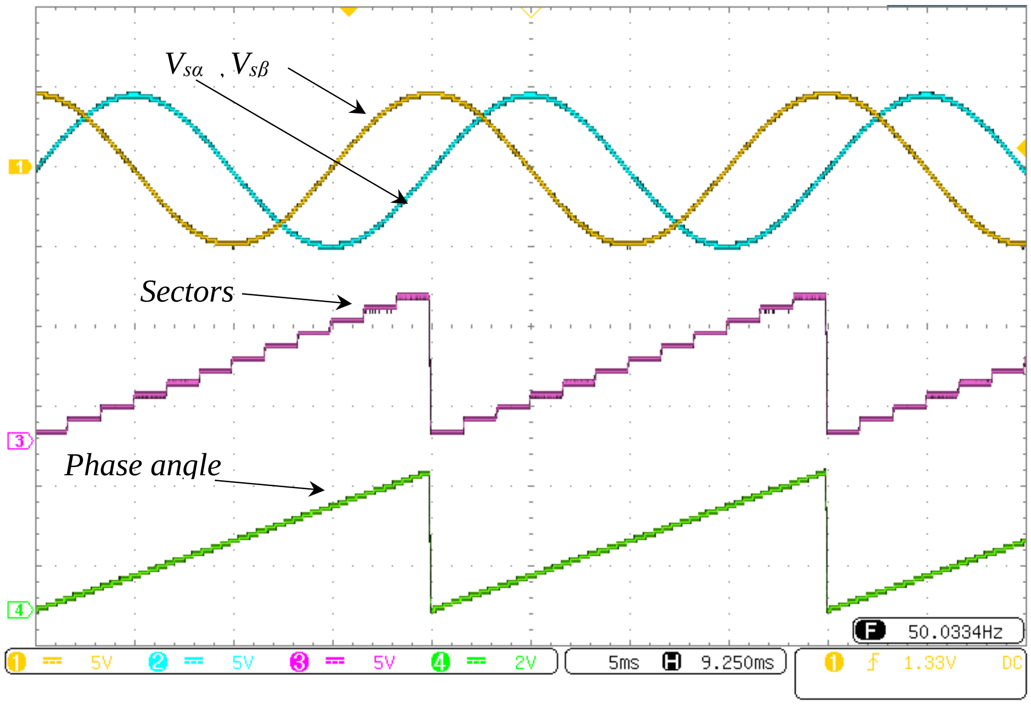

Figure II.21 : Experimental results of source voltage on stationary coordinates (v_α, v_β), sectors and phase angle.

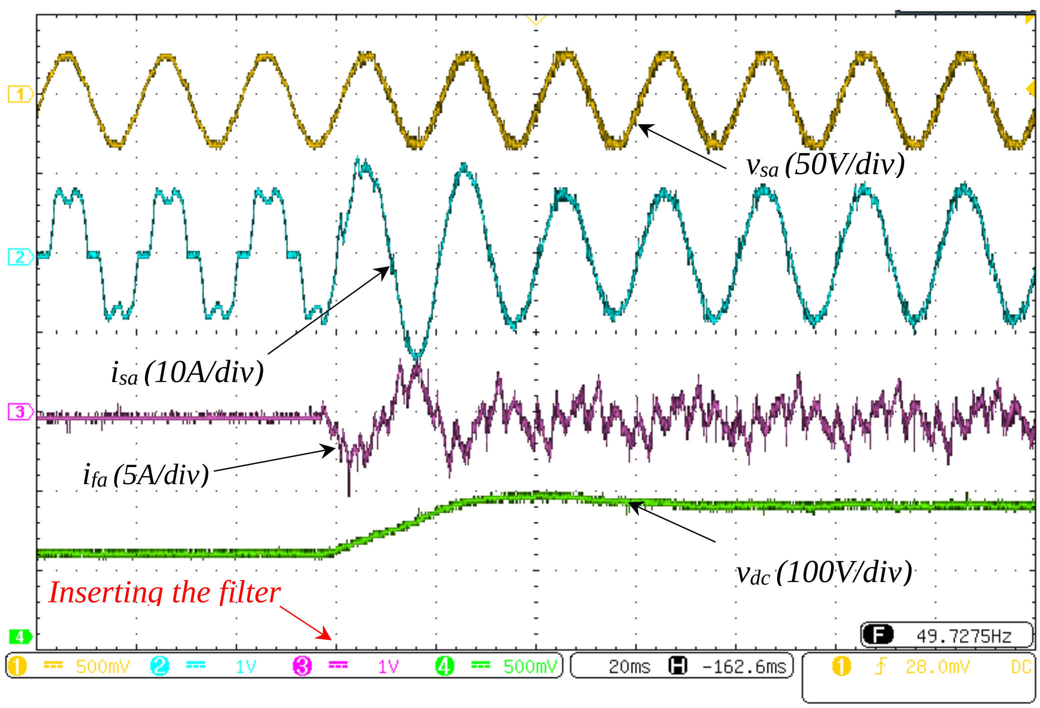

Figure II.22 : Experimental results of source voltage *(v_s)*, source current *(i_s)*, filter current*(i_f)*, DC bus voltage waveforms *(v_{dc})* during the connection of SAPF.

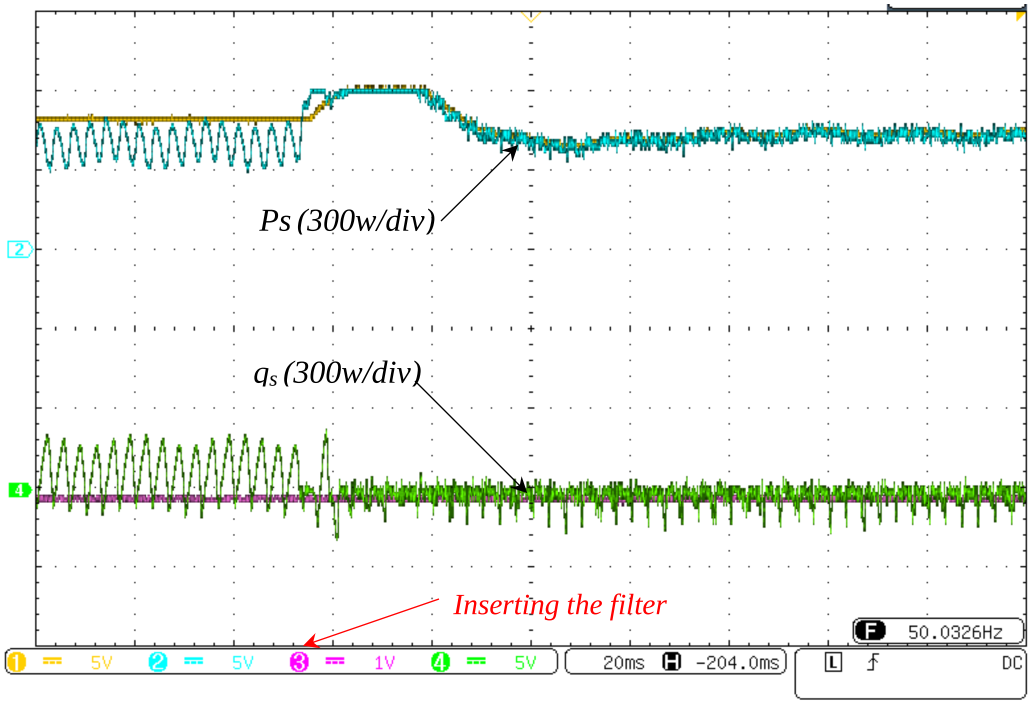

Figure II.23 : Experimental results of source active and reactive power *(p_s , q_s)* with their references *(p_{sref} , q_{sref})* during the connection of SAPF

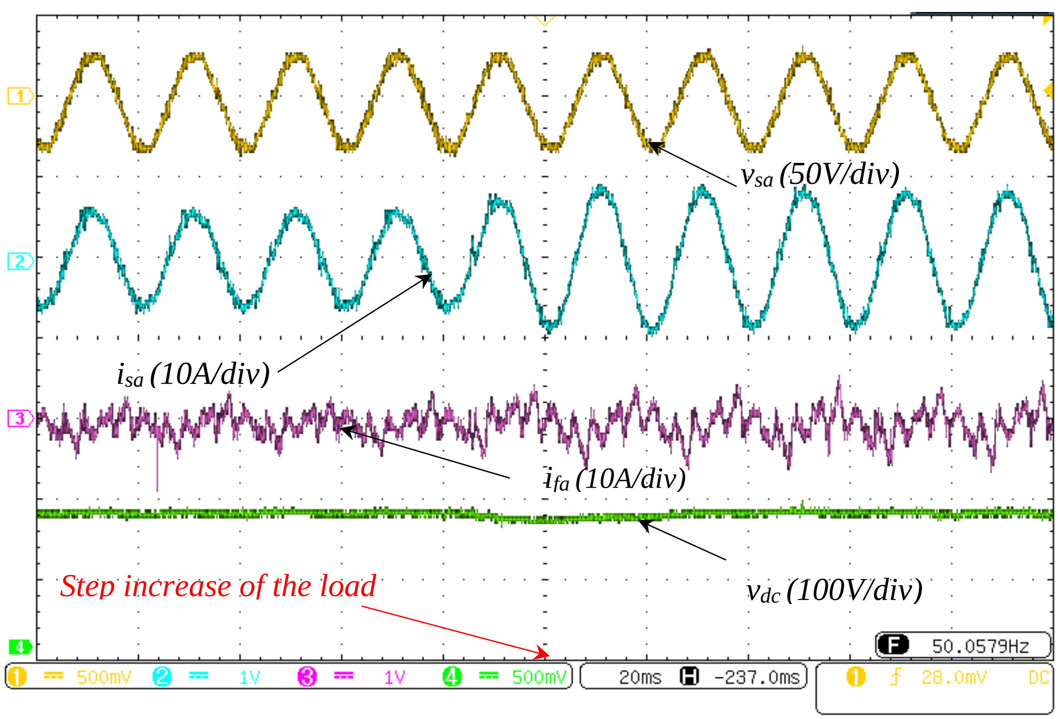

Figure II.24 : Experimental results of source voltage *(v_s)*, source current *(i_s)*, filter current*(i_f)*, DC bus voltage waveforms *(v_{dc})* during step increase of the load.

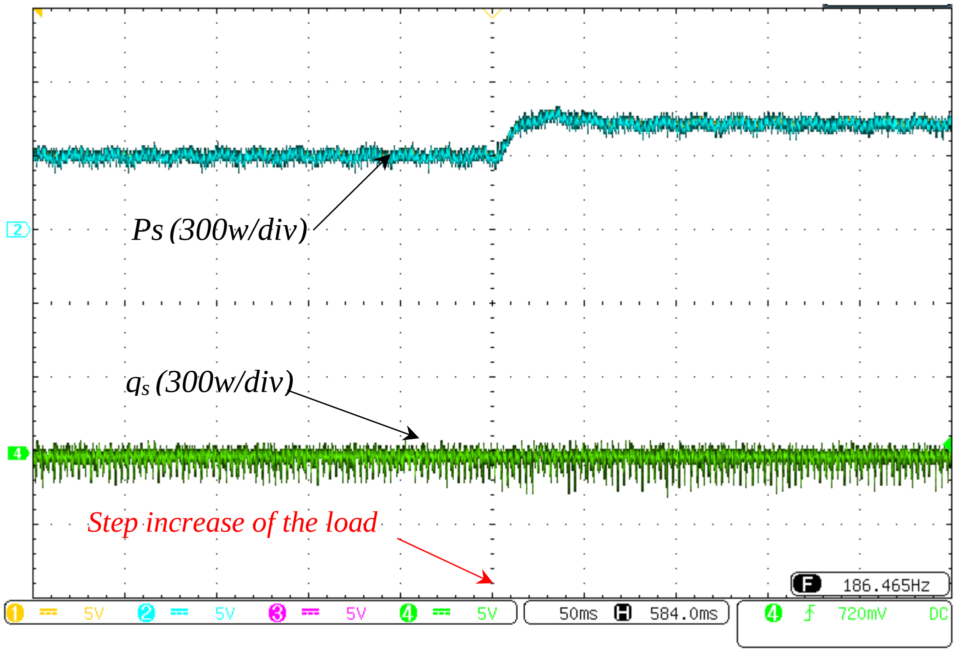

Figure II.25 : Experimental results of source active and reactive power *(p_s , q_s)* with their references *(p_{sref} , q_{sref})* during step increase of the load.

A sudden variation of the load was performed, The experimental results shown in Figures II. (24-25) confirm those of the simulation and prove the good performance of the system even under sudden variation of the load.

(a)

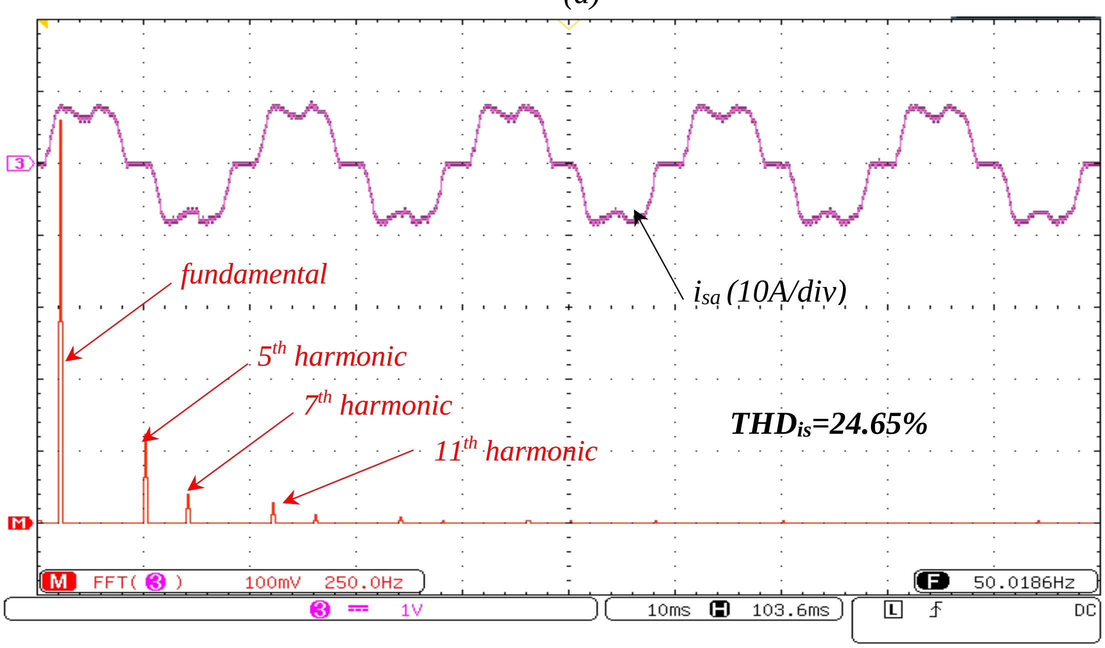

(b)

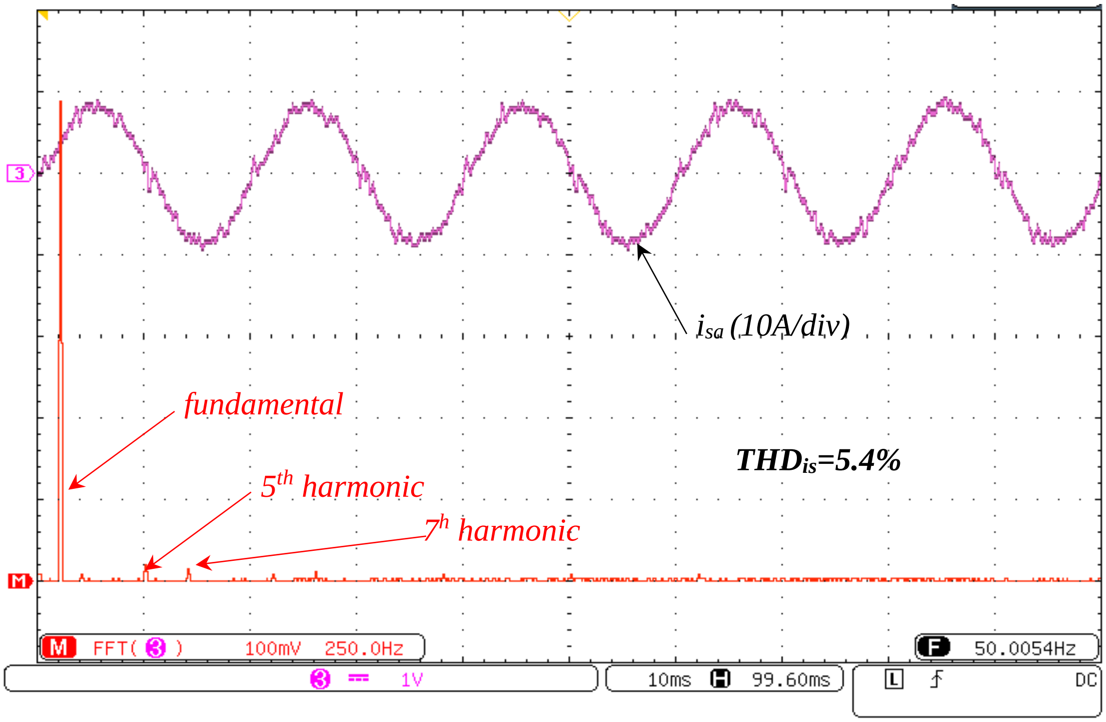

Figure II.26 : Experimental results of FFT analysis of source current before filtering *(a)* after filtering *(b)*

Figure II.26 shows the spectral analysis of the source current before and after the compensation, it is clear that the DPC approach is able to reduce the total harmonic distortion to 5.4%. However, the results can be improved if the control is performed with better performance control board.

II.6. Conclusion

In this chapter, an overview of shunt active power filter has been performed, where its advantages and disadvantages have been clearly presented. Analysis and design considerations of shunt active power filter have been discussed. Furth more, some of widely employed control strategies for shunt active power filter have been shown, including VOC, VOC-SVM, DPC, DPC-SVM, virtual flux and predictive control.

Direct power control strategy has been selected, in this study, due to its simplicity and reliability. Moreover, it provides satisfactory results. However, it suffers with thee variable switching frequency. The last mentioned problem will be treated in the next chapter by introducing a promising control approaches.

Chapter III: Predictive Control based Shunt Active Power Filter

III.1. Introduction

Predictive control of power converters and electrical drives is an essential work on modern methodology that has the potential to advance the performance of future energy processing and control systems[39]. High efficiency, fast operation and high power densities are the main features of modern power electronic converters, which are achieved through the use of high frequency switching devices and high performance control strategy. This leads to different control strategies of power converter

In this chapter, two control strategies based on predictive concept for SAPF are presented, The first predictive strategy is based on selecting the optimum control vector to be applied to the output of VSI. Among the set of possible vectors, the one that minimizes the cost function, is applied during each sampling period. Thus, the switches of the three-phase bridge are controlled with a variable switching frequency.

The second predictive control strategy developed in this thesis is to apply an average control vector to the output of the inverter during a determined period. The average of the control vector is calculated based on a predictive model to minimize the error between the controlled variables and their references. It is developed based on Deadbeat control concept. In this control strategy, the space vector modulation technique is used to convert the calculated average control vector at the beginning of the switching period into a sequence of distributed adjacent control vectors. This leads to a control of the VSI switches with a constant switching frequency.

III.2. Overview of predictive control approach[53–55]

Predictive control is a very wide class of controllers that have found rather recent application in the control of power converters. Research on this topic has been increased in the last years due to the possibilities of today's microprocessors used for the control[53]. The main characteristic of predictive control is the use of the model of the system for the prediction of the future behavior of the controlled variables. This information is used by the controller in order to obtain the optimal actuation, according to a predefined optimization criterion[56]. The proposed classification for different control methods is shown in Figure III.1.

Hysteresis based predictive control tries to keep controlled variables between hysteresis bands. Using predictive current control, switching instants can be determined by error boundaries. When referenced vector touches the controller band then prediction and optimization of next switching state occurs[57] . The principle of trajectory based predictive control is to force the system's variables onto precalculated trajectories as in direct torque control[41].

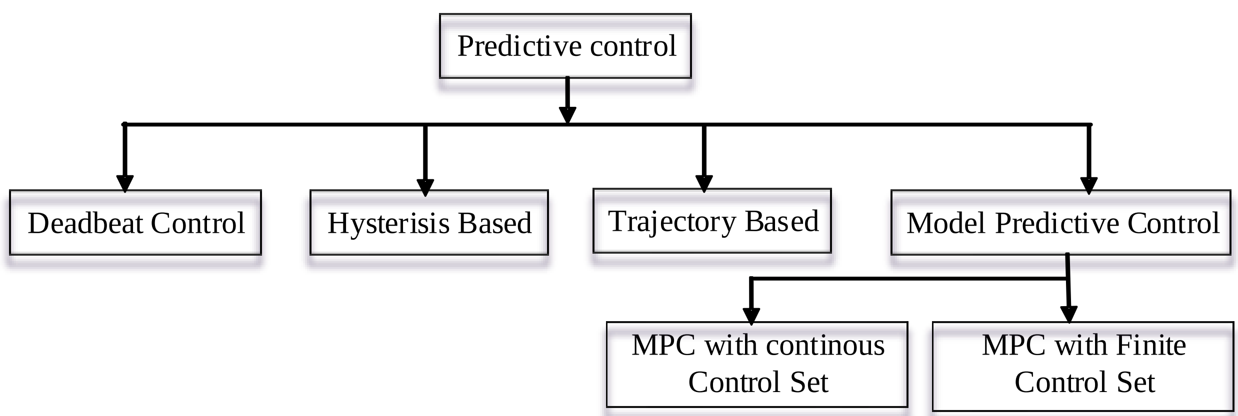

Figure III.1 : Classification of predictive control methods used in power electronics.

Another type of predictive controller is the deadbeat controller. It uses the model of the system to calculate reference voltage vector, in order to set the controlled variable error to zero within one sampling time. Next, the referenced voltage vector is realized by modulator. It has been applied for current control in three phase inverters [58,59] . This method is being used, when a fast dynamic response is required. However, parameters mismatch, unmodeled delays, and other errors in the model deteriorate control performance. Model Predictive Control (MPC) has been successfully used in practical applications in recent decades. Theoretical results and applications have been presented in many books and survey papers[53,60,61]. The MPC can be divided into two main groups: with continuous control sets, where modulator realizes switching states, and finite control set MPC, which directly controls power converter switches.

The finite control-set model predictive control method (FCS-MPC) meets very well discrete nature of power converters. Taking into account the finite set of possible switching states of the power converter, which depends on the possible combinations of the “on” and “off” switching states of the power switches, the optimization problem is reduced to the evaluation of all possible states, and selection of the one which minimizes value of the defined cost function. In view of switching frequency the FCS-MPC methods can be divided into two groups: Variable Switching Frequency (VSF)[62–67] and Constant Switching Frequency (CSF)[55,68–70]. One advantage of predictive control is that its concepts are very simple and intuitive. Using predictive control it is possible to avoid the cascaded structure, which is typically used in a linear control scheme.

III.3. Finite-Control Set Model Predictive Control (FCS-MPC)

III.3.1. Working Principle of FCS-MPC

A general working principle of MPC for a shunt active filter based on three-phase two level inverter is shown in Figure. 1. The model predictive control takes as input measurements from the three-phase source, $i_{sabc}(k)$, $v_{sabc}(k)$ to calculate the actual values of the controlled variables $p_s(k)$ and $q_s(k)$. The discrete time model of SAPF is used to calculate predictions of the controlled variables at the next sampling instant $p_s(k+1)$ and $q_s(k+1)$. The number of samples ahead predictions of the controlled variables can be higher than one in case of long prediction horizon. The predicted values are calculated for the possible switching combinations used in VSI. In three-phase two-level VSI, 8 switching combinations can be done as explained in the previous chapter. The predicted quantities p_s, q_s and their respective reference values p_{sref}, q_{sref} are optimized using a cost-function optimization criterion to generate the optimum switching signal *Sa*, *Sb* and *Sc* for the VSI. This process repeats every sampling period to calculate prediction values and generate the optimum switching signals[71].

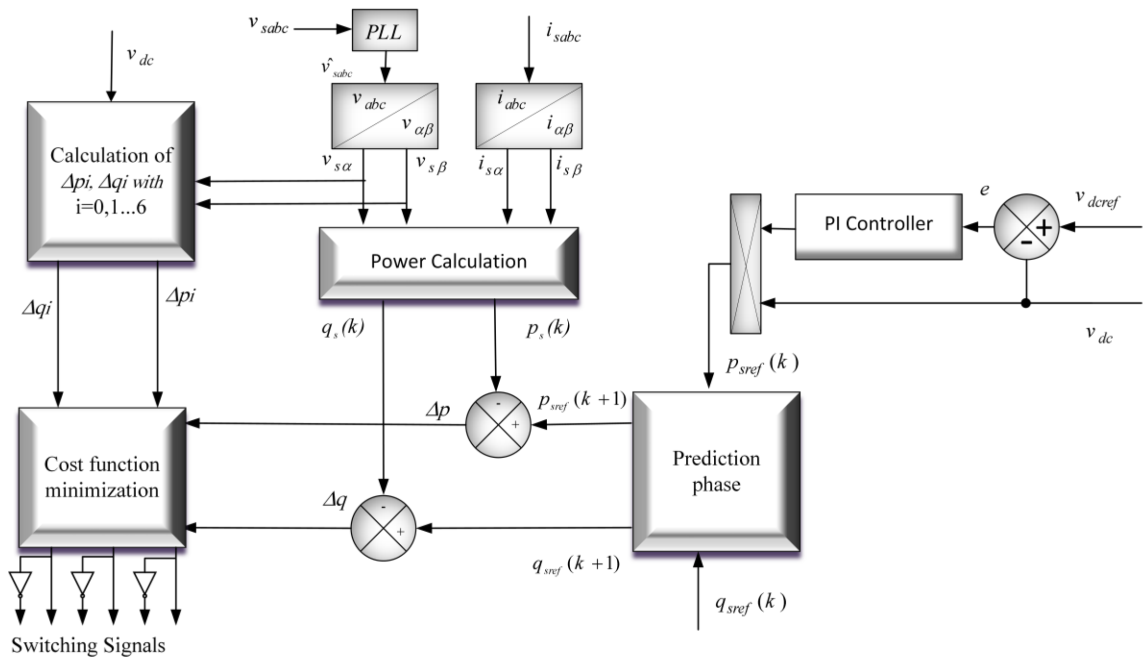

Figure III.2 : Working principle of FCS-MPC.

III.3.1.1. Dynamic model for FCS-MPC

Dynamic model of SAPF enables MPC to predict the sequence of future system states and outputs for a given sequence of controlled variables. The dynamic evolution of SAPF in the continuous-time domain is described in previous chapter in Equation (II.3).

By neglecting the effect of filter resistance, the Equation (II.3) can be written as:

$$L_f \frac{di_{fx}}{dt} = u_{fx} - v_{sx} \quad , x=a,b,c \qquad \text{(III.1)}$$

Where:

$$v_{sx} = v_x - L_s \frac{di_{sx}}{dt} + R_s . i_{sx} \qquad \text{(III.2)}$$

v_s denoted the source voltage at PCC, u_f denoted the voltage at the output of the inverter.

the state-space representation.

The controlled variable in the studied model are the active and reactive powers. Their expressions in a stationary reference frame (α, β) are defined based on Akagi power theory for three-phase balanced system:

$$\begin{bmatrix} p_s \\ q_s \end{bmatrix} = \begin{bmatrix} v_{s\alpha} & v_{s\beta} \\ v_{s\beta} & -v_{s\alpha} \end{bmatrix} \begin{bmatrix} i_{s\alpha} \\ i_{s\beta} \end{bmatrix} \tag{III.3}$$

The variation of instantaneous active and reactive powers can be obtained using the time derivative as follows:

$$\frac{d}{dt}\begin{bmatrix} p_s \\ q_s \end{bmatrix} = \frac{d}{dt}\begin{bmatrix} v_{s\alpha} & v_{s\beta} \\ v_{s\beta} & -v_{s\alpha} \end{bmatrix} \begin{bmatrix} i_{s\alpha} \\ i_{s\beta} \end{bmatrix} + \begin{bmatrix} v_{s\alpha} & v_{s\beta} \\ v_{s\beta} & -v_{s\alpha} \end{bmatrix} \frac{d}{dt}\begin{bmatrix} i_{s\alpha} \\ i_{s\beta} \end{bmatrix} \tag{III.4}$$

If the sampling period T_S, is assumed to be sufficiently small compared to the period of the source voltage (Ts << T), $v_{s\alpha}$ and $v_{s\beta}$ can be considered constant during the sampling period. Based on this assumption, the previous equation can be written as :

$$\frac{d}{dt}\begin{bmatrix} p_s \\ q_s \end{bmatrix} = \begin{bmatrix} v_{s\alpha} & v_{s\beta} \\ v_{s\beta} & -v_{s\alpha} \end{bmatrix} \frac{d}{dt}\begin{bmatrix} i_{s\alpha} \\ i_{s\beta} \end{bmatrix} \tag{III.5}$$

Euler forward discretization method shown in Equation (III.5) can be used to approximate the derivatives for first order systems:

$$\frac{dx}{dt} = \frac{x\,(\mathrm{k}+1) - \mathrm{x}(\mathrm{k})}{dt} \tag{III.6}$$

By applying Euler forward method on Equation (III.4) yield:

$$\begin{bmatrix} p_s(k+1) - p_s(k) \\ q_s(k+1) - q_s(k) \end{bmatrix} = \begin{bmatrix} v_{s\alpha} & v_{s\beta} \\ v_{s\beta} & -v_{s\alpha} \end{bmatrix} \begin{bmatrix} i_{s\alpha}(k+1) - i_{s\alpha}(k) \\ i_{s\beta}(k+1) - i_{s\beta}(k) \end{bmatrix} \tag{III.7}$$

In SAPF, the load consumes non-sinusoidal current that is composed mainly by the source current in addition to the current generated by the filter. Wherever, the fundamental current is ensured by the source and the filter provides the harmonic currents as detailed below.

$$i_{lx} = i_{sx} + i_{fx}\,, \quad x = a,b,c \tag{III.8}$$

$$i_{lx} = i_{\text{fundamental x}} + i_{harmonic\ \text{x}} \tag{III.9}$$

$$i_{fx} - i_{harmonic\ \text{x}} = i_{\text{fundamental x}} - i_{sx} \tag{III.10}$$

Where:

i_l : Current consumed by the load.

i_f : Current generated by the filter.

$i_{fundamental}$: Fundamental component of the current.

$i_{harmonic}$: Harmonic components of the current.

It is noticed that the variation in filter current is equal to that of source current but with opposite sign:

$$i_{fx} - i_{harmonic\ x} = -(i_{sx} - i_{fundamental\ x}) \tag{III.11}$$

Then $\Delta i_{fx} = -\Delta i_{sx}$ (III.12)

For a small variation of source and filter, currents the Equation (III.12) can be written as follows:

$$di_{fx} = -di_{sx} \tag{III.13}$$

The last expression allows obtaining the variation in filter current as well as the voltage at the point of common coupling PCC without the need to measure filter current. Thus, the Equation (III.1) can be written as:

$$L_f \frac{di_{sx}}{dt} = v_{sx} - u_{fx} , \qquad x = a, b, c \tag{III.14}$$

Discretization of the previous equation for a sampling period T_s after transformation in α-β coordinates yields:

$$\begin{bmatrix} i_{s\alpha}(k+1)-i_{s\alpha}(k) \\ i_{s\beta}(k+1)-i_{s\beta}(k) \end{bmatrix} = \frac{T_s}{L_f}\left(\begin{bmatrix} v_{s\alpha}(k) \\ v_{s\beta}(k) \end{bmatrix} - \begin{bmatrix} u_{f\alpha}(k) \\ u_{f\beta}(k) \end{bmatrix}\right) \tag{III.15}$$

By inserting the previous expression into Equation (III.7) , the predictive model of SAPF in discreet-time domain is obtained:

$$\begin{bmatrix} p_s(k+1)-p_s(k) \\ q_s(k+1)-q_s(k) \end{bmatrix} = \frac{T_s}{L_f}\begin{bmatrix} v_{s\alpha}(k) & v_{s\beta}(k) \\ v_{s\beta}(k) & -v_{s\alpha}(k) \end{bmatrix}\left(\begin{bmatrix} v_{s\alpha}(k) \\ v_{s\beta}(k) \end{bmatrix} - \begin{bmatrix} u_{f\alpha}(k) \\ u_{f\beta}(k) \end{bmatrix}\right) \tag{III.16}$$

The predictive values of active and reactive power are given in Equation (III.17).

$$\begin{bmatrix} p_s(k+1) \\ q_s(k+1) \end{bmatrix} = \frac{T_s}{L_f}\begin{bmatrix} v_{s\alpha}(k) & v_{s\beta}(k) \\ v_{s\beta}(k) & -v_{s\alpha}(k) \end{bmatrix}\left(\begin{bmatrix} v_{s\alpha}(k) \\ v_{s\beta}(k) \end{bmatrix} - \begin{bmatrix} u_{f\alpha}(k) \\ u_{f\beta}(k) \end{bmatrix}\right) + \begin{bmatrix} p_s(k) \\ q_s(k) \end{bmatrix} \tag{III.17}$$

It is observed that the sampling period, as well as filter and source inductance, are the main parameters that take an important role in the prediction stage.

The objective of the predictive algorithm consists in tracking the active and reactive power values by making the error between the reference value and the actual value near to zero as much as possible:

$$\begin{cases} p_{sref}(k)-p_s(k) \approx 0 \\ q_{sref}(k)-q_s(k) \approx 0 \end{cases} \tag{III.18}$$

For an optimal convergence towards the desired values of powers, the following equations must be verified.

$$\begin{cases} \Delta p = P_{sref}(k+1)-p_s(k) \\ \Delta p = q_{sref}(k+1)-q_s(k) \end{cases} \tag{III.19}$$

Moreover, only seven possible variations can be made on the active and reactive powers, by applying each of the seven control vectors during a sampling period. These variations, named *$\Delta P_i(k)$* and *$\Delta q_i(k)$*, are expressed based on the Equation (III.17) as follows:

$$\begin{bmatrix} \Delta p_i \\ \Delta q_i \end{bmatrix} = \frac{T_s}{L_f}\begin{bmatrix} v_{s\alpha}(k) & v_{s\beta}(k) \\ v_{s\beta}(k) & -v_{s\alpha}(k) \end{bmatrix}\left(\begin{bmatrix} v_{s\alpha}(k) \\ v_{s\beta}(k) \end{bmatrix} - \begin{bmatrix} u_{f\alpha i}(k) \\ u_{f\beta i}(k) \end{bmatrix}\right), \quad i=0,1,2\ldots.6 \tag{III.20}$$

By considering that the reference value of active power is varied linearly between two successive sampling period, as described in Figure III.3. This consideration takes the assumption that the variation of the error of the voltage regulation loop during two successive sampling periods is null.

Whereas, the reference value of reactive power is often imposed constant with zero value in order to ensure an operation with unity power factor. As a result, the reference values of active and reactive power for the next sampling period can be estimated by the following:

$$\begin{bmatrix} p_{sref}(k+1) \\ q_{sref}(k+1) \end{bmatrix} = \begin{bmatrix} 2p_{sref}(k) - p_{sref}(k-1) \\ q_{sref}(k) \end{bmatrix} \quad \text{(III.21)}$$

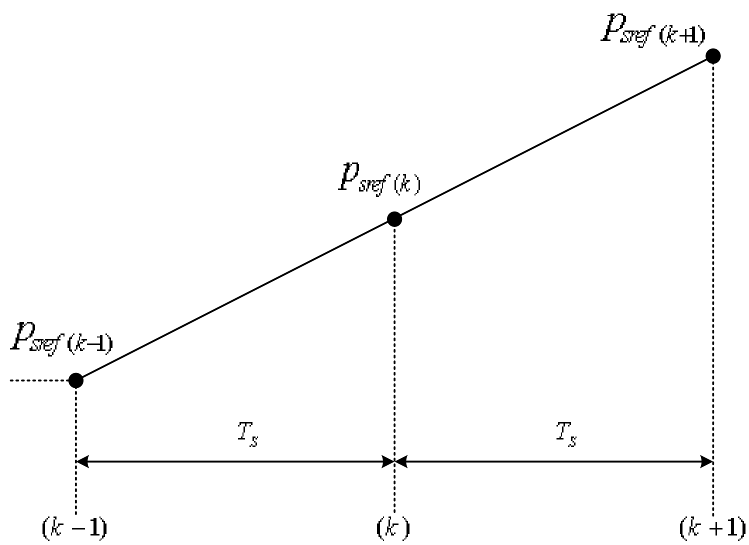

Figure III.3 : Predictive value estimation of reference active power

III.3.1.2. Cost function

MPC method is based on the evaluation of the cost function for a number of switching states according to the used converter.

The adopted cost function aims to minimize the active and reactive power tracking errors, which is defined as:

$$C_f = \lambda_p(\Delta p - \Delta p_i)^2 + \lambda_q(\Delta q - \Delta q_i)^2 \quad i=0,1,2\ldots.6 \quad \text{(III.22)}$$

Typically, the two weighting factor λ_q , λ_p are set to 1. However, the weighting can be adjusted to achieve better control performance. In addition, it is better to use dynamic weighting factors to handle the nonlinearity of the power converter and achieve high performance.

Among all the possible VSI control vectors, the one that minimizes the defined cost function C_f is applied during the next sampling period.

III.3.2. Advantages and Challenges of FCS-MPC[39,72]

MPC has several important advantages such as:

- Concepts are very intuitive and easy to understand.
- Compared to conventional control strategies, model predictive control presents a fast response and an easier implementation.
- It can be applied to a great variety of systems.
- MPC is a multivariable control method that is ideally suited for MIMO systems.
- Easy inclusion of nonlinearities in the model.

However, some disadvantages have to be highlighted:

- Larger number of calculations, compared to conventional controllers
- The quality of the model has a direct influence on the quality of the resulting controller, and if the parameters of the system change in time, some adaptation or estimation algorithm has to be considered.
- The same converter states can be applied for more sampling intervals, resulting in a
- Variable converter switching frequency.
- There is no limitation on the number of switching devices that can be used resulting in increased switching loss in case of high switching frequency.

III.3.3. Simulation results

The simulation of the global system is performed under the Matlab\Simulink environment. The simulation parameters are similar to those used in the previous tests, which are illustrated in Table A.1 (see Appendix). The studied system FCS-MPC based SAPF is investigated under different operating conditions.

Firstly, simulation is carried out with a three-phase balanced source voltage. The SAPF is operated at *(t=0.16s)*. The simulation results are presented in Figure III.4 and Figure III.5. before connecting the filter, the source current and load current have identical distorted waveforms, DC bus voltage is equal to the peak of the input phase-to-phase voltage *(100V)*. After inserting SAPF, the filter start injecting the needed current for source current compensation, the source current becomes sinusoidal after transient period of *(Δt=0.1s)*, and capacitor voltage tends towards its reference and reaches steady state within 4 cycles.

In order to assess the quality of the source current, FFT analysis has been performed. The measurements obtained are shown in Figure III.6. These measurements show that the current absorbed are strongly distorted *(THDis = 24.24%)*. However, lower Total Harmonic Distortion is achieved after connecting the filter *(THDis = 0.90%)*. It is worthy to mention that FCS-MPC provides better harmonic compensation as compared to DPC strategy.

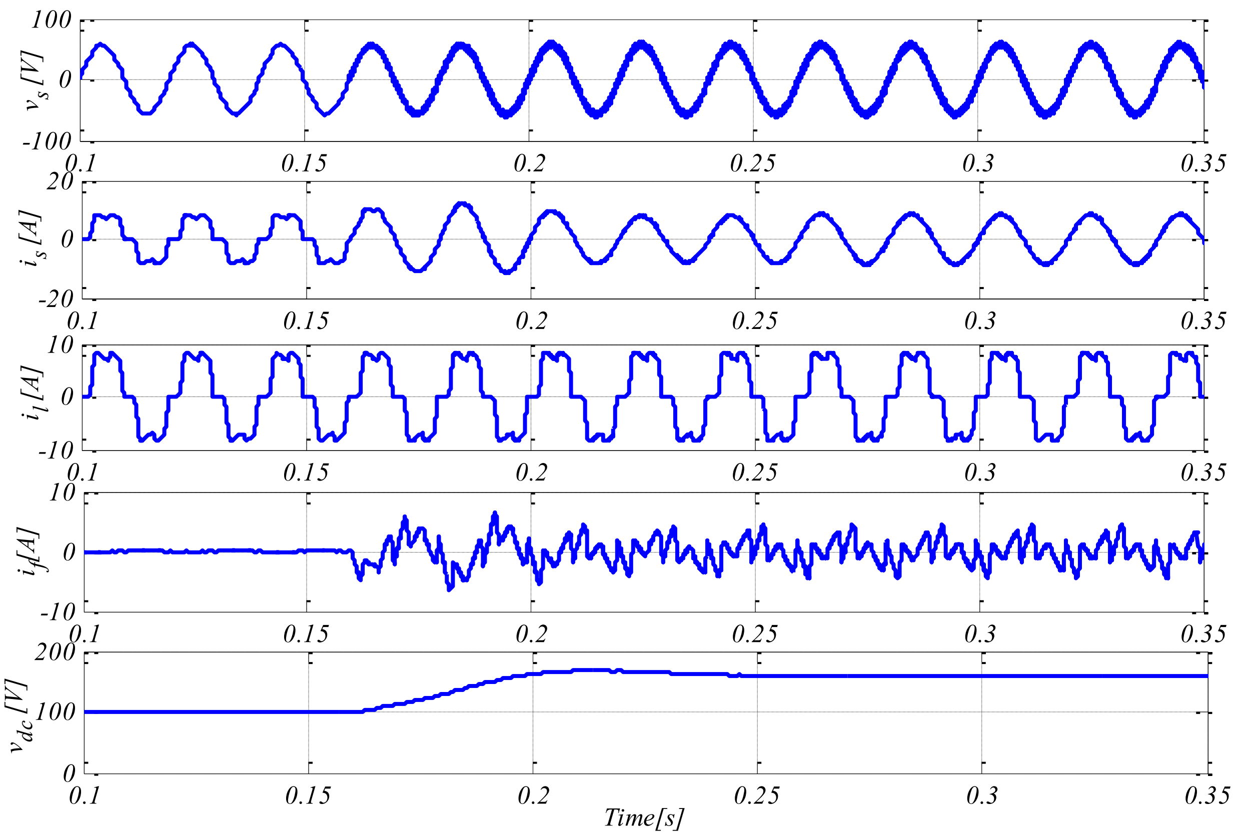

Figure III.4 : Simulation results of source voltage *(v_s)*, source current *(i_s)*,load current*(i_l)*, filter current*(i_f)*, DC bus voltage waveforms *(v_{dc})*, SAPF is operated at *t=0.16s*

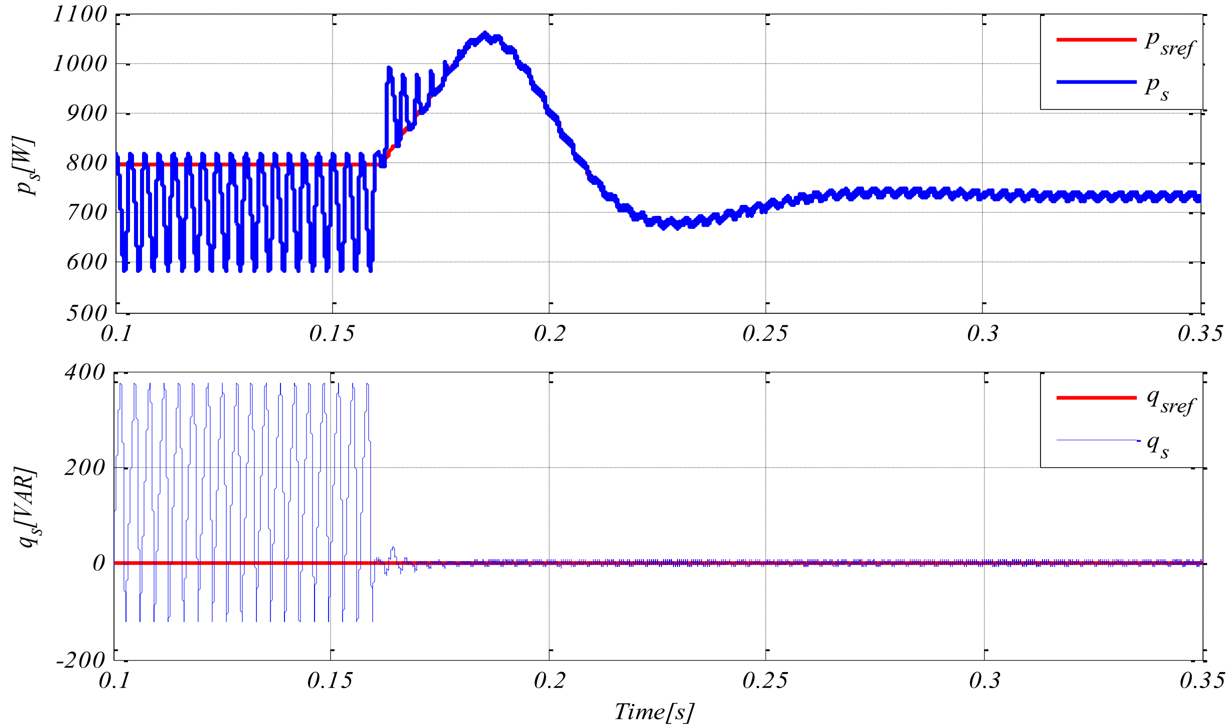

Figure III.5 : Simulation results of source active and reactive power *(p_s , q_s)* with their references *(p_{sref} , q_{sref})*, SAPF is operated at *t=0.16s.*

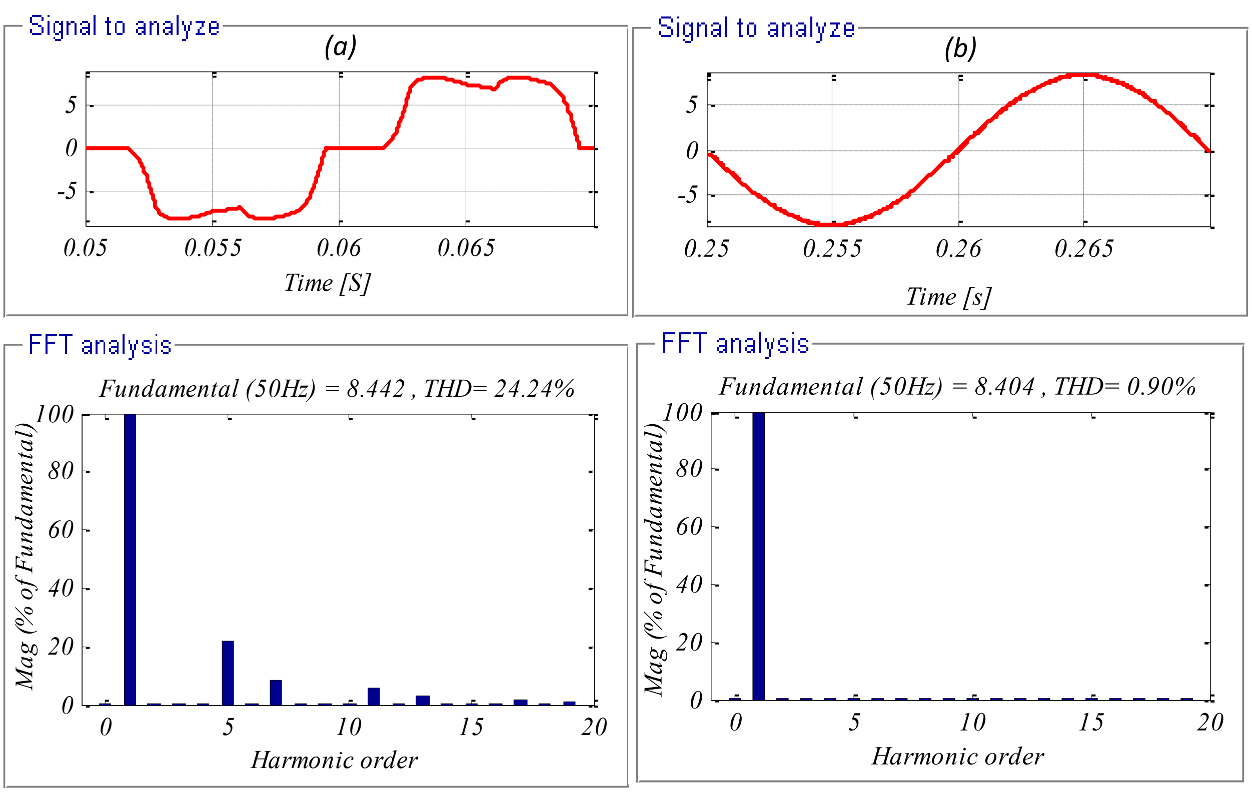

Figure III.6 : Simulation results of FFT analysis of source current before filtering *(a)* and after filtering *(b).*

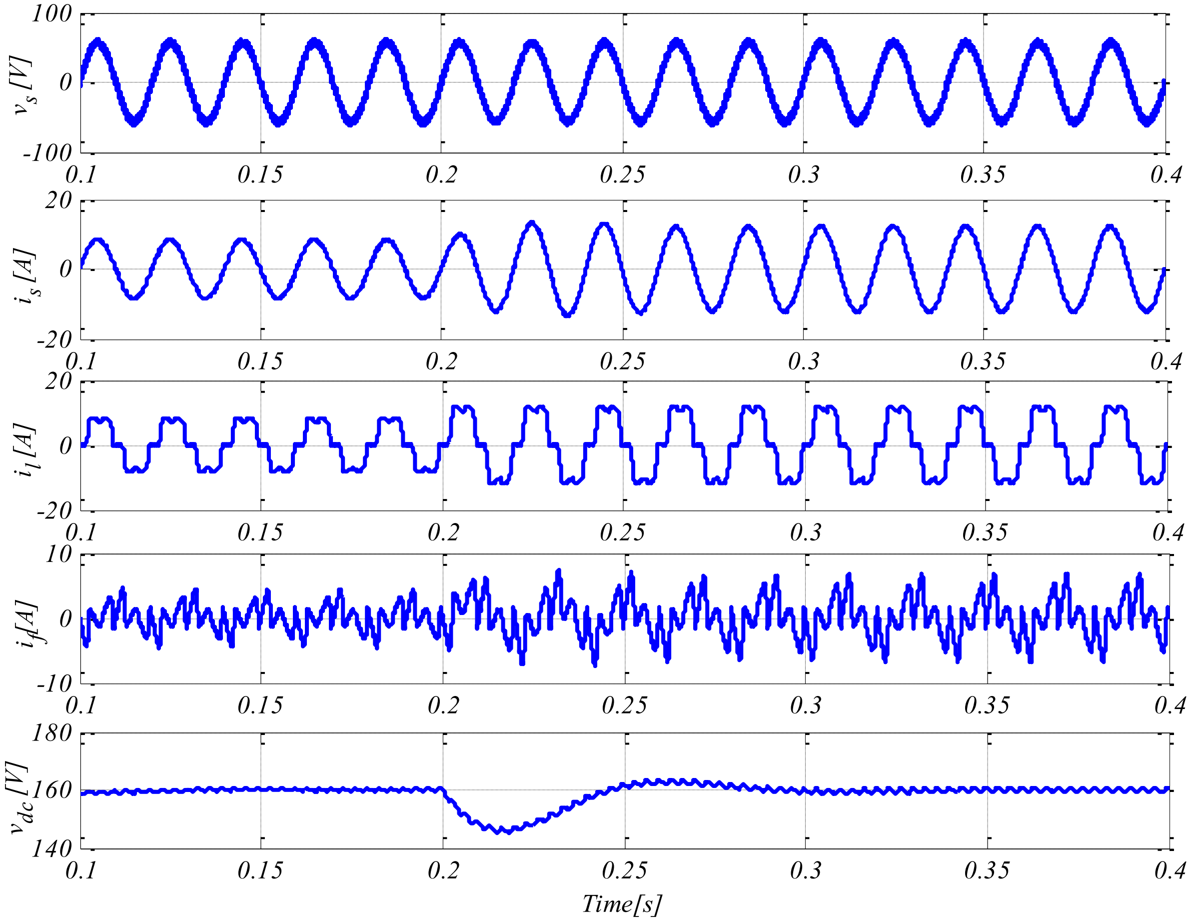

Figure III.7 : Simulation results of source voltage *(v_s)*, source current *(i_s)*,load current*(i_l)*, filter current*(i_f)*, DC bus voltage waveforms *(v_{dc})*, step increase of the load at *t=0.2s.*

Step increase of the load at the output of the rectifier has been performed in this stage to evaluate the robustness of the control strategy. The resistance value of the load is decreased from *22.66* Ω to *11.33* Ω (step variation of 50%). Figure III.7 and III.8 show that the various waveforms during load variation.

It is noticed in Figure III.7, when the load current is increased, capacitor voltage decreases for a period of *(Δt=0.1s)* then returns to its reference value. The source current is increased and maintains its sinusoidal waveform. No effect is noticed on the source voltage.

The reactive power is increased once the load is changed with good tracking performance and lower power ripple as compared to that obtained in DPC, whereas, good reactive power compensation is performed even after increasing the load current.

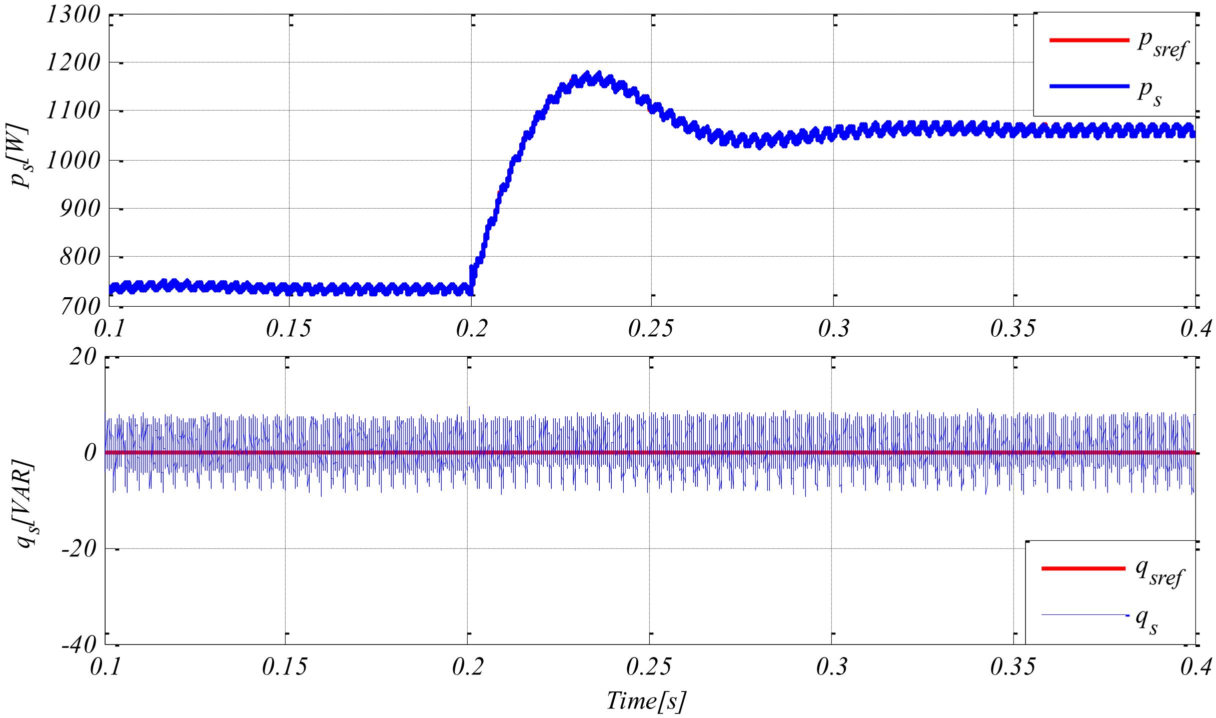

Figure III.8 : Simulation results of source active and reactive power (p_s , q_s) with their references (p_{sref} , q_{sref}), step increase of the load at $t=0.2s$

III.3.4. Experimental results

To evaluate the performance of FCS-MPC based SAPF, the overall system is validated in experimental setup shown in Figure II.22. The experimental tests have been conducted with the same parameters used in simulation, expect the sampling time that is set to *t=5e-5s* instead of *t=5e-6s* as in simulation tests due to limitation of the control board. The same tests performed in simulation have been validated experimentally under operating condition quite similar. Hence, the experimental results are similar and corroborate the simulation results presented previously. The same interpretation of the waveforms can be given.

However, spectral analysis of the source current in experimental measurement shows significant difference with the simulated one. The justification of this difference may refer to different parameters are not considered in simulation such as the dead time in addition to the sampling period difference. Spectral analysis shows that the source current total harmonic distortion is reduced to *2.9%* after the compensation, which make the source current in compliance with IEEE-519 standards.

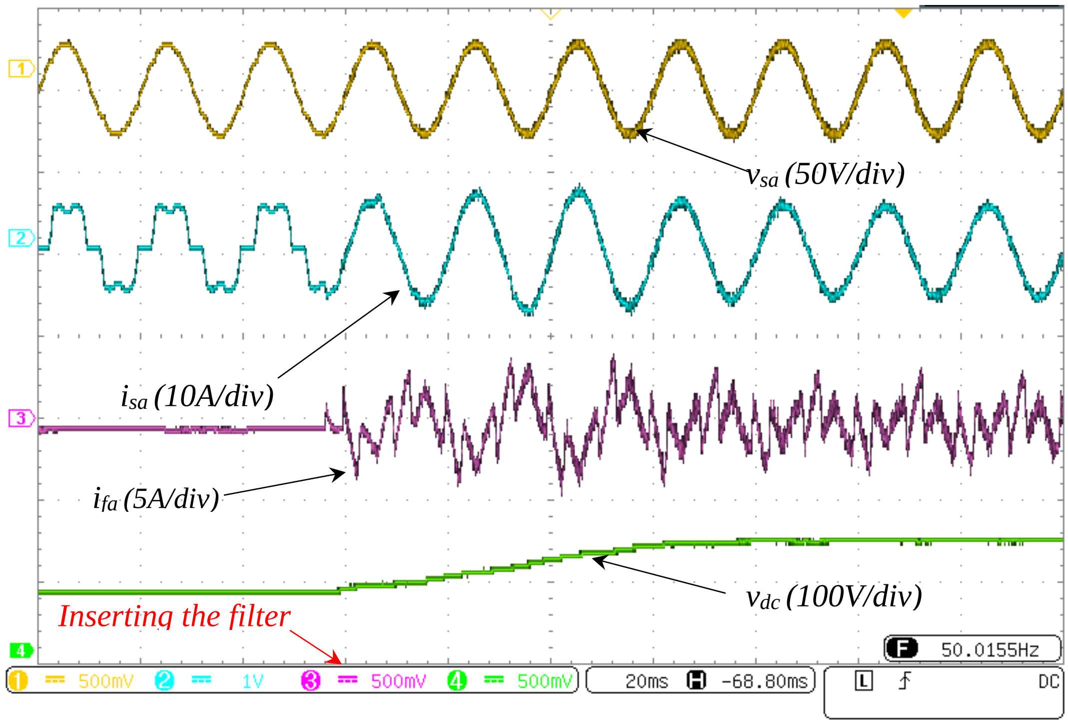

Figure III.9 : Experimental results of source voltage *(v_s)*, source current *(i_s)*, filter current*(i_f)*, DC bus voltage waveforms *(v_{dc})* during the connection of SAPF.

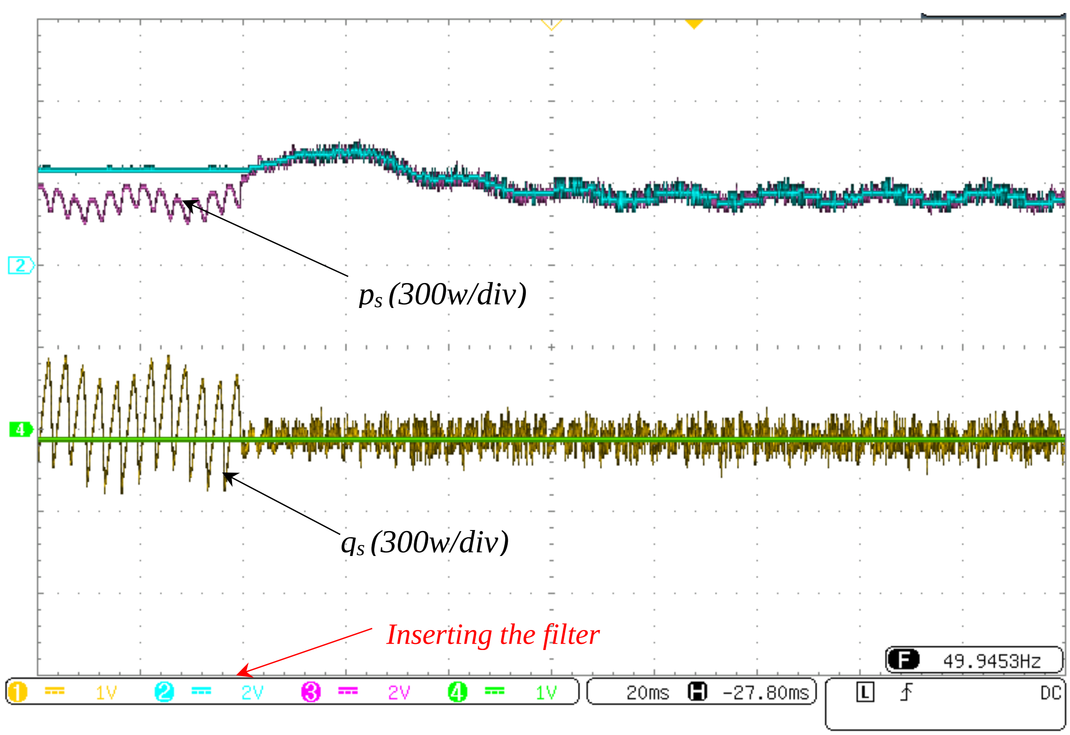

Figure III.10 : Experimental results of source active and reactive power *(p_s , q_s)* with their references *(p_{sref} , q_{sref})* during the connection of SAPF.

(a)

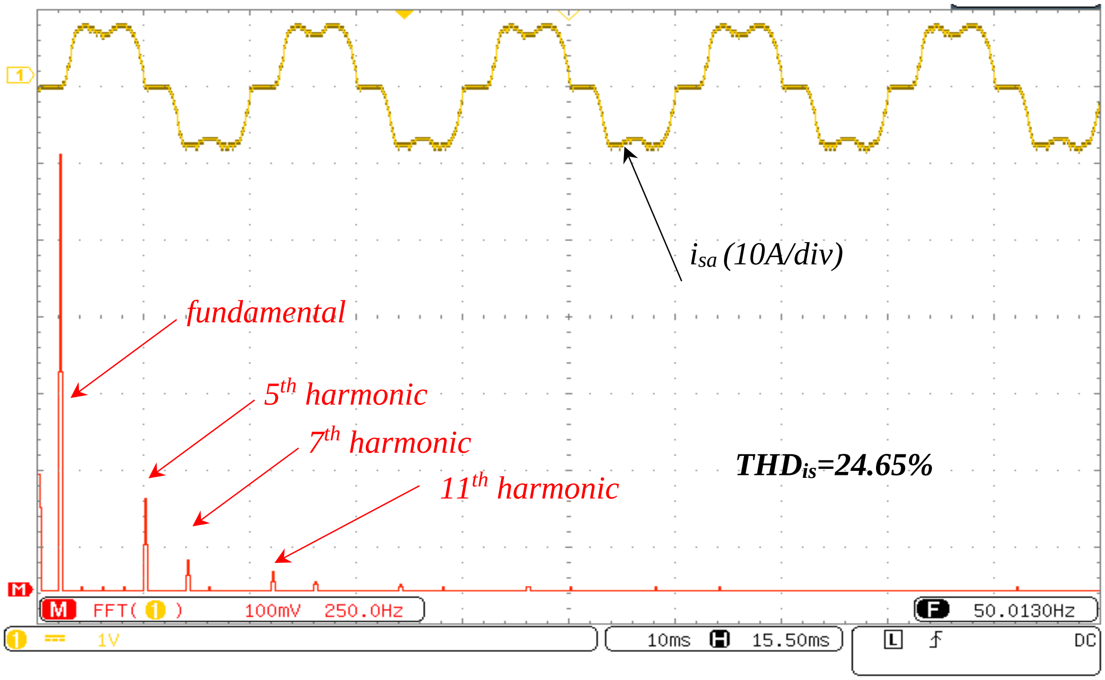

(b)

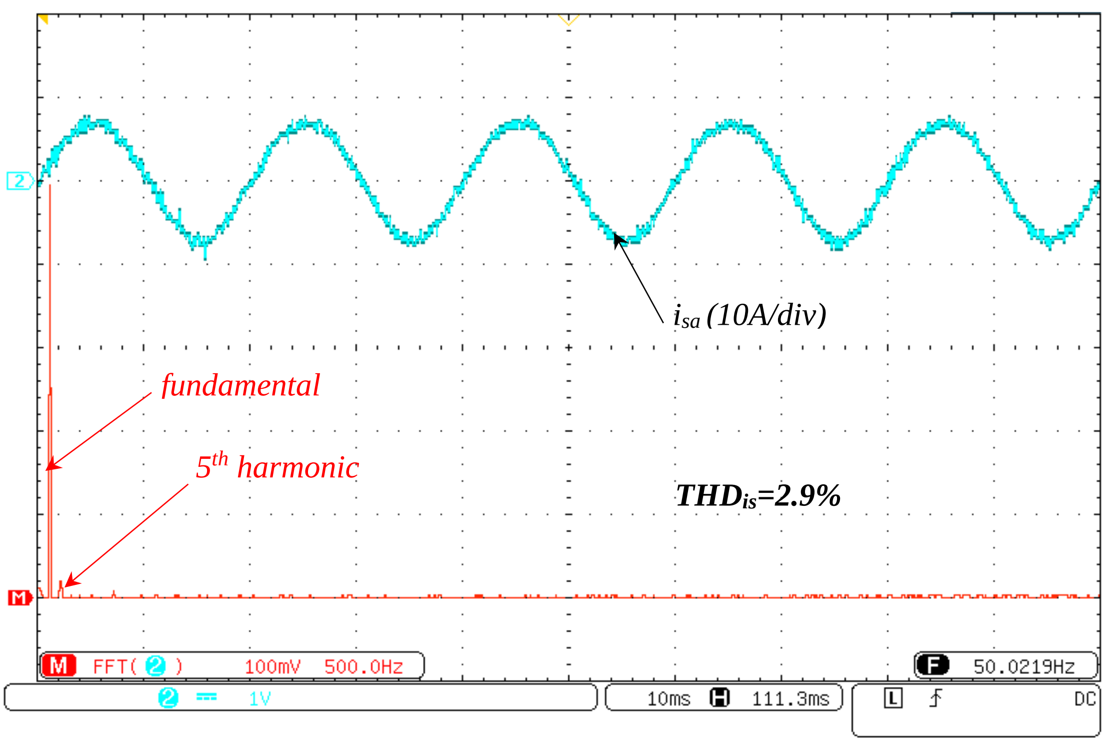

Figure III.11 : Experimental results of FFT analysis of source current before filtering *(a)* and after filtering *(b).*

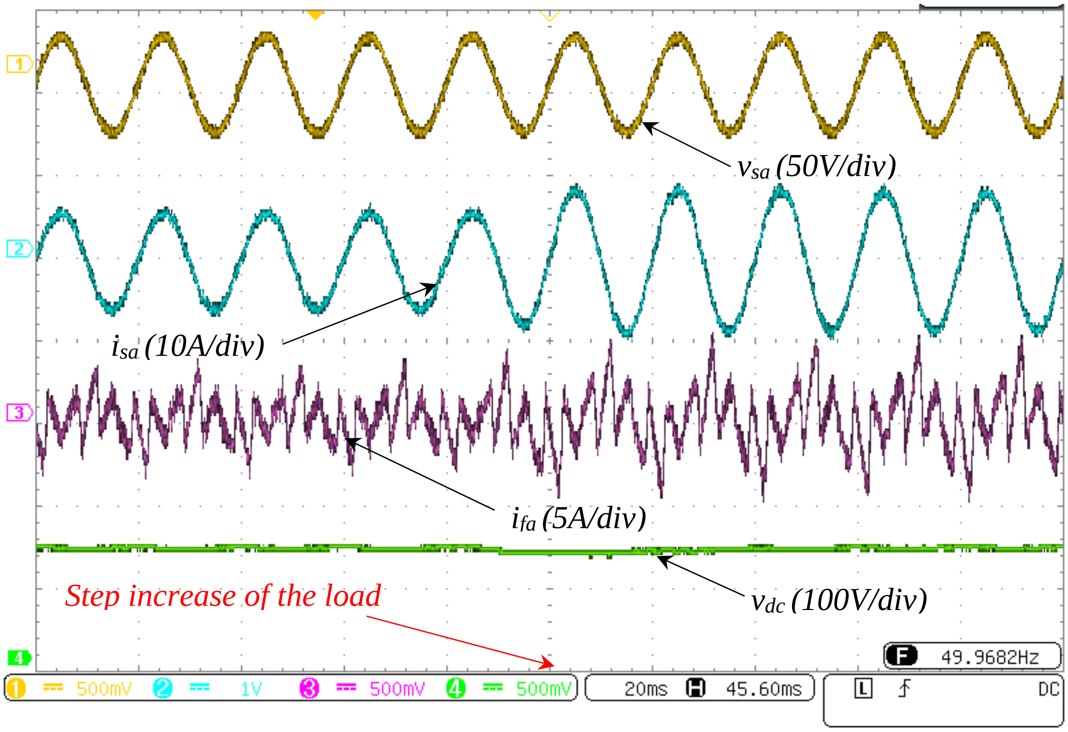

Figure III.12 : Experimental results of source voltage *(v_s)*, source current *(i_s)*, filter current*(i_f)*, DC bus voltage waveforms *(v_{dc})* during step increase of the load.

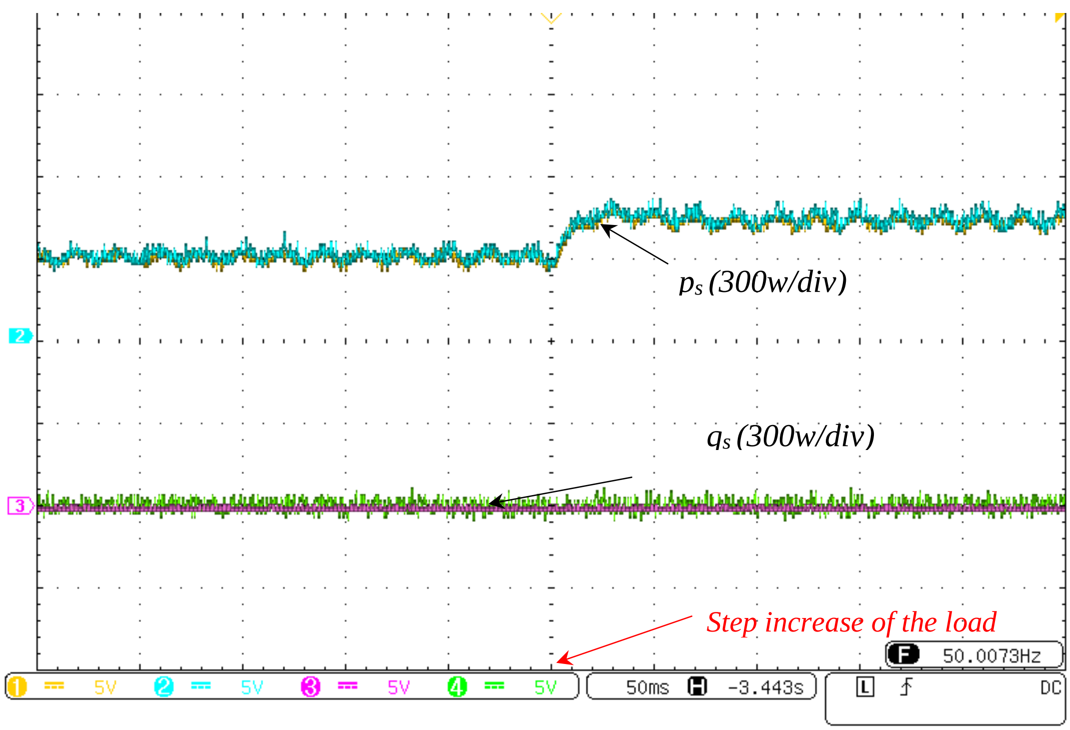

Figure III.13 : Experimental results of source active and reactive power *(p_s , q_s)* with their references *(p_{sref} , q_{sref})* during step increase of SAPF.

III.4. PDPC-SVM (Deadbeat control)

III.4.1. Working principle of Predictive DPC-SVM

Following the principle of MPC, The proposed predictive DPC-SVM technique requires a predictive model in discrete-time domain to select the best voltage vectors. This approach operates with constant switching frequency using space-vector modulation (SVM). For this purpose, a predictive control algorithm based on deadbeat control approach, was developed to compute the required average voltage control vector in *(α–β)* reference frame, to be applied during each sampling period *Ts*, in order to minimize the active and reactive power errors at the next sampling period and provide good tracking performance. The average voltage vector is converted into a sequence of switching states (adjacent voltage vectors) by means of SVM technique. The general working principle of P-DPC-SVM approach is illustrated in Figure.III.14.

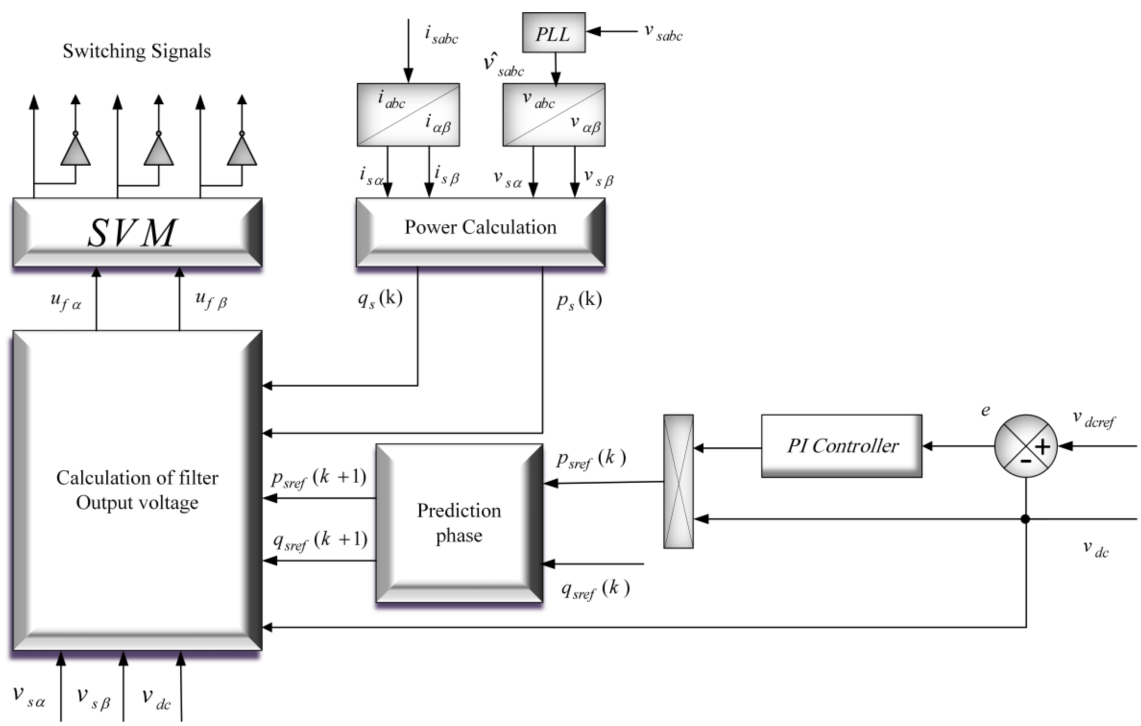

Figure III.14 : Working principle of Predictive DPC-SVM.

III.4.1.1. Dynamic model for Predictive DPC-SVM

For an optimal convergence towards the desired power values, the following equation must be verified.

$$\begin{cases} p_s(k+1) - P_{sref}(k+1) = 0 \\ q_s(k+1) - q_{sref}(k+1) = 0 \end{cases} \tag{III.23}$$

Then

$$\begin{cases} p_s(k+1) = p_{sref}(k+1) \\ q_s(k+1) = q_{sref}(k+1) \end{cases} \tag{III.24}$$

Substituting (III.24) into (III.16) yields:

$$\begin{bmatrix} p_{sref}(k+1) - p_s(k) \\ q_{sref}(k+1) - q_s(k) \end{bmatrix} = \frac{T_s}{L_f} \begin{bmatrix} v_{s\alpha}(k) & v_{s\beta}(k) \\ v_{s\beta}(k) & -v_{s\alpha}(k) \end{bmatrix} \left(\begin{bmatrix} v_{s\alpha}(k) \\ v_{s\beta}(k) \end{bmatrix} - \begin{bmatrix} u_{f\alpha}(k) \\ u_{f\beta}(k) \end{bmatrix} \right) \tag{III.25}$$

By using the equations (III.21) and (III.25) The average control vector to be applied during the next sampling period [kT_s $(k+1)T_s$] is obtained by the following equation:

$$\begin{bmatrix} u_{f\alpha}(k) \\ u_{f\beta}(k) \end{bmatrix} = \begin{bmatrix} v_{s\alpha}(k) \\ v_{s\beta}(k) \end{bmatrix} - \frac{L_f}{T_s(v_{s\alpha}^2 + v_{s\beta}^2)} \begin{bmatrix} v_{s\alpha}(k) & v_{s\beta}(k) \\ v_{s\beta}(k) & -v_{s\alpha}(k) \end{bmatrix} \begin{bmatrix} 2p_{sref}(k) - p_{sref}(k-1) - p_s(k) \\ q_{sref}(k) - q_s(k) \end{bmatrix} \tag{III.26}$$

III.4.1.2. Space Vector Modulation[73]

SVM is one of the preferred modulation techniques and is widely used for control of power converters. As explained earlier in section II.2.2.3, the operation of two-level VSI. There are eight possible combinations of switching states in the two-level inverter as listed in Table II.1. A typical space vector diagram for the two-level inverter is shown in Figure. III.15, where the six active vectors $\vec{V}_1$ to $\vec{V}_6$ form a regular hexagon with six equal sectors. The zero vector $\vec{V}_0$ lies on the center of the hexagon.

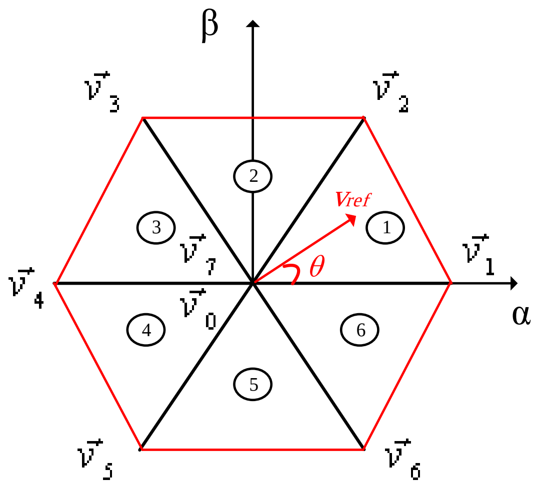

Figure III.15 : Space vector diagram for the two-level inverter.

For a given magnitude (length) and position, $\vec{V}_{ref}$ can be synthesized by three nearby stationary vectors, based on which the switching states of the inverter can be selected and gate signals for the active switches can be generated.

Assuming that a sampling period T_h is sufficiently small, the reference vector $\vec{V}_{ref}$ can be considered constant during T_h. Under this assumption, $\vec{V}_{ref}$ can be approximate by two adjacent active vectors and one zero vector as follows:

$$\vec{V}_{ref} T_h = \vec{V}_i T_i + \vec{V}_{i+1} T_{i+1} + \vec{V}_0 T_0 \tag{III.27}$$

For example, when $\vec{V}_{ref}$ falls into sector 1 as shown in Figure III.16, it can be synthesized by $\vec{V}_1$, $\vec{V}_6$, and $\vec{V}_0$ as follows:

$$\vec{V}_{ref} T_h = \vec{V}_1 T_1 + \vec{V}_2 T_2 + \vec{V}_0 T_0 \tag{III.28}$$

Where T_1, T_2, and T_0 are the dwell times for the vectors $\vec{V}_1$, $\vec{V}_2$, and $\vec{V}_0$, respectively.

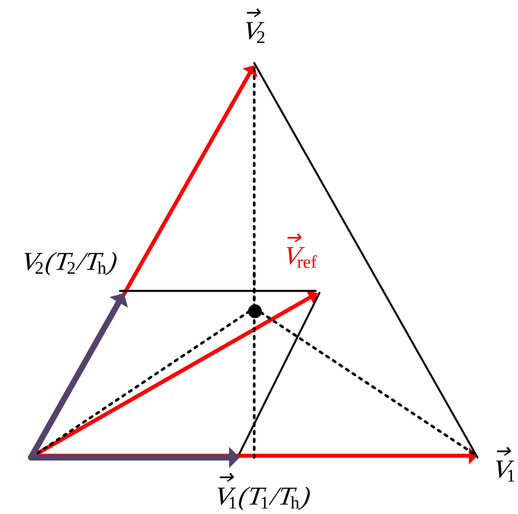

Figure III.16 : $\vec{V}_{ref}$ synthesized by $\vec{V}_1$, $\vec{V}_2$, and $\vec{V}_0$.

The determination of times T_1 , T_2 and T_0 corresponding to voltage vectors are obtained by

$$\begin{cases} T_1 = \dfrac{\sqrt{6}v_{s\alpha} - \sqrt{2}v_{s\beta}}{2v_{dc}} \\ T_2 = \dfrac{\sqrt{2}v_{s\beta}}{v_{dc}} T_h \\ T_0 = T_h - T_1 - T_2 \end{cases} \quad \text{(III.29)}$$

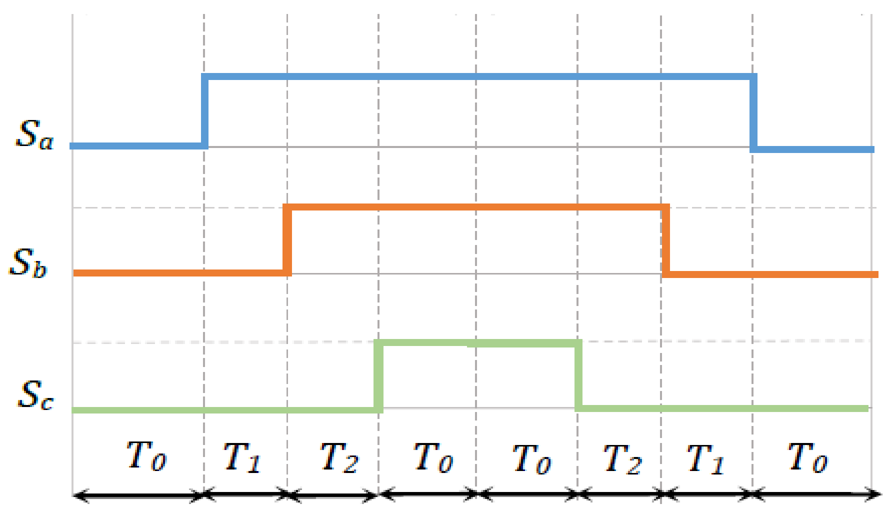

Figure III.17 : Switching times of sector 1.

III.4.2. Simulation results

The utilized simulation parameters are similar to those used in the previous tests, which are illustrated in Table A.1 (see Appendix). The studied system P-DPC-SVM based SAPF are investigated under different operating conditions.

Figure III.18 and Figure III.19 sows the simulation results during the operation of SAPF. Initially, the system operates without SAPF, the source currents are identical to that of the nonlinear load characterized by a distorted waveform containing only odd and not multiple of three order harmonics, no current is injected from the filter and the DC bus capacitor is charged to the peak of the input phase-to-phase voltage *(100V)*. Once the SAPF start operating at *t=0.16s,* the filter starts producing the necessary current *(i_f)* that make the source current sinusoidal and in phase with the source voltage after a transient period of *(Δt=0.02s)*.

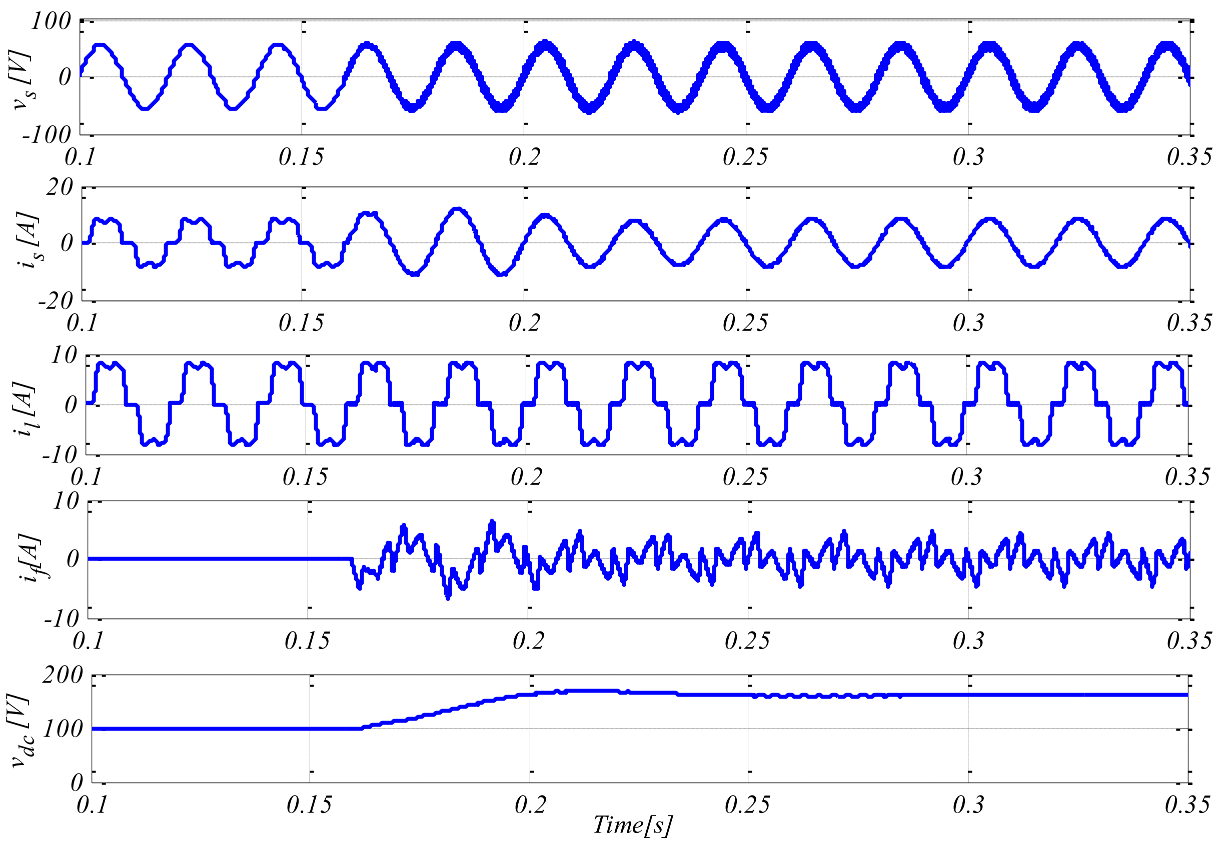

Figure III.18 : Simulation results of source voltage *(v_s)*, source current *(i_s)*,load current*(i_l)*, filter current*(i_f)*, DC bus voltage waveforms *(v_{dc})*, SAPF is operated at *t=0.16s*

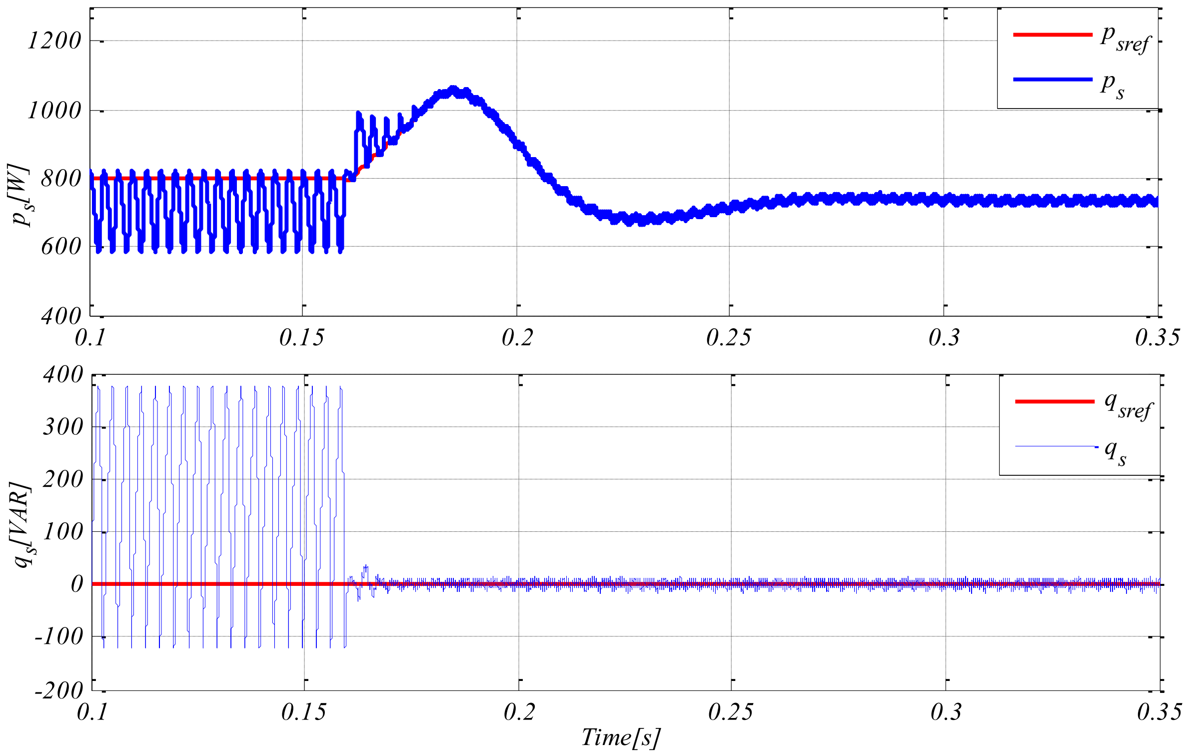

Figure III.19 : Simulation results of source active and reactive power *(p_s , q_s)* with their references *(p_{sref} , q_{sref})*, SAPF is operated at *t=0.16s*

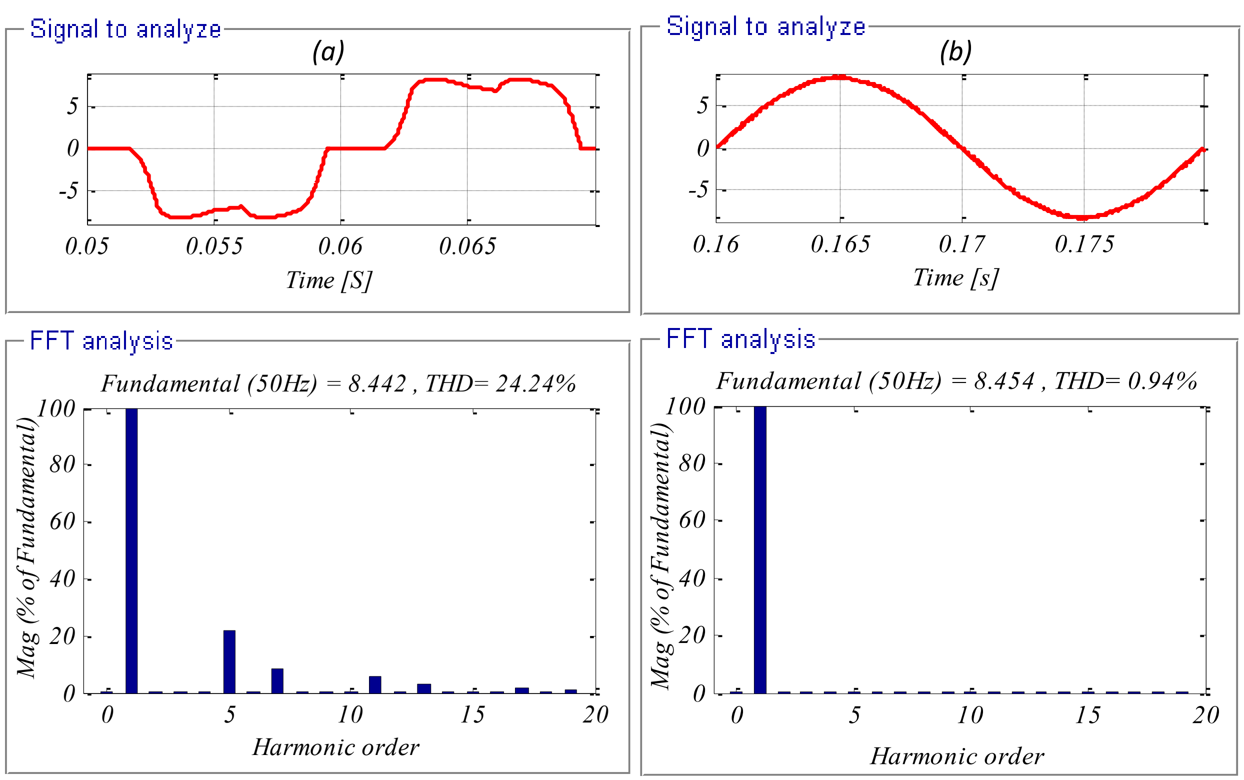

Figure III.20 : Simulation results of FFT analysis of source current before filtering *(a)* and after filtering *(b).*

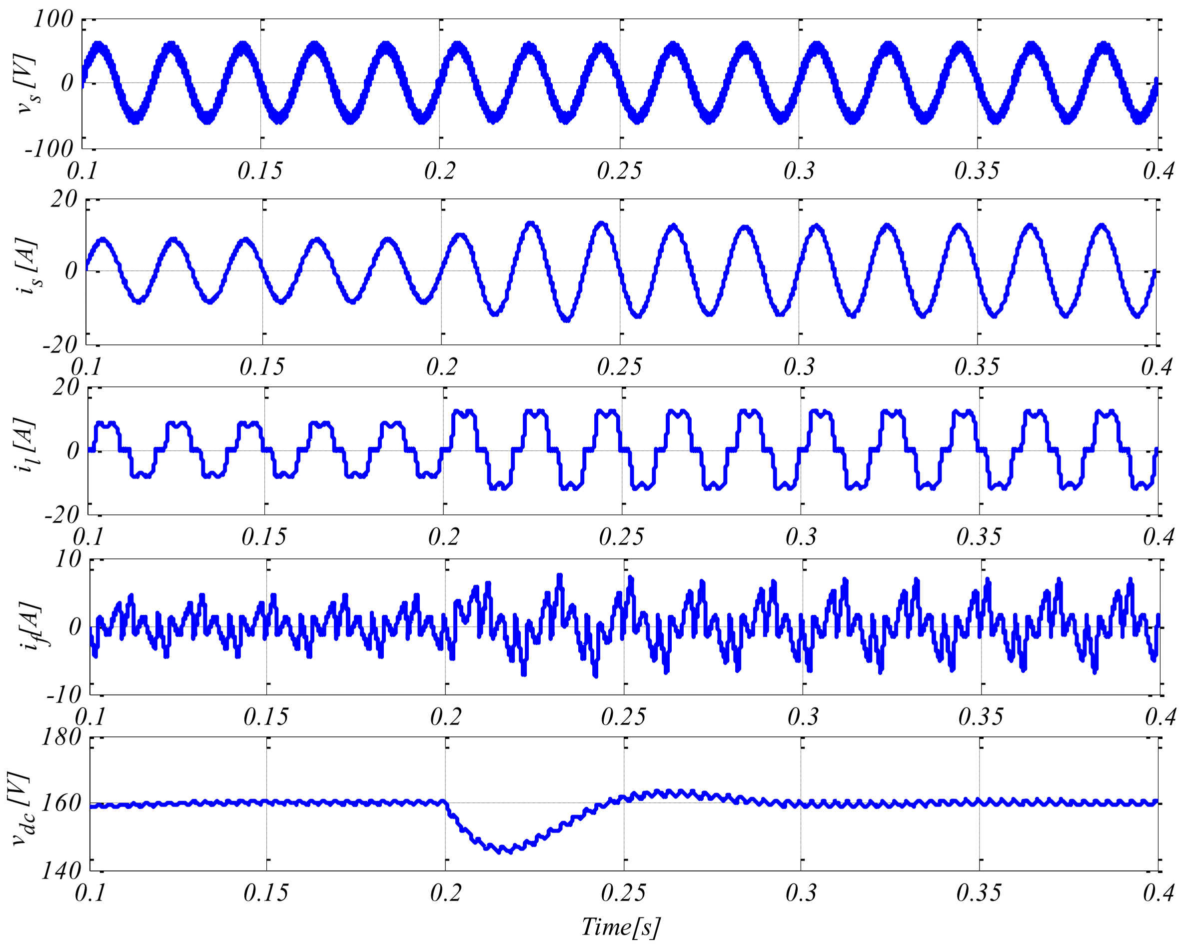

Figure III.21 : Simulation results of source voltage *(v_s)*, source current *(i_s)*,load current*(i_l)*, filter current*(i_f)*, DC bus voltage waveforms *(v_{dc})*, step increase of the load at *t=0.2s*

To study the robustness of the control strategy, the system experienced a sudden variation of the nonlinear load (50% variation). Figure III.22 shows that at *t=0.2s*, the load currents is suddenly increased while that of the source retain its dynamic and its sinusoidal form, thanks to the robustness of the control strategy, no disturbance is noticed in the source voltages. In addition, the DC bus voltage followed its reference $v_{dc}=160V$ after a transient period of $\Delta t=0.1s$.

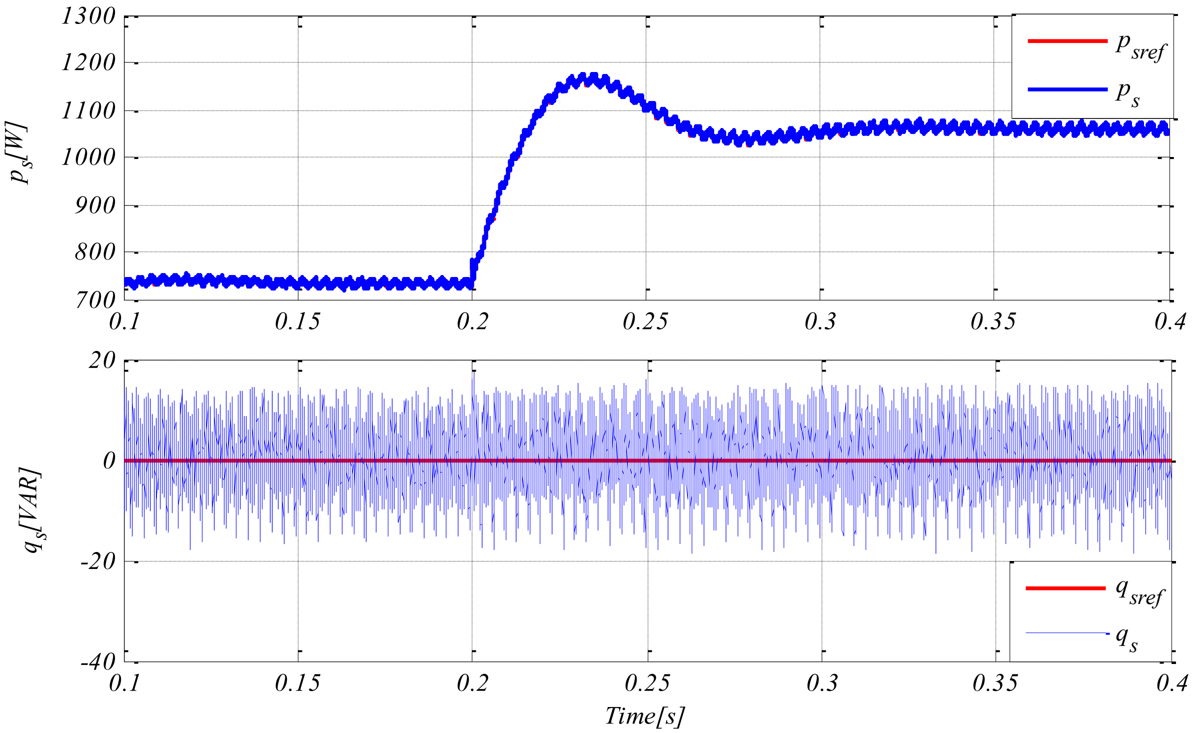

Figure III.22: Simulation results of source active and reactive power *(p_s , q_s)* with their references *(p_{sref} , q_{sref})*, step increase of the load at *t=0.2s.*

III.4.3. Experimental results

The experimental tests have been conducted with the same parameters used in simulation, expect the sampling time that is set to *t=5e-5s* instead of *t=5e-6s* as in simulation tests due to limitation of the control board. The same tests performed in simulation have been validated experimentally under the operating condition quite similar. Hence, the experimental results are similar and corroborate the simulation results presented previously. The same interpretation of the waveforms can be given.

However, spectral analysis of the source current in experimental measurement shows significant difference with the simulated one. The justification of this difference may refer to different parameters are not considered in simulation such as the dead time in addition to the sampling period difference. Spectral analysis shows that the source current total harmonic distortion is reduced to 3.4% after the compensation, which make the source current in compliance with IEEE-519 standards.

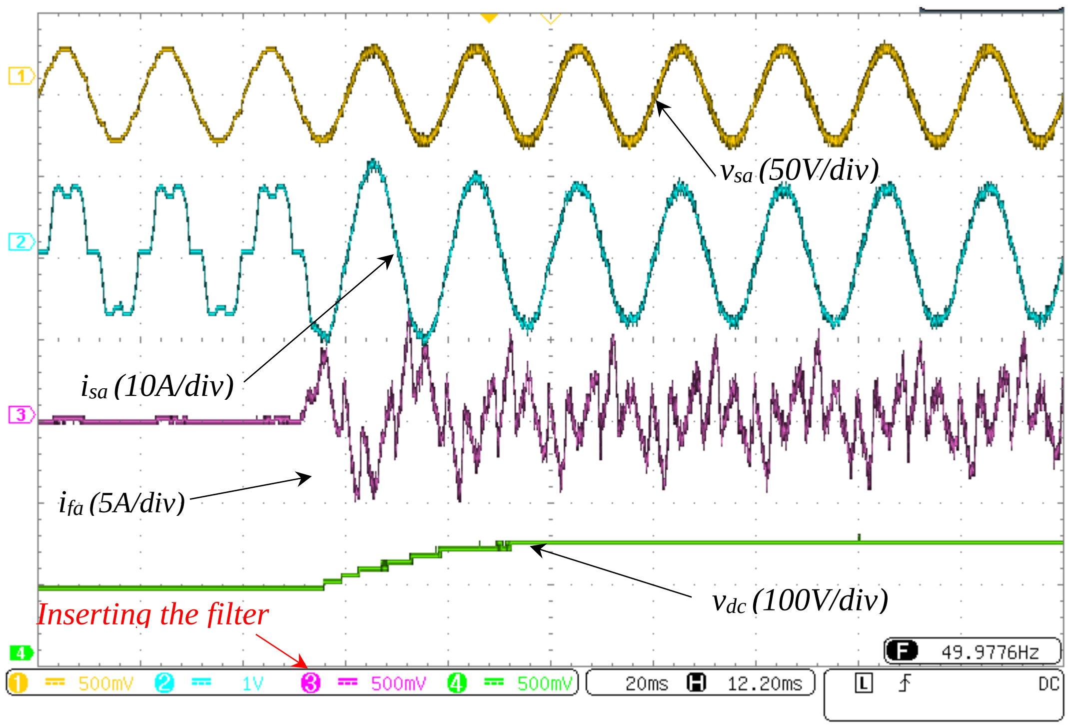

Figure III.23 : Experimental results of source voltage *(v_s)*, source current *(i_s)*, filter current*(i_f)*, DC bus voltage waveforms *(v_{dc})* during the connection of SAPF.

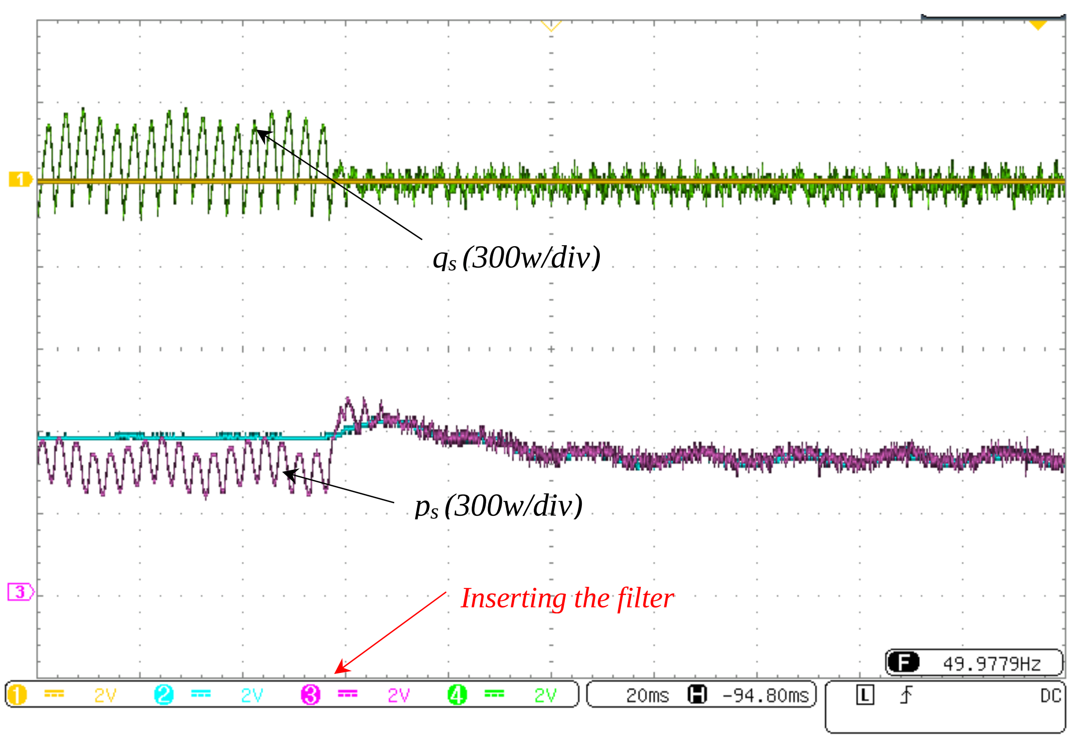

Figure III.24: Experimental results of source active and reactive power *(p_s , q_s)* with their references *(p_{sref} , q_{sref})* during the connection of SAPF.

(a)

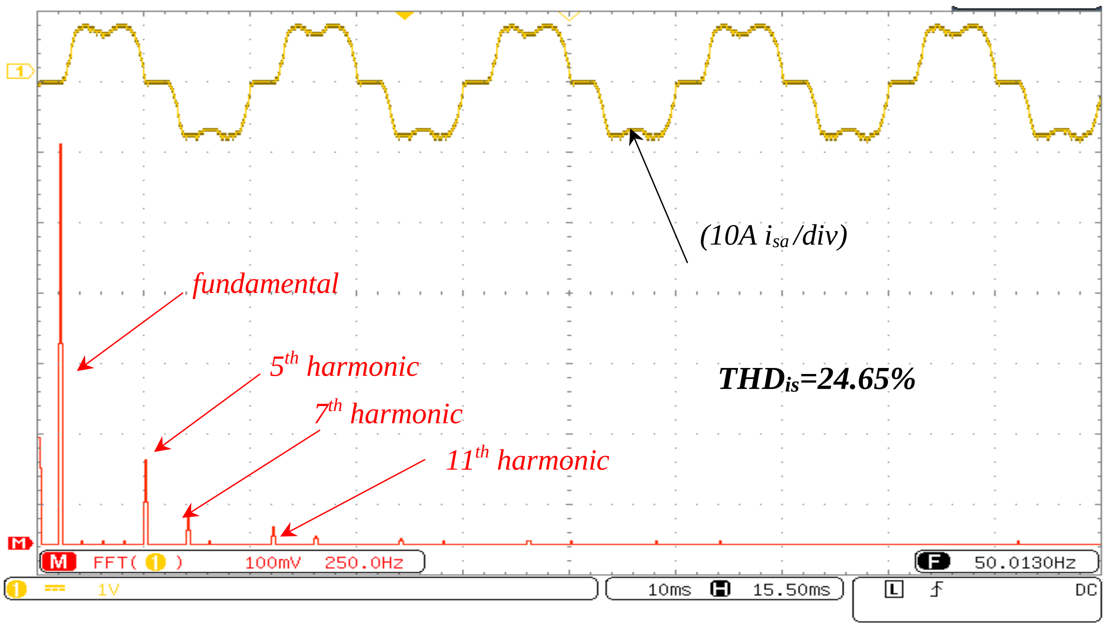

(b)

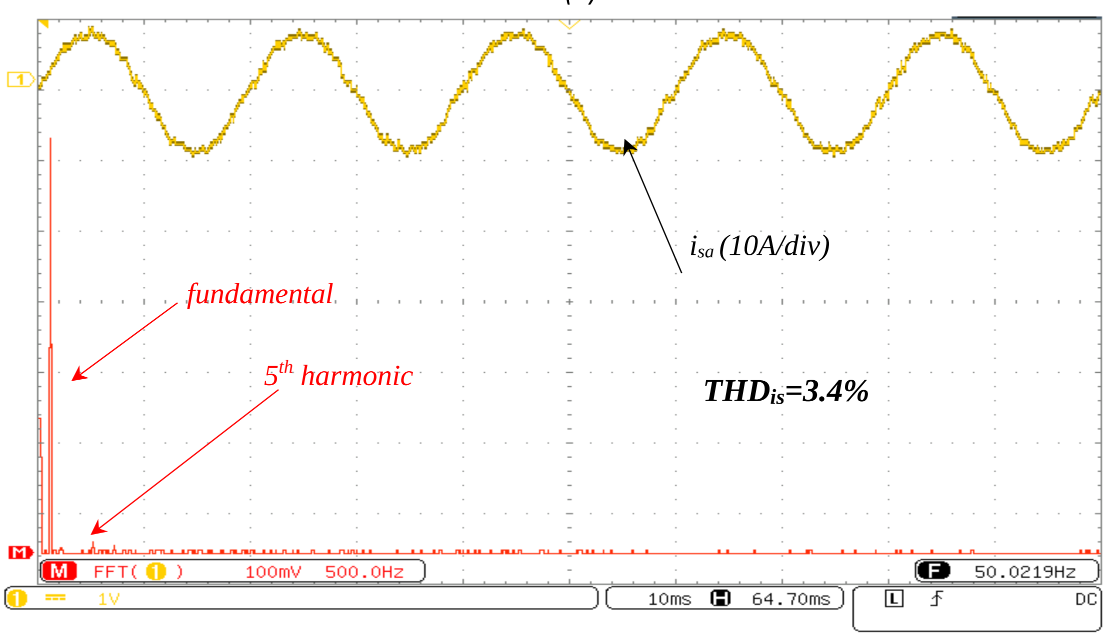

Figure III.25: Experimental results of FFT analysis of source current before filtering *(a)* and after filtering *(b)*.

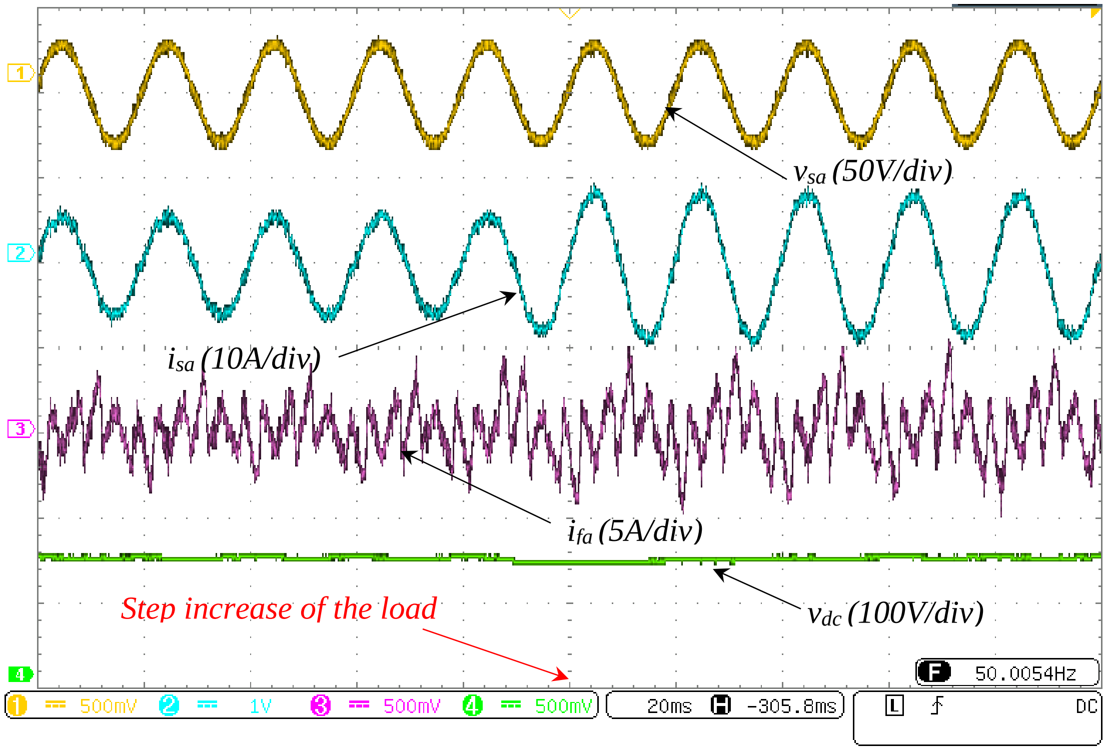

Figure III.26 : Experimental results of source voltage *(v_s)*, source current *(i_s)*, filter current*(i_f)*, DC bus voltage waveforms *(v_{dc})* during step increase of the load.

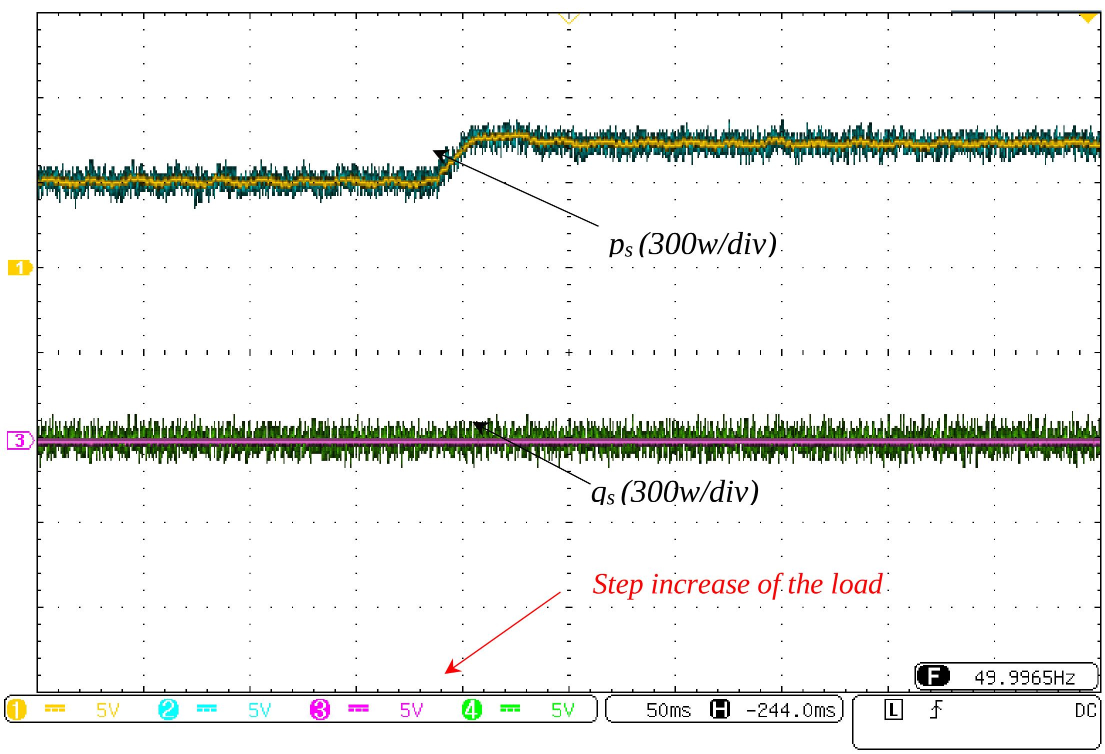

Figure III.27: Experimental results of source active and reactive power *(p_s , q_s)* with their references *(p_{sref} , q_{sref})* during step increase of the load.

III.4.4. Comparative study

In this stage, a comparative study of the three different control strategies performed in this thesis. DPC, FCS-MPC, and P-DPC-SVM. It can be stated based on the results abstained in different simulation and experimental tests that:

- The SAPF filter is able to inject the proper reactive power to achieve displacement power factor near to one.
- The SAPF filter is able provide the suitable current harmonic content to reduce the input current THD.
- Good dynamic performance is obtained.

However, the accuracy of compensation, tracking performance, and the quality of filtering are differ from each other.

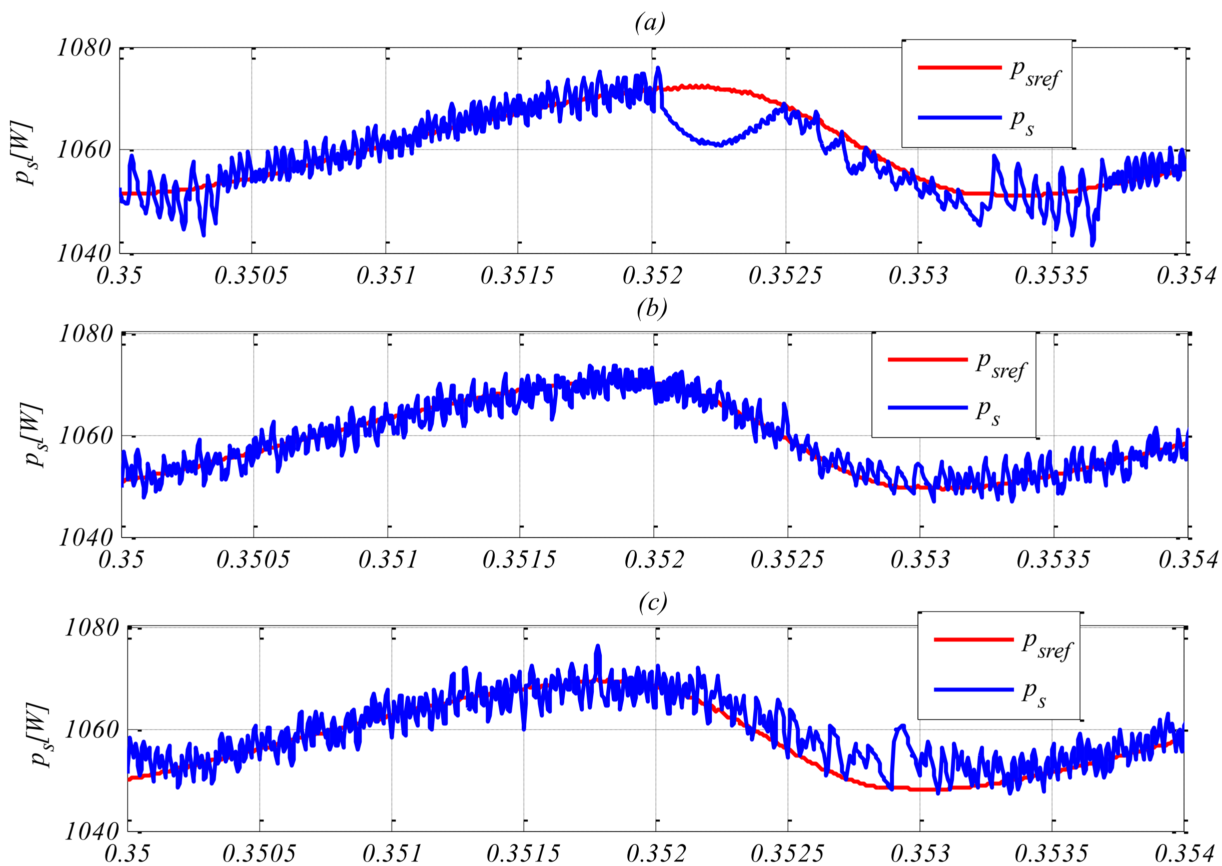

Figure III.28: Tracking performance of active power in steady state for DPC *(a)* FCS-MPC *(b)* , and P-DPC-SVM *(c).*

Figure III.28 presents the active powers with their references for the three control strategies in steady state. Good tracking performance for the three control strategies is noticed. However, FCS-MPC shows superior tracking performance of active power as compared to DPC and P-DPC-SVM control strategy. The difference between FCS-MPC and P-DPC-SVM is noticed in small period of time 0.3525<t<0.3535. Whereas, quite similar performance is obtained in the remain period of time.

Figure III.29 shows the reactive powers with their references for the three control strategies in steady state. Good reactive power compensation for the three control strategies is noticed. However, better compensation is noticed in case of FCS-MPC and P-DPC-SVM with small superiority of FCS-MPC.

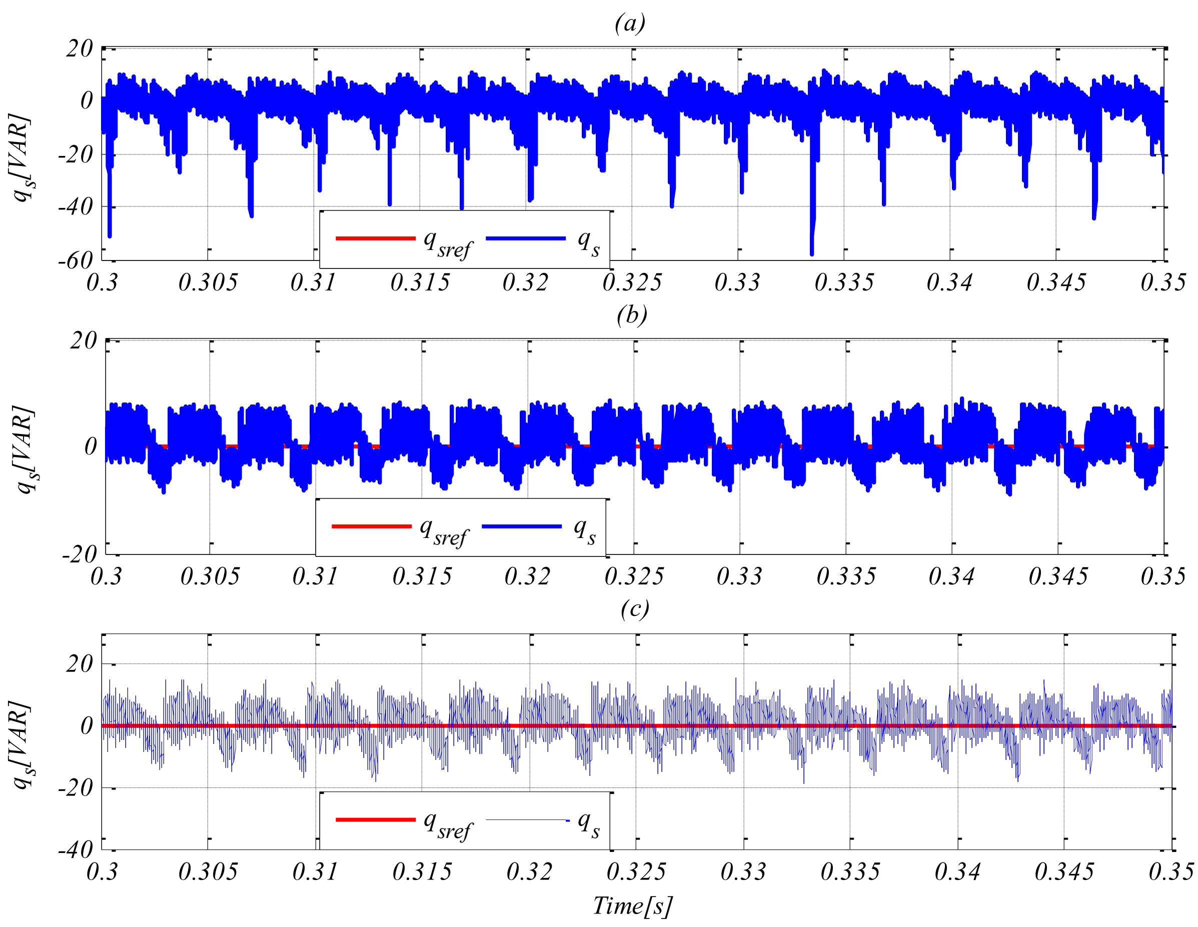

Figure III.29: Tracking performance of reactive power in steady state for DPC *(a)* FCS-MPC *(b)* , and P-DPC-SVM *(c).*

The evaluation of the three control strategies are performed in terms of quality of filtering in steady state. The simulation and experimental results are illustrated in table III.1.

FCS-MPC and P-DPC-SVM provide satisfactory results that meet IEEE 519-1992 standard requirement. Slight superiority in filtering is noticed in FCS-MPC. However, P-DPC-SVM presents some advantages as compared to FCS-MPC such as:

Table III.1: Total harmonic distortion of source current of different control strategies.

CONTROL STRATEGY	THD of Source Current i_{sa} before Inserting SAPF		THD of Source Current i_{sa} after Inserting SAPF	
	Simulation	Experiment	Simulation	Experiment
DPC	24.24 %	24.65 %	1.20 %	5.4 %
FCS-MPC		24.65 %	0.90 %	2.9 %
P-DPC-SVM		24.65 %	0.94 %	3.4 %

- It does not require a high amount of calculations, compared to FCS-MPC scheme, which reduces the cost of implementation.
- It operates with fixed switching frequency, which increase the efficacy and reliability of the converter.
- It operates with lower switching frequency, which reduces the power losses.

III.5. Conclusion

In this chapter, we have presented an overview of different predictive control strategies. Then, two types of predictive control are investigated on shunt active power filter. Firstly, Finite Control Set Model Predictive Control has been modelled and validated by simulation and experimentally. In the second part, Predictive Direct Power Control with space vector modulation is presented. The simulation and experimental results of P-DPC-SVM based SAPF are presented and discussed. Finally, we have closed this chapter by a comparative study of different control strategies investigated in this thesis.

As a conclusion, Predictive direct power control can produce good reference tracking performances and dynamic response. However, the quality of filtering provided is little bit inferior when compared with FCS-MPC. Due to fixed switching frequency that result in low switching losses and good reliability of power converter, P-DPC-SVM is selected to be used for photovoltaic integration in the next chapter

Chapter IV: Optimized Shunt Active Power Associated with PV System

IV.1. Introduction

Nowadays, the use of renewable energies is more than necessary; it is a global strategic issue. Indeed, it would be a tool against global warming. It is crucial to preserve resources and the environment while meeting the global demand for energy. Solar energy is one of the so-called renewable energies in the sense that the sun is almost an inexhaustible resource[1].

Over the past 20 years, the PV power industry has experienced significant growth. PV power generation has become more and more common. The capacity of PV systems ranges from milliwatts for portable devices such as calculators, to gigawatts for power plants connected to the electricity grid. A grid-connected PV power system can be economically installed, and can be rated as low as just a few hundred watts[74].

In this chapter, an overview of photovoltaic energy will be presented, the modelling of PV panel and DC/DC boost converter will be discussed. In addition, different type of MPPT will be presented. The Particle swarm optimization algorithm will be discussed. In the last part, the simulation and experimental will be presented and discussed.

IV.2. Overview of Photovoltaic Energy

IV.2.1. PV module

A PV module is comprised of individual solar cells that are electrically connected in series and parallel to achieve a desired DC output voltage and current for the PV module. Each solar cell is made from semiconducting materials that use sunlight to separate electrons from atoms to create an electric DC current.

The typical current–voltage (I-V) and power–voltage (P-V) characteristics of a PV module under standard test condition (STC); illumination of 1kW/m^2, and cell temperature of 25°C are shown in Figure IV.1 [75].

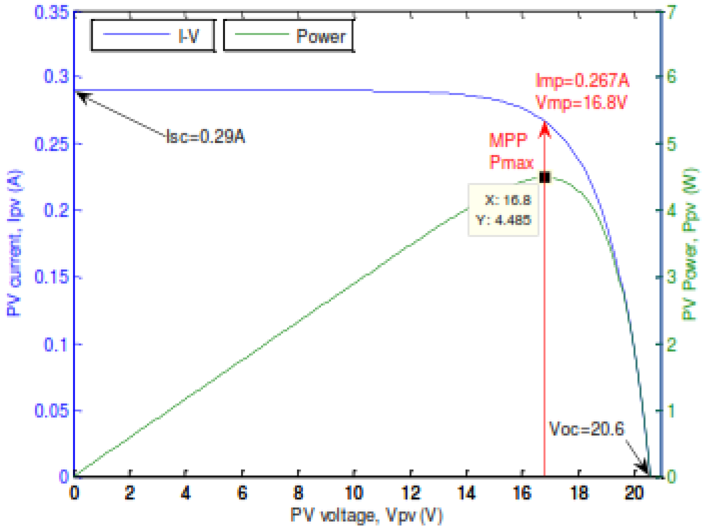

Figure IV.1 : I-V and P-V curves of PV module.

Short-circuit current *(I_{sc})* and open-circuit voltage *(V_{oc})* are the maximum current and voltage that the PV module can produce. However, the instantaneous power output of the PV module is the product of the output current and the terminal voltage of the PV module, so neither of these conditions are appropriate operating point for the PV module (short-circuit voltage *(V_{sc})* and open-circuit current *(I_{oc})* are zero, which leads to zero power production.

IV.2.1.1. Modeling of PV module

PV module is treated as a number of PV cells associated in series and in parallel[76]. Multiple mathematical models for PV cells are found in the literature [77,78]. The adopted PV module is designed based on a single-diode model of PV cell represented by Equation (IV.1) [78].

$$I_{pv} = I_{sc} - I_0.[\exp(\frac{V_{cell} + R_s.I_{cell}}{V_t.\alpha}) - 1] - \frac{V + R_s.I_{cell}}{R_p} \quad (IV.1)$$

Where:

I_{sc} : Photo-current generated by PV cell.

I_0 : Saturation current of the diode.

V_t: Thermal voltage of PV cell.

R_p: The equivalent parallel resistance.

R_s: The equivalent series resistance.

α: Diode ideality factor.

V_{cell}: Voltage at the output of PV cell.

I_{cell}: Current generated by PV cell.

IV.2.2. Standalone PV Systems[74]

Standalone PV systems supply power to local loads, and so are independent of the grid distribution network. Their history can be traced back to the 1950s, when PV technology was widely used for space power supplies. Solar radiation is more intense in space because it is not attenuated by the atmosphere and not blocked by clouds. The outer atmosphere is considered an ideal environment for solar PV power generation. However, their recent application has mostly been on Earth. The major applications of standalone systems include satellites, spacecraft, space stations, remote homes, villages, street lights, communication sites, water pumps, and vehicles. Nowadays, these systems are mainly installed in areas where grid connections are unavailable. Standalone PV systems can supply either DC, AC or both, depending on the load requirement.

IV.2.3. Grid-Connected PV Systems

A grid-connected photovoltaic system can be defined as the connection between the solar cells and the public electricity grid via a suitable inverter, because a PV module delivers only DC power. The complete grid-connected photovoltaic system is illustrated in Figure III.2 [79], which is comprised of a number of units. The first unit is a solar array, which transforms sunlight into electric current. The second unit is an electronic power converter, which in turn is divided into two parts; the DC/DC boost converter is used to step up the relatively low solar panel DC voltage to the desired level for input to the DC/AC inverter. The inverter is operated in current control mode to inject a unity power factor current waveform into the grid. Finally, a low voltage transformer is used as galvanic isolation between the grid and photovoltaic system [79].

Grid-connected PV systems have clear advantages for massive solar power production since the utility grid is a significant energy buffer that can accommodate the intermittency of solar power generation[74].

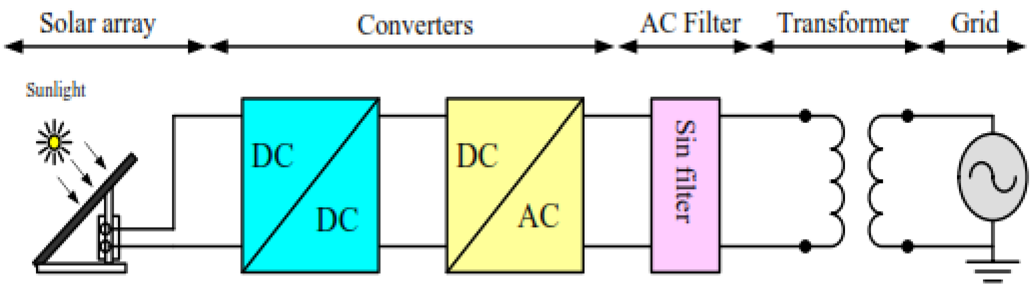

Figure IV.2 : Schematic of grid-connected PV system.

Grid-connected PV systems can be subdivided into two kinds:

- Decentralized grid-connected PV systems.
- Central grid-connected PV systems.

IV.2.3.1. Decentralized Grid-Connected PV Systems[80]

Decentralized grid-connected PV systems have mostly a small power range and are installed on the roof of buildings (rooftop or flat-roof installation) or integrated into building facades.

Energy storage is not necessary in this case. On sunny days, the solar generator provides power, e.g., for the electrical appliances in the house. Excess energy is supplied to the public grid. During the night and overcast days, the house draws its power from grid. In this way, the electricity

grid can be regarded as a large "storage unit." In the case of a favorable rate-based tariff for PV electricity, as is in force in some countries, it is more advantageous to feed all solar electricity into the grid.

IV.2.3.2. Central Grid-Connected PV Systems[80]

Central grid-connected PV systems have an installed power up to the MW range. With such central photovoltaic power stations, it is possible to feed directly into the medium or high voltage grid. Mostly central photovoltaic power stations are set up on otherwise unused land, but in some cases an installation on buildings, mostly on the flat roof of greater buildings, is also possible.

Both decentralized and central grid-connected PV systems consist of the following two main components:

- PV module.
- Inverter.

IV.2.4. PV System Configuration Options[81]

A string is a series connection of PV modules that, by definition, has a higher output voltage (which is useful for easier power conversion), and equal current though every module. Partial shading on any module will limit its current output, which in turn limits the current (and hence power output) for all modules on the same string, unless the shaded module is short-circuited out with the use of a bypass diode. Three string-based topologies are examined (central inverters, string inverters, multi-string inverters).

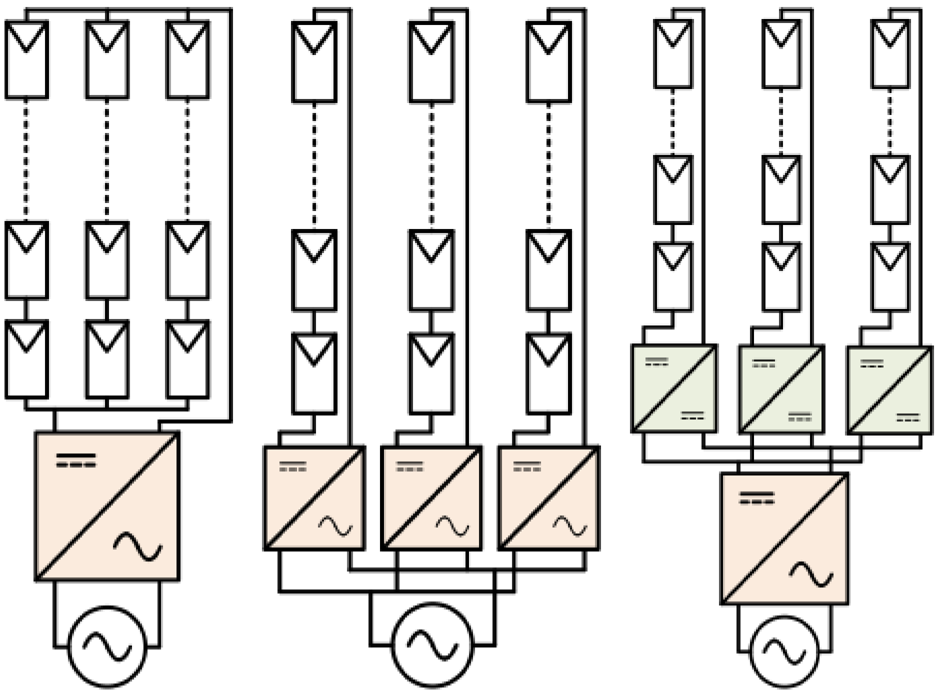

(a) **(b)** **(c)**

Figure IV.3 : String-based solar PV system configurations: *(a)* Central inverter, *(b)* String inverters, *(c)* Multi-string inverters.

IV.2.4.1. Central Inverter[81]

A central inverter takes an entire array of strings in parallel as a single DC input then converts it for export to the AC network, as shown in Figure III.3-a**.** This conversion may be done with a single DC-AC stage or though an extra DC-DC stage that should be added if the input voltage is not high enough, or if the inverter is designed to operate with a regulated DC voltage[82]. A single MPPT controller is implemented on the entire solar array, meaning any orientation, manufacturing, or irradiance differences will result in a suboptimal output for the entire system. Additionally, since all strings are connected in parallel, the DC voltage set by the MPPT controller is equal across all strings meaning that individual strings may also not be operating at their MPP[83].

IV.2.4.2. String Inverter[81]

A string inverter is similar to the central inverter, however in an effort to increase the number of MPPT controllers each inverter only operates on a single string (to ensure more panels operate closer to their MPP), as shown in Figure III.3-b. Each of these inverters may be a single DC-AC inverter, though again a step-up DC-DC stage can be added if the string voltage is not sufficiently high for direction inversion, or if the inverter's DC input requires tighter regulation. In order to expand the system, additional PV strings and inverters will be added, connected in parallel directly to the AC network[84].

IV.2.4.3. Multi-String Inverter[81]

A multi-string inverter combines the previous two ideas of a central inverter and per-string MPPT controllers. This is done with the use of multiple DC-DC converters performing MPPT on individual strings, with their outputs connected in parallel to a common DC bus. This power is then processed by a single inverter for connection to the AC network as shown in Figure III.3-c [82].

IV.2.5. PV Power Converters technology [85]

Since the power per PV generating unit is relatively low while its cost of energy is still at a relatively high level, there is a strong demand to improve the efficiency. Furthermore, as illustrated in Figure III.4, the power converters for PV applications are power-dependent, where the efficiency reaches to 98.8%.

It is also observed in Figure III.4 that there is a significant difference in efficiency and market share for three power conversion configurations; the multi-string inverter (module converter),

string inverter, and central inverter technologies[86,87]. The market shares of central inverters and string inverters are almost equal, which is mainly a consequence of the strong demand in electricity generation and the fast decrease in the module price. In contrast, the module PV converters are evolving[86] [24].

Central inverters are adopted in large-scale commercial and utility-scale PV power systems with the power rating of above 100kWp, and string inverters are more commonly seen in applications with the power below 100kWp (e.g., residential and small-scale commercial systems).

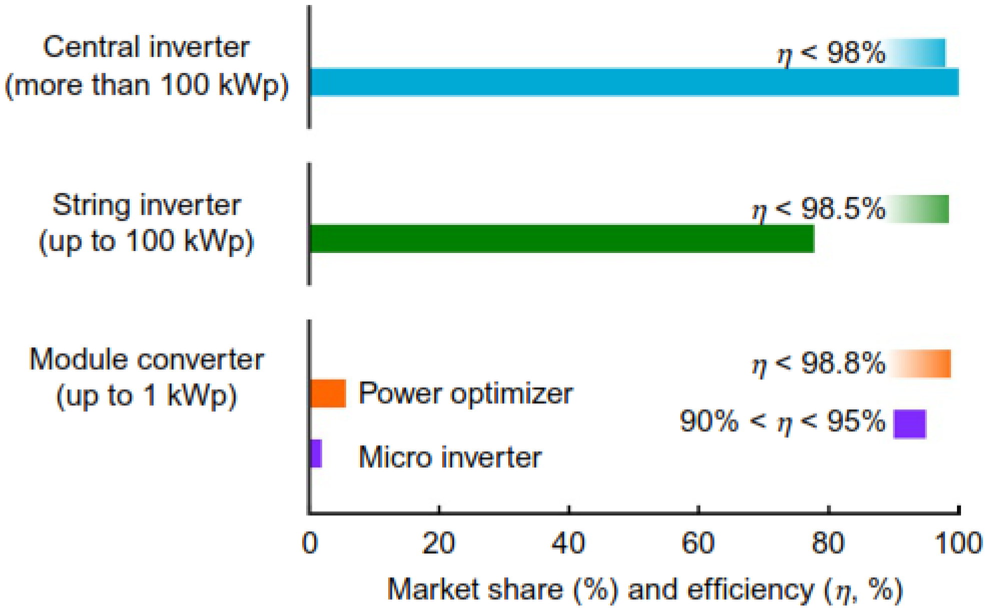

Figure IV.4 : Market share of PV converters (percentage of the central inverter market) in 2016 and the corresponding efficiencies [109], where the power rating ranges for each technology are also indicated.

For even low-power applications (rooftop small PV units and off-grid systems), power optimizers and micro inverters are preferable in terms of efficiency and power optimization. Notably, in practical projects, multiple string inverters are also adopted to collect higher power considering the system overall reliability. The most important concerns in respect to the cost of PV energy.

IV.2.6. DC-DC Conversion stage[79]

Many solar arrays have a low level output voltage[88]. For this reason, a DC-DC boost converter is required to boost the low voltage to (380 - 400 DC voltage) for compatibility with the requirements of grid connection. Bratcu, Munteanu et al. [89] presented a method, which consists of a series topology of per-panel DC–DC converters; these are connected to a single-phase DC/AC inverter. This method has some advantages over the parallel connection case, as it is possible to operate each boost with a small step-up ratio, resulting in good efficiency at low cost. Haeberlin[90] described different methods of achieving the inverter DC link voltage without the need for a DC/DC converter. There are various combinations of series and parallel configurations to get a high DC voltage level from the PV module. The simple method is to use a series connection for only a few PV panels. This approach has high inverter efficiency, simplicity and low cost. This approach is still the first choice for medium and large PV applications, because it has a higher power level, and does not even have Maximum Power Point Tracking MPPT for each string. In string inverters configuration, each string has MPPT, but the cost of this module is higher per KW due to the low power rating compared with the centralized inverter.

IV.2.6.1. Maximum Power Point Tracking Algorithms

To maximize the energy generated by the solar modules, it is desired to maintain operation at the highest point on the P-V curve, known as the maximum power point (MPP). Since the P-V curve varies with irradiance and cell temperature, a MPPT controller should be used to ensure the module is connected at the optimal voltage to deliver the best possible performance. It is possible for partial shading to create multiple local maxima so MPPT controllers should make sure they do not settle at these points instead of the global maximum[91]. A comparison of various MPPT techniques is given in Table IV.1. The most common types of MPPT control strategies are:

- Perturb and Observe (P&O): This controller operates by varying the PV voltage and measuring the change in output power[92].
- Hill climbing: Hill climbing is similar to P&O, but introduces perturbations in the duty ratio ratio instead of the PV voltage[93].
- Three-Point Weight Comparison: Variation of P&O where the current point is compared to the two preceding ones to ensure the MPP is tracked even under sudden irradiance changes.

- Incremental Conductance (IC): Compares instantaneous with incremental conductance to determine which side of MPP the current operating point is on. This controller allows the operating point to be maintained at the MPP instead of oscillating around it like the P&O method[94] [44].

Table IV.1: Main characteristics of various MPPT techniques [91].

MPPT Technique	Analog or Digital	Periodic Tuning	Convergence Speed	Implementation Complexity	Sensed Parameters
Hill Climbing /(P&O)	Both	No	Varies	Low	Voltage, Current
Incremental Conductance	Digital	No	Varies	Medium	Voltage, Current
Fractional open-circuit Voltage	both	Yes	Medium	Low	Voltage
Fractional Short-Circuit Current	both	Yes	Medium	Medium	Current
Fuzzy Logic Control	Digital	Yes	Fast	High	Varies
Neural Networks	Digital	Yes	Fast	High	Varies
Current Sweep	Digital	Yes	Slow	High	Voltage, Current

- Fractional Open-Circuit Voltage: Set the PV current momentarily to zero and measure the open circuit voltage, then set the reference voltage to around 71-78% (commonly 76%) of the open circuit voltage. This works due to the near linear relationship between the MPP voltage and the open circuit voltage[91].

- Fractional Short-Circuit Current: Similarly to the fractional open-circuit voltage

  method, this is based on the fact that the MPP current is roughly proportional to the short circuit current (approximately 78-92%).

- Current Sweep: Perform a periodic sweep to obtain the array I-V characteristics and use this to compute the location of the MPP.

- Artificial intelligence based MPPT such as Fuzzy Logic Control, Neural Networks[95–97].

IV.2.6.2. Sliding mode based MPPT

Sliding mode control for non-linear systems has become a motivating solution. It is considered one of the most used control approaches thanks to its advantages.(robustness, good stability, very low response time)[98,99]. It is characterized by the discontinuity of the control at the passages by a sliding surface. So everything depends on the appropriate choice of this surface [100]. Therefore, for simplicity, the Equation (IV.2) has been transformed for the sliding surface for SM-MPPT.

$$S = \frac{dP_{pv}}{dI_{pv}} \quad \text{(IV.2)}$$

Then

$$S = I_{pv}\frac{dV_{pv}}{dI_{pv}} + V_{pv} \quad \text{(IV.3)}$$

the structure of the sliding mode controller focuses on two main parts: a continuous part and another discontinuous part[98] as presented below:

$$u = u_{con} + u_{disc} \quad \text{(IV.4)}$$

The first part, it is extracted from the condition (IV.2) that satisfies Lyapunov stability theory[101]. $d\dot{S} = 0$ (IV.5)

The continuous part is presented as follows:

$$u_{con} = 1 - \frac{V_{pv}}{V_{dc}} \quad \text{(IV.6)}$$

The second part is important in nonlinear control because its role is to eliminate the effects of inaccuracies and disturbances on the model of the system when the system has not reached the sliding surface [100]. It is defined by:

$$u_{disc} = K.sign(S) \quad \text{(IV.7)}$$

K : is the maximum value desired at the output of the controller to assure steady-state stabilization.

The output of the SMC can be represented by Equation (IV.8).

$$u = \begin{vmatrix} 1 & if & (u_{con} + u_{disc}) > 1 \\ (u_{con} + u_{disc}) & if & 0 < (u_{con} + u_{disc}) < 1 \\ 0 & if & (u_{con} + u_{disc}) < 0 \end{vmatrix} \quad \text{(IV.8)}$$

IV.3. Particle Optimization Algorithm

PSO is an intelligent optimization algorithm, it is belongs to a class of optimization algorithms called Metaheuristic. PSO is based on paradigm of swarm intelligence, and it is inspired by social behavior of animals like fish and birds. Initially PSO is introduced by james kennedy and Russell C Aberhart in 1995 [102]. In last 20 years, the introduction of PSO became one of most useful and most popular algorithm to solve various optimization problems in various fields. One of key points behind the PSO is its simplicity. However, it is a powerful algorithm.

IV.3.1. Working Principle of PSO

In swarm intelligence, an intelligent behavior is created by means of some agents like birds, ants and fishes. This level of intelligence is absolutely unreachable for any member of the swarm, but with cooperation among the members of swarm.

PSO contains a population of candidate solution called a swarm, and this swarm is a set of particles[102]. Any particle has a position in the search space *(x)*. Therefore, any particle has a velocity *(v)*, which describes the movement of a particle in the sense of direction, distance and the step size.

In addition to position and velocity, every particle has a memory of its own best position and best experience. This is denoted by personal best. However, the best experience of all particles known as global best *(G_{best})* [103]. PSO mechanism is illustrated in Figure IV.5.

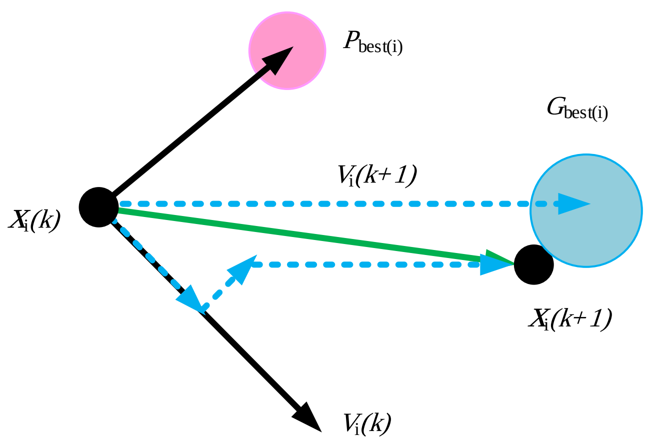

Figure IV.5 : Schematic of PSO mechanism.

IV.3.2. Mathematical model of PSO Algorithm

Particles of the swarm are interacting and learning from each other obeying some simple rules to find the best solution for an optimization problem[104]. The mathematical model of the motion of particles can be described as follows:

$$v_i(k+1)=\beta(k)v_i(k)+r_1c_1(P_{best(i)}(k)-x_i(k))+r_2c_2(G_{best(i)}(k)-x_i(k)) \quad \text{(IV.9)}$$

$$x_i(k+1)=x_i(k)+v_i(k+1) \quad \text{(IV.10)}$$

Where:

i : Number of particle.

k : Current number of iteration.

r_1, r_2 are random number confined between 0 and 1.

c_1, c_2 are acceleration coefficients.

β : is the inertia coefficient that is defined by Equation (IV.11) as indicated in[105,106].

$$\beta(k)=\beta_{\max}-\left(\frac{\beta_{\max}-\beta_{\min}}{\beta_{\max}}\right).k \quad \text{(IV.11)}$$

The new position of a particle is a probably a better location, because it is created according to the previous decision about the movement of this particle, and it uses the previous experience of the particle itself as well as the previous experience of the whole swarm.

IV.4. Association of the SAPF with PV system

IV.4.1. Configuration of the system

The proposed system relies on four main parts as depicted in Figure IV.6; power supply, nonlinear load, voltage source inverter (VSI) and double stage PV system. The inverter has double functions. Firstly, it operates as shunt active filter by minimizing the current harmonic distortion of the grid and suppressing the phase shift that are caused by nonlinear load and in the second place, it injects PV power into the load/grid. PV panels are connected to VSI via boost converter to operate with MPPT. The three-phase network is connected to a nonlinear load via three inductors. The nonlinear load is shaped from three-phase diode rectifier with a resistive load, which is the most common source of harmonic currents. Two level VSI based on six IGBT switches with a capacitor for energy storage is connected at the point of common coupling (PCC) through inductors *(L_f)*.

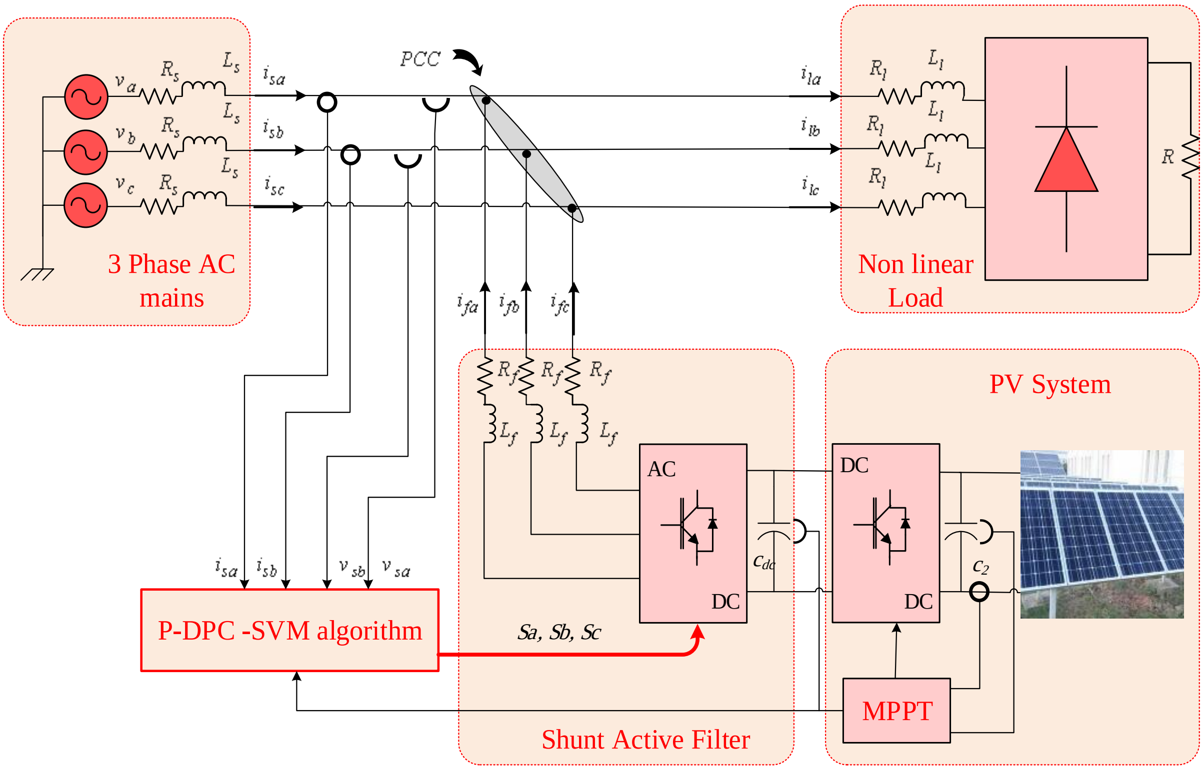

Figure IV.6 : General configuration of SAPF connected with PV system.

IV.4.2. Optimization of system parameters

IV.4.2.1. Optimization of Anti-Windup PI controller

PI controller with anti-windup provides a good performance in DC bus voltage regulation for the proposed P-DPC-SVM. However, anti-windup PI controller needs an accurate mathematical model, which is unreachable in the case of parameter variations and system nonlinearity. Consequently, PI controller that is designed based on the conventional method fails to achieve optimal performance and better results under different operating modes. Hence, the PSO algorithm has been proposed to improve the performance of the anti-windup PI controller. It executes an offline search in three search space to obtain optimized parameters of PI controller (Integral gain K_i, Proportional gain K_p and Anti-windup gain (G_a) that give better dynamic and steady performance .

The optimization problem, which is being solved by PSO, is an objective function that would like to minimize its cost value. The objective function is based on the instantaneous error of DC bus voltage control loop *e(t)* and instantaneous $THD_{is}(t)$ of current supply as described in Figure IV.7.

$$ITAE = \int t.|J(t)|.dt \qquad \text{(IV.12)}$$

$$IAE = \int |J(t)|.dt \tag{IV.13}$$

$$ISE = \int (J(t))^2 .dt \tag{IV.14}$$

Whereas:

$$J(t) = e(t) + THD_{i_s}(t) \tag{IV.15}$$

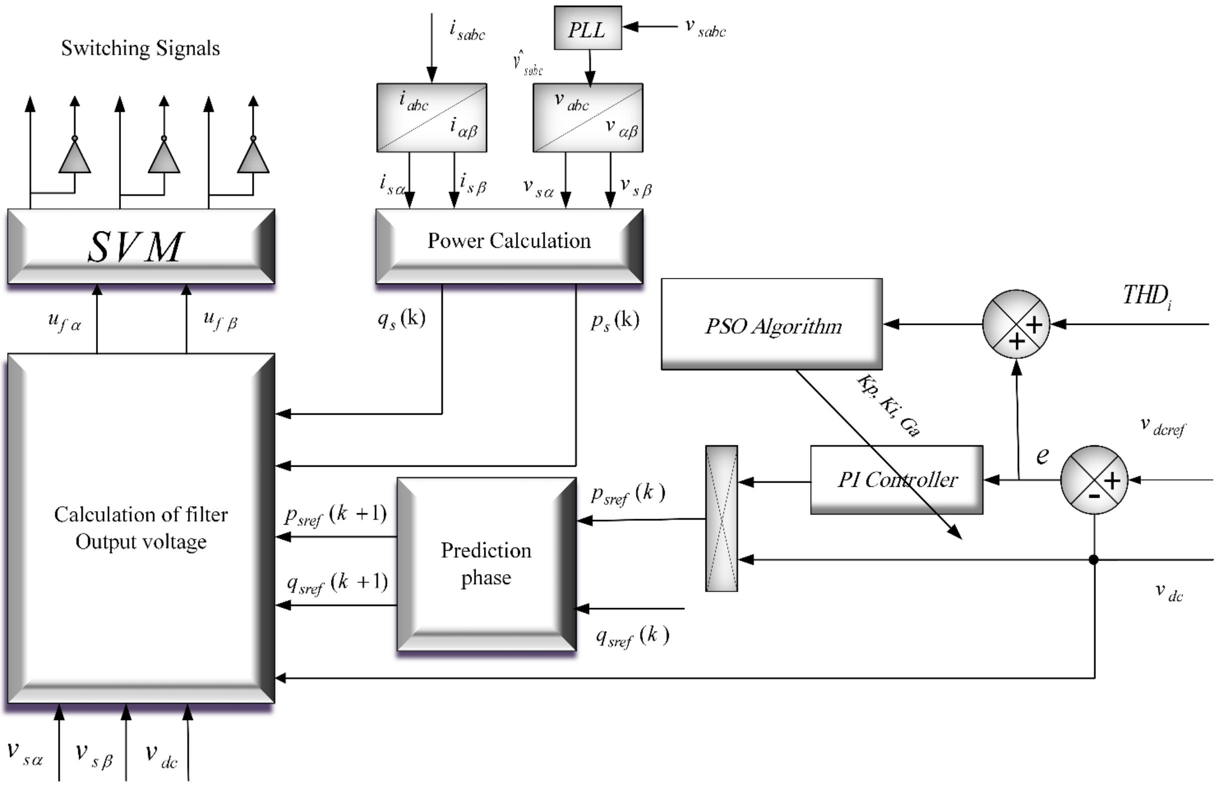

Figure IV.7 : Control scheme of P-DPC-SVM with optimized Anti-windup PI controller.

The performance of the three objective functions are evaluated according to PSO mechanism described by the flowchart in Figure IV.8 , where the initial parameters of PSO algorithm are listed in Table A.2 (see Appendix). The suitable objective function for DC bus voltage regulation was selected according to its corresponding fitness value. After many experiments, the lowest fitness has been obtained using ITAE objective function. The obtained parameters are given in Table A.3 (see Appendix).

IV.4.2.2. Optimization of Sliding mode MPPT

Sliding mode gain is properly adjusted for each sliding mode application in the aim of satisfying the stability condition of the system because there is no generalized rule to determine SMC gain [107]. PSO algorithm has been used to determine the optimal gain for sliding mode MPPT considering the objective function ITAE in standalone mode as shown in Figure IV.9.

$$ITAE = \int t.\left|e_{pv}(t)\right|.dt \qquad (IV.16)$$

Where: $e_{PV}(t) = P_{PVref}(t) - P_{PV}(t)$ (IV.17)

$P_{pvref}(t)$: Reference value of output PV power.

$P_{pv}(t)$: Measured value of output PV power.

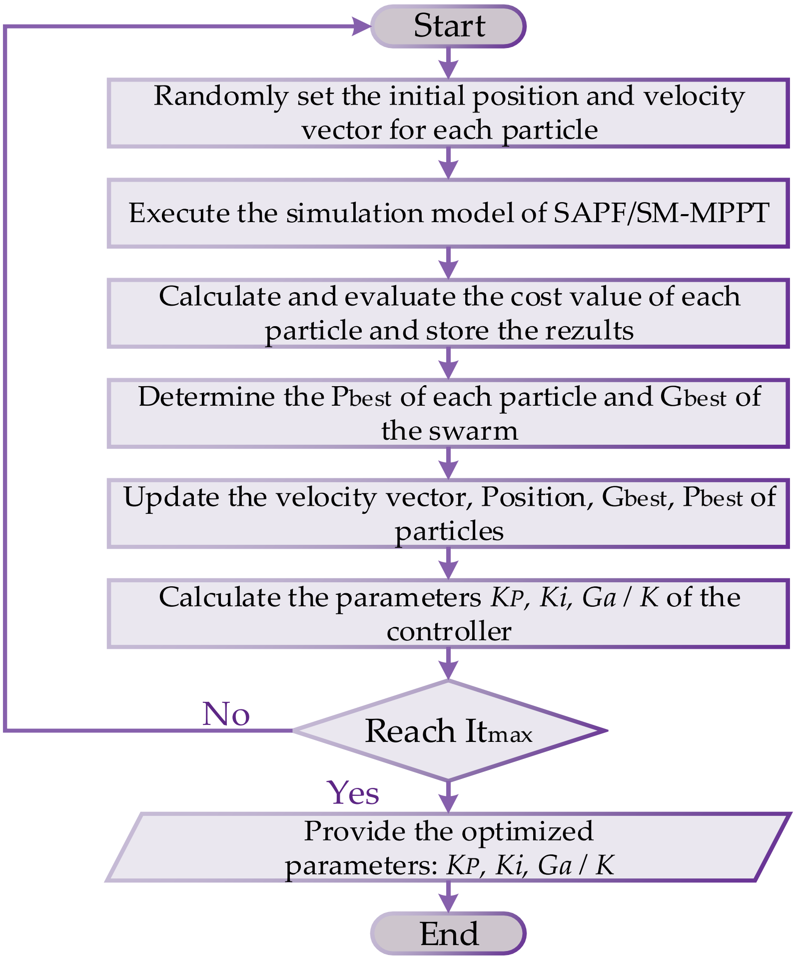

Figure IV.8 : Flowchart of PSO algorithm.

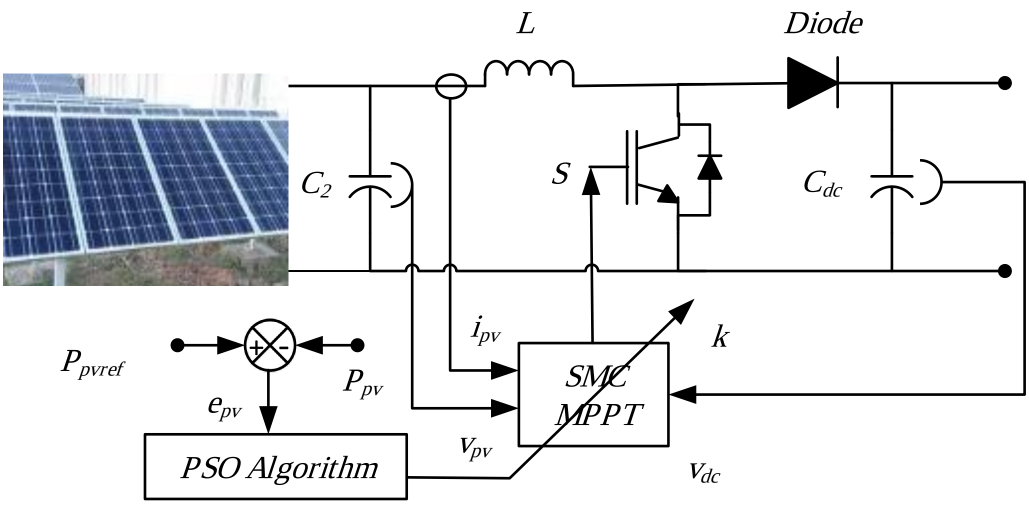

Figure IV.9 : Optimized sliding mode MPPT.

Figure IV.10 shows the convergence of the objective functions during simulations for PI parameters optimization and for SM-MPPT optimization using ITAE as objective function.

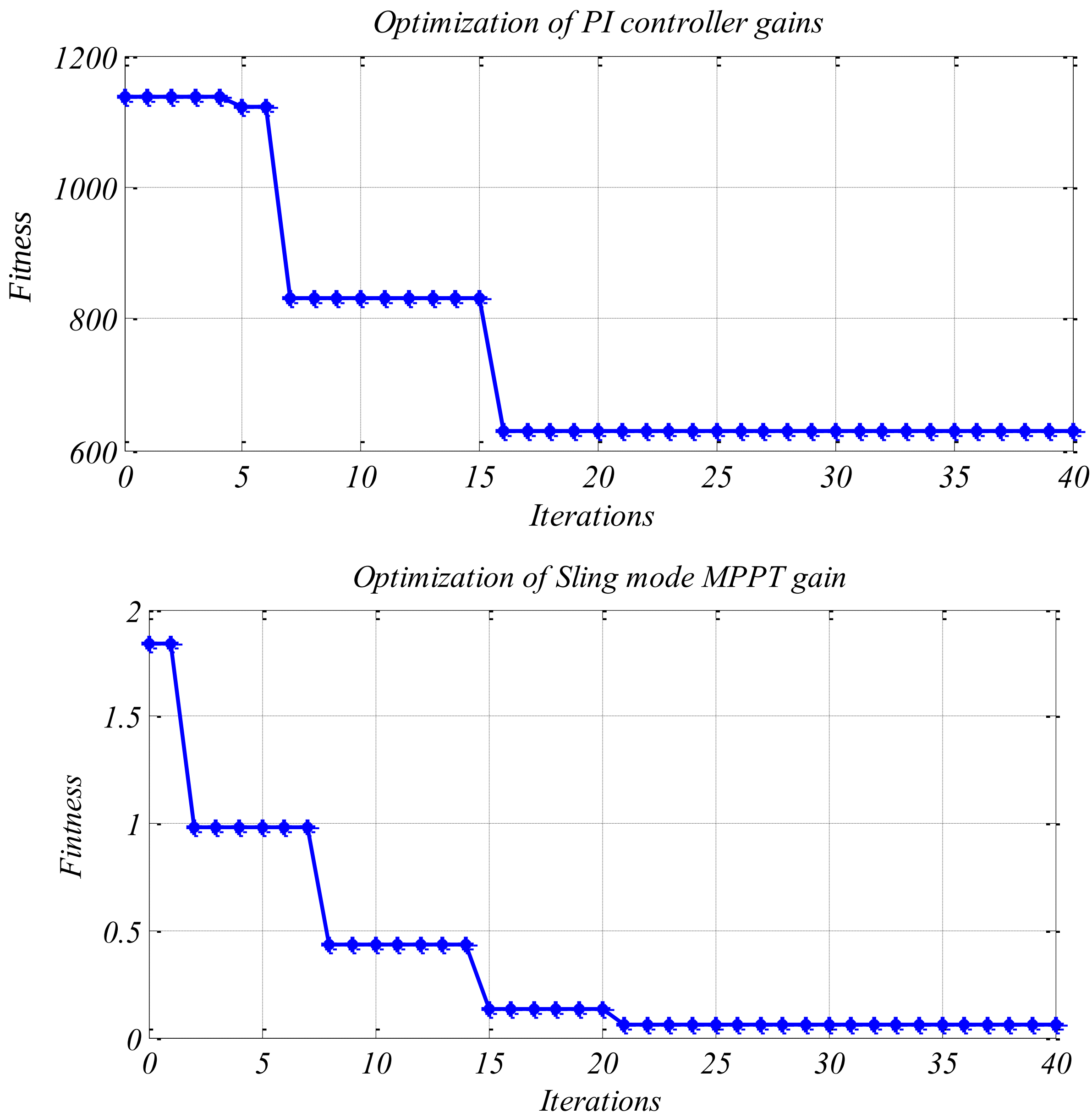

Figure IV.10 : Convergence of the objective functions.

IV.5. Simulation results

The simulation of the global system is performed under the Matlab\Simulink environment. The simulation parameters are are illustrated in Table A.1 (see Appendix). The studied system P-DPC-SVM based SAPF connected with PV system is investigated under different operating conditions.

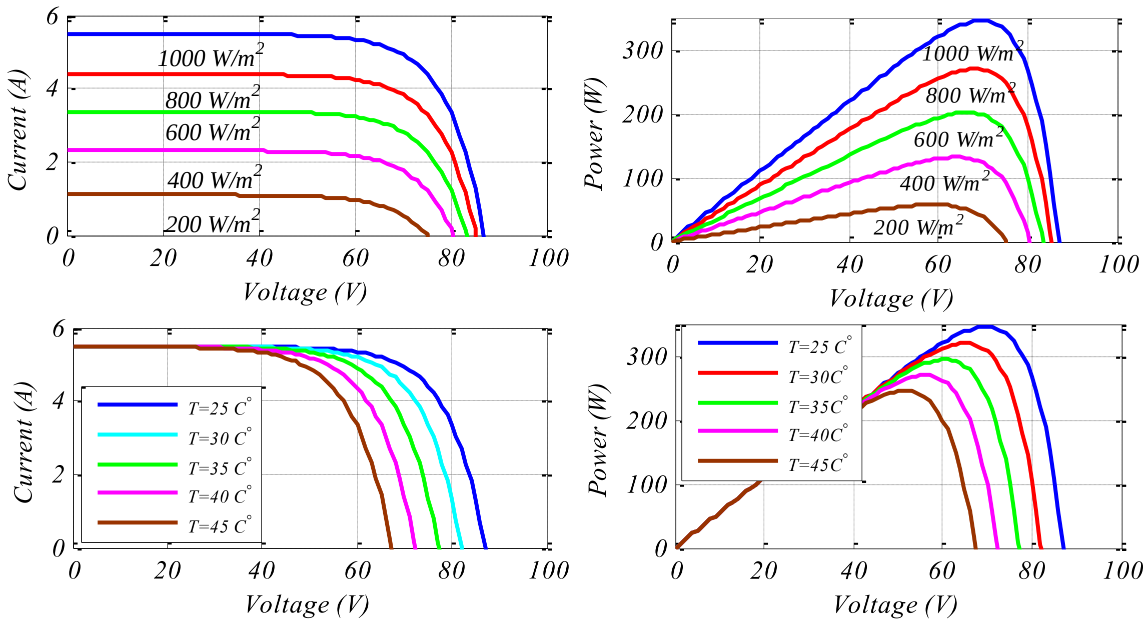

Figure IV.11 : P-V and I-V characteristics of the overall PV system.

Firstly, The PV system is composed of four PV modules (ALPV85-125M-36), which are connected in series to achieve the desired voltage level and to raise the power of the whole PV system. The parameters of the PV panel are listed in Table A.4 (see Appendix). whereas the P-V and I-V characteristics of the overall PV system in different climate conditions are given in Figure IV.11.

To demonstrate the efficiency and the robustness of SM-MPPT algorithm, simulation test is made under variable illumination in standalone mode. The photovoltaic generator is composed of four PV panels of 85 W associated in series.

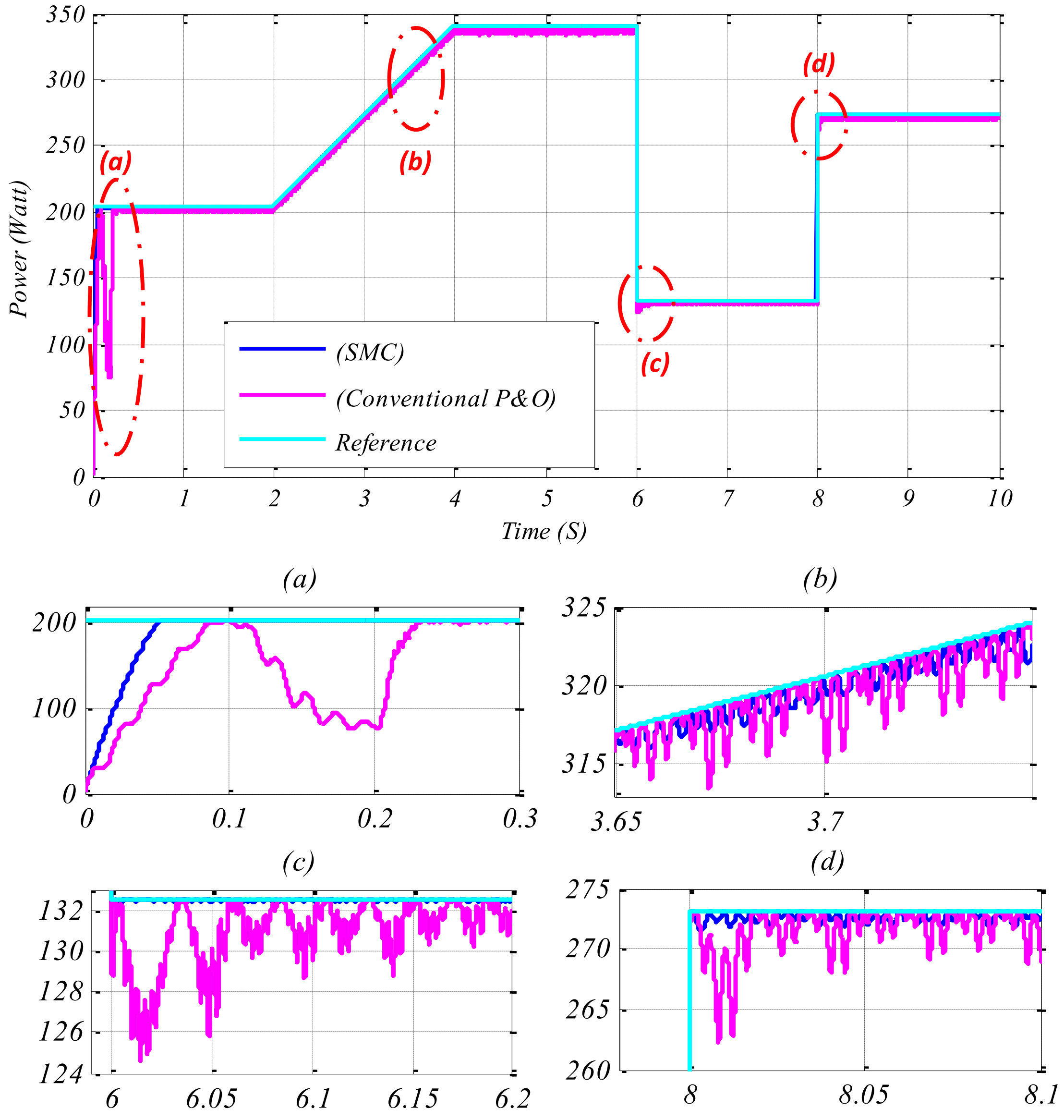

Figure IV.12 : Output PV Power waveform under variable illumination.

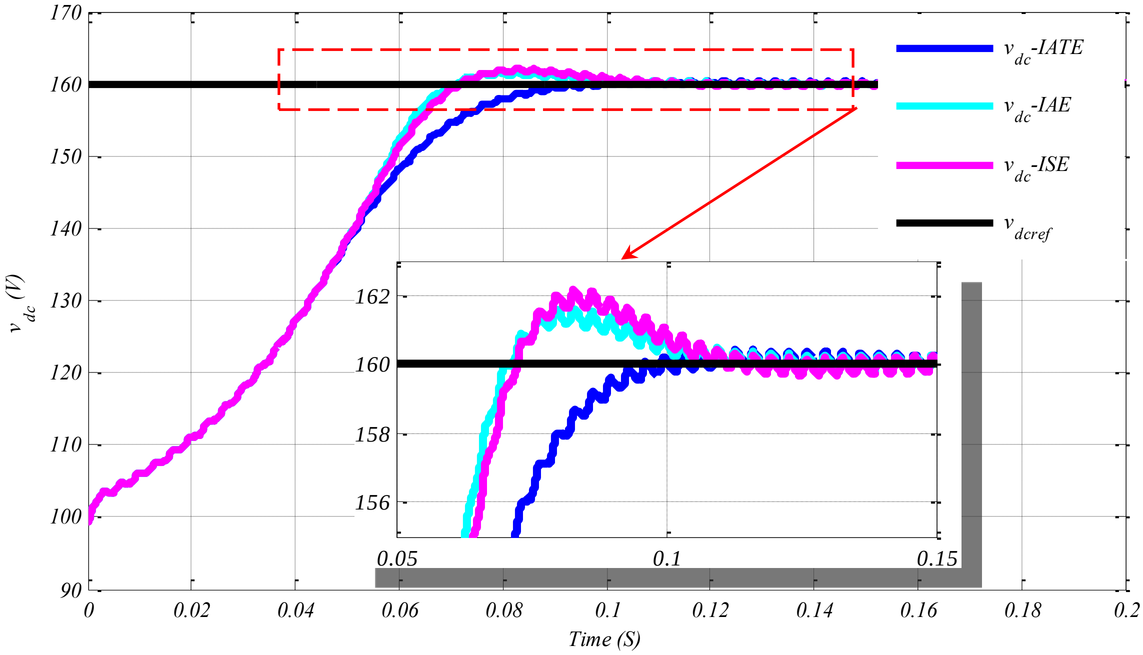

Figure IV.13 : Convergence of DC side voltage using different objective functions.

The output power of PV generator using Sliding mode MPPT based PSO is compared to that obtained using a conventional P_O algorithm. As it is noticed on the curves of Figure IV.13. Sliding mode MPPT optimized by PSO perfectly follows the theoretical reference. It follows the maximum power with a very good stability and lower oscillation. Although , the panels are still at their optimal power despite the sudden variation of illumination. In addition, the proposed MPPT reaches the MPP with a very short convergence time when compared to a P_O algorithm.

Figure IV.13 depicts the convergence of DC bus voltage after employing the enhanced anti-windup PI parameters in all cases . It is clearly deduced that Anti-windup-PSO based on ITAE objective function can reduce voltage overshoot and offer lowest settlement time. Thus, the optimized gains obtained in the case of ITAE objective function are adopted in all experiments.

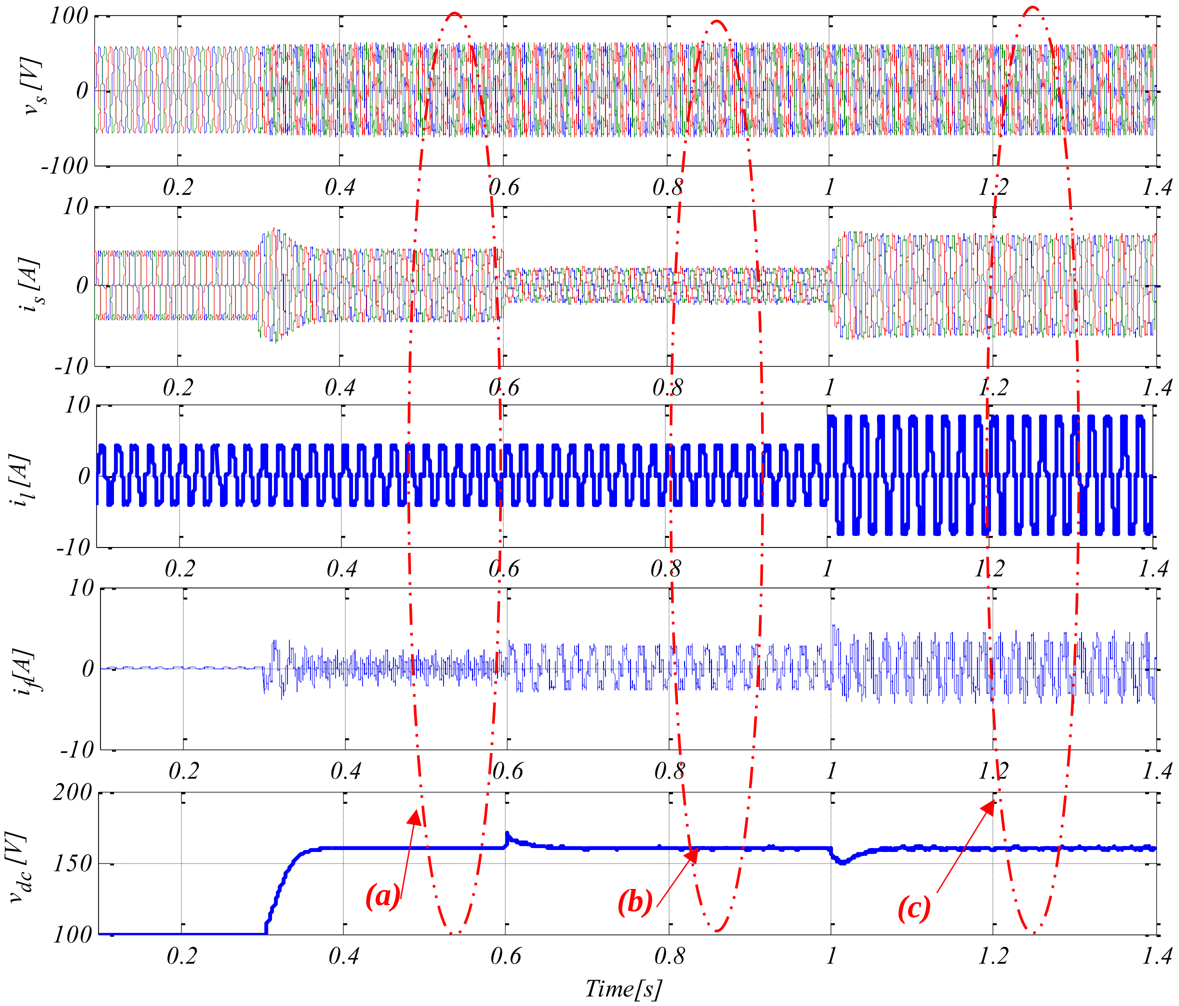

Figure IV.14 : Simulation results under different operating conditions.

Figure IV.14 shows simulation results during connecting the SPAF and inserting the PV system. Firstly, SAPF is connected at *t= 0.3 s*, The system starts the compensation where the source provides the necessary fundamental current to the load and harmonics are ensured by SAPF . Once PV system is connected at *t=0.6s*, it injects its maximum power into the grid and the source ensure the remain, although the source current presents variation in amplitude due to the injected current from the PV system , whereas the form remains quasi-sinusoidal during the variations.

Regarding the DC bus voltage, follows its reference and it stays constant all over the experiment with low overshoot voltage at the moment of connecting the PV system and small undershoot voltage once the load is increased.

(a)

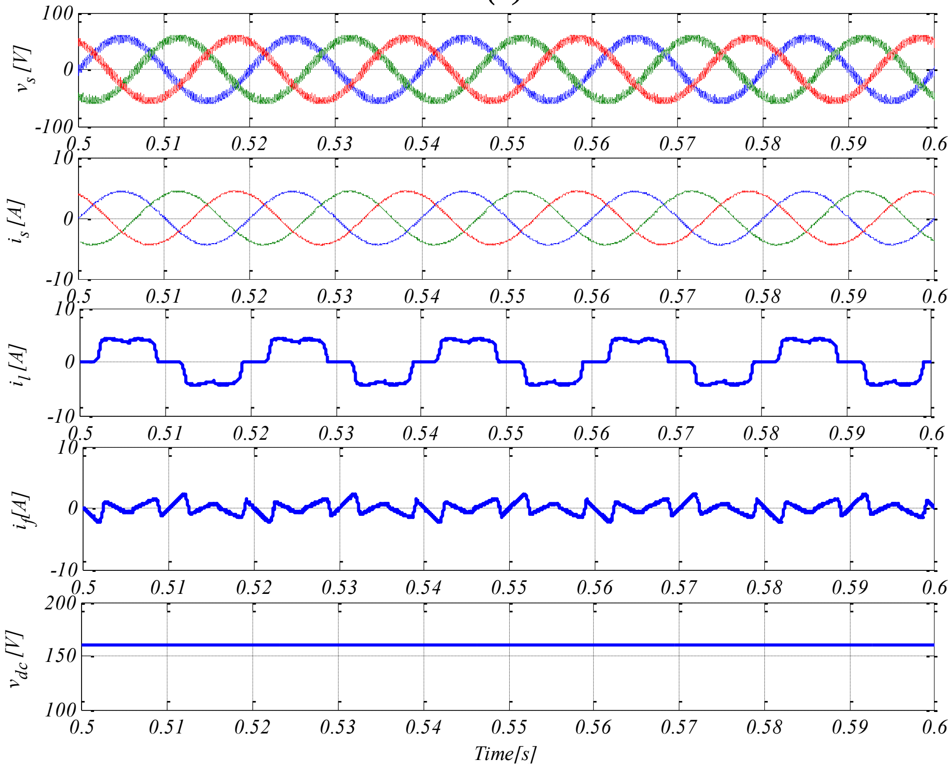

Figure IV.15: Simulation results when SAPF is operating and PV system is disconnected *(a)*.

(b)

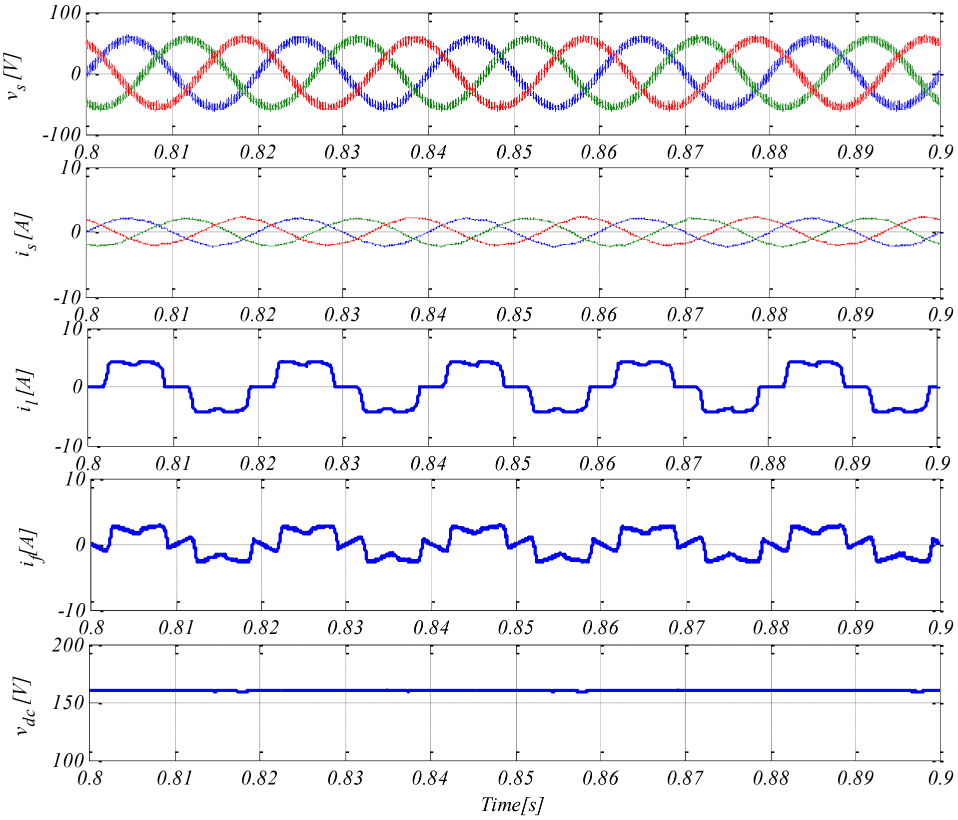

Figure IV.16 : Simulation results when SAPF and PV system are operating *(b)*.

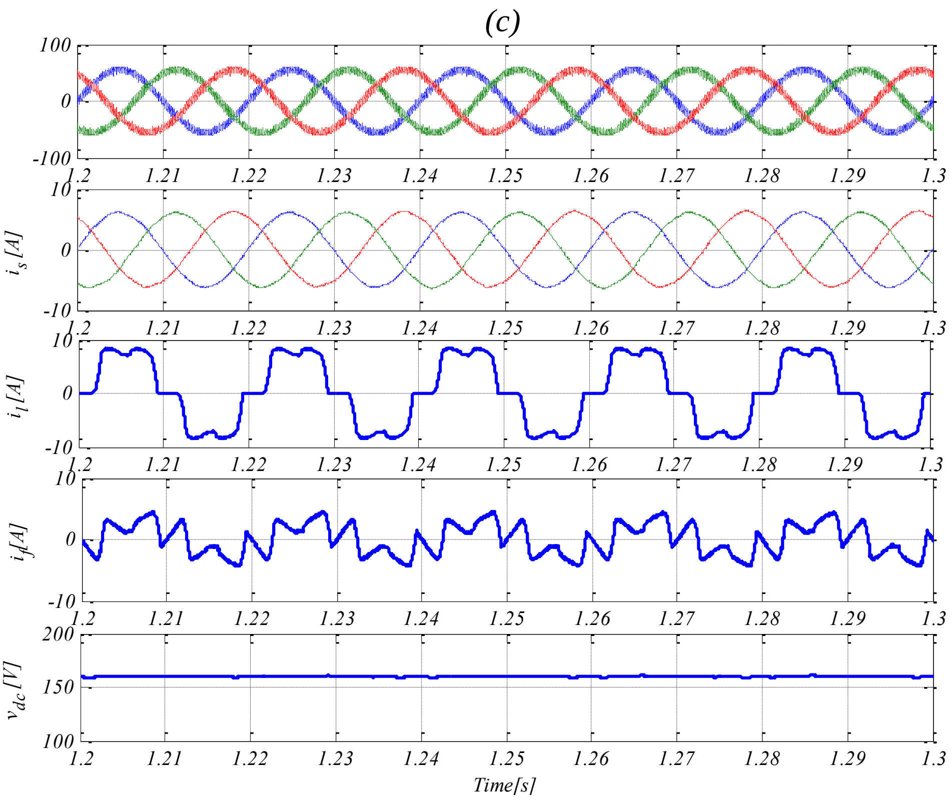

Figure IV.17 : Simulation results when the load is increased *(c).*

It is worthy to mention that the injected current in the state of absence of PV system is different from that injected during the presence of PV, because the first contains only harmonic and reactive current but the second contains harmonic, reactive and active current.

It is observed in Figure IV.18 that the source active power is directly influenced by the injected photovoltaic power and the load demand. Whereas, the reactive energy continues to oscillate around zero to ensure the power factor correction.

The source current waveform, after connecting the proposed system, has been analyzed to evaluate its THD, It can be deduced that the proposed contains less harmonics in source current as presented in Figure IV.19 with a THD equal to 1.94 % after connecting SAPF-PV.

Simulation results in steady state and in various transient states show good performance, thanks to this strategy of control, P-DPC-SVM for grid connected PV system, the system presents very interesting dynamic performance in terms of time response and steady state error with very acceptable harmonic current distortion (confirms IEEE standars-519).

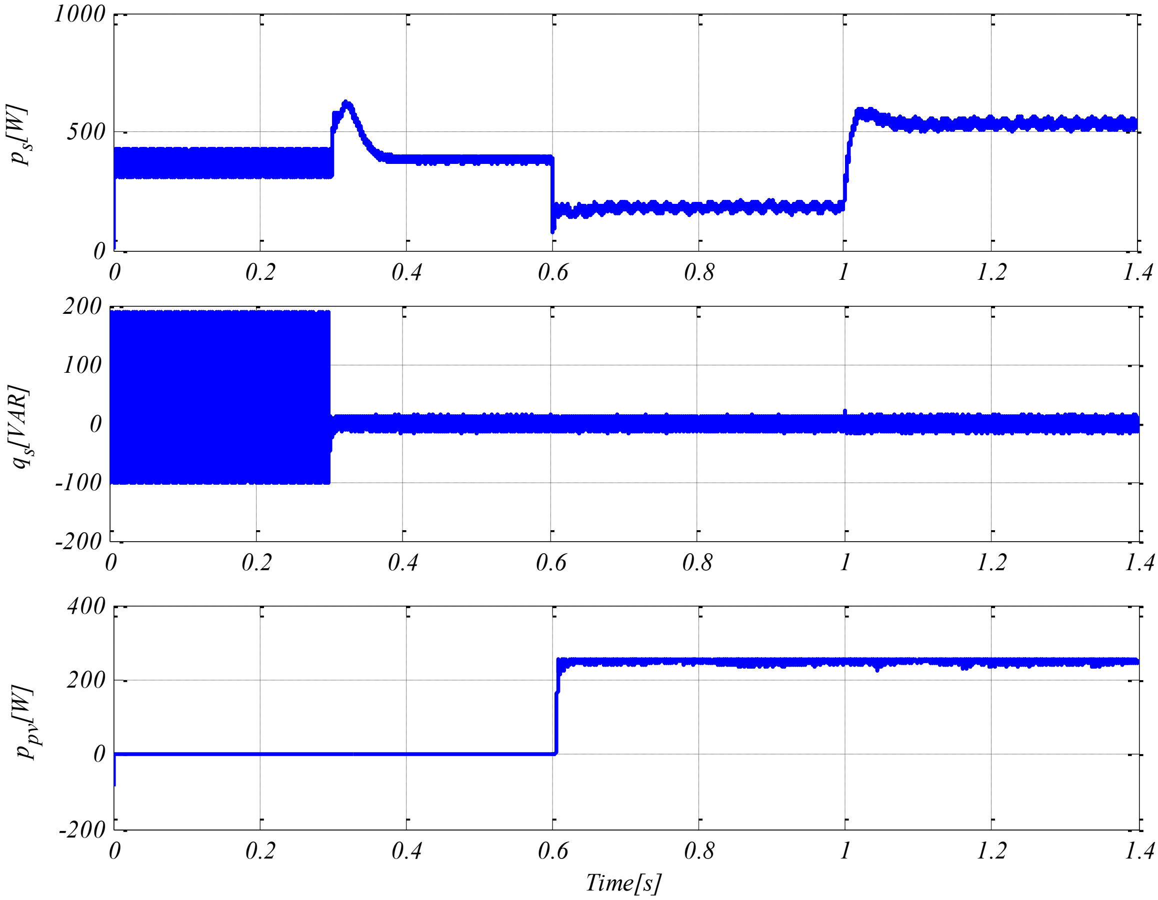

Figure IV.18 : Simulation results of source power and PV power under different operating conditions.

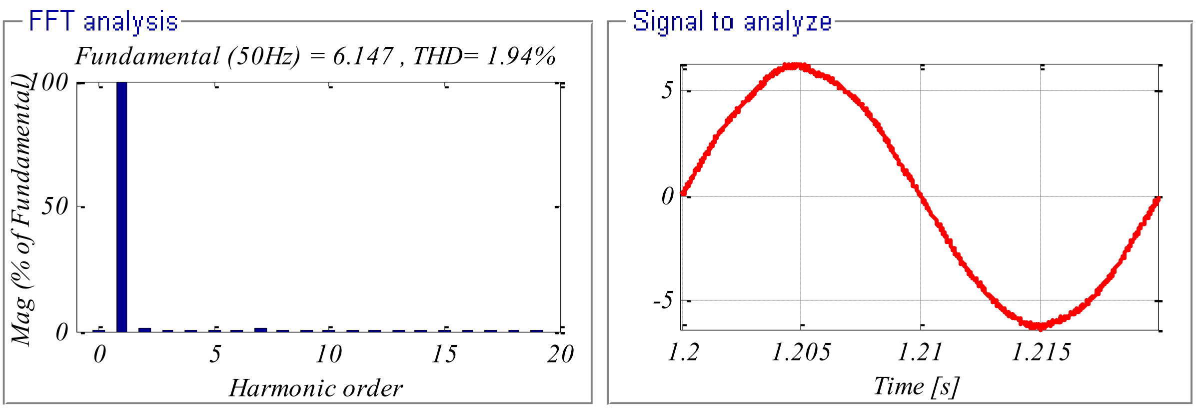

Figure IV.19 : Simulated FFT analysis of source current after connecting PV system .

IV.6. Experimental results

The proposed system has been investigated in an experimental test bench developed in the laboratory as shown in Figure IV.20 . The experimental pattern is designed for low voltage rate due to laboratory limitations. It consists mainly of the following:

- Three phase power supply based on three-phase autotransformer.
- Two-level inverter and boost converter manufactured by SEMIKRON based on IGBTs (SKM 50 GB 123D) in addition to three-phase diode bridge rectifier.
- Measurement and visualization tools.
- Coils and resistor load.
- Four PV Panels (ALPV85-125M-36).

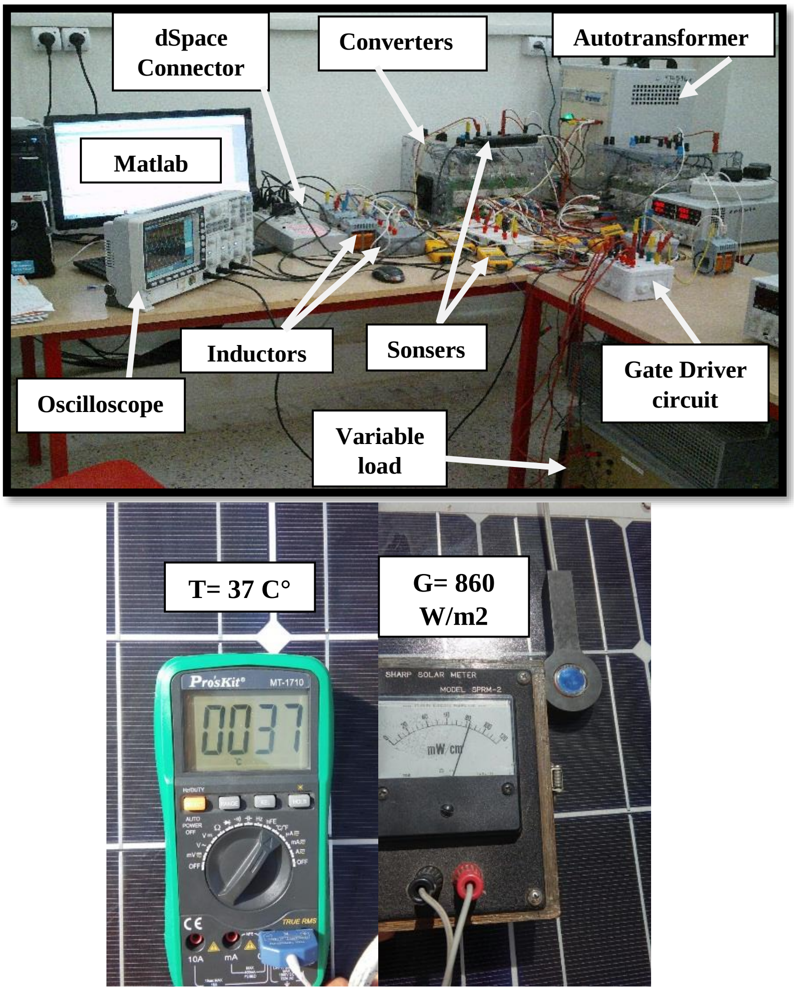

Figure IV.20 : Experimental test bench in LMSE laboratory.

For real-time implementation dSpace 1104 is used, the computing time of the process is set to the lowest possible sample time of the DSP *(10^{-4} s)*. The detailed system parameters are given in Table A.1 (see Appendix).

The installation of the PV modules depends on its geographical location. It is necessary to choose the optimal orientation and inclination for the location. This allows producing a maximum of energy. The modules are oriented south (azimuth 0 °) and inclined 34.8 ° relative to the horizontal which is the optimum tilt angle in that location as demonstrated in [108].

(a)

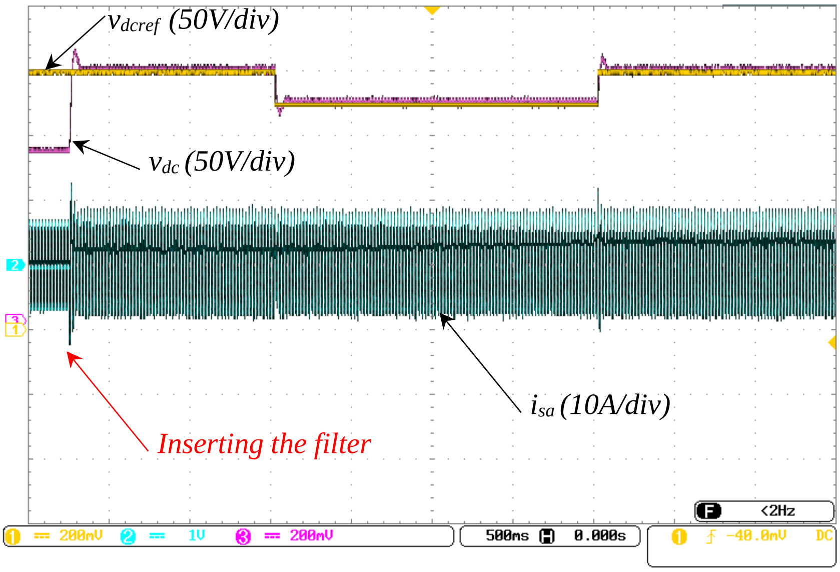

(b)

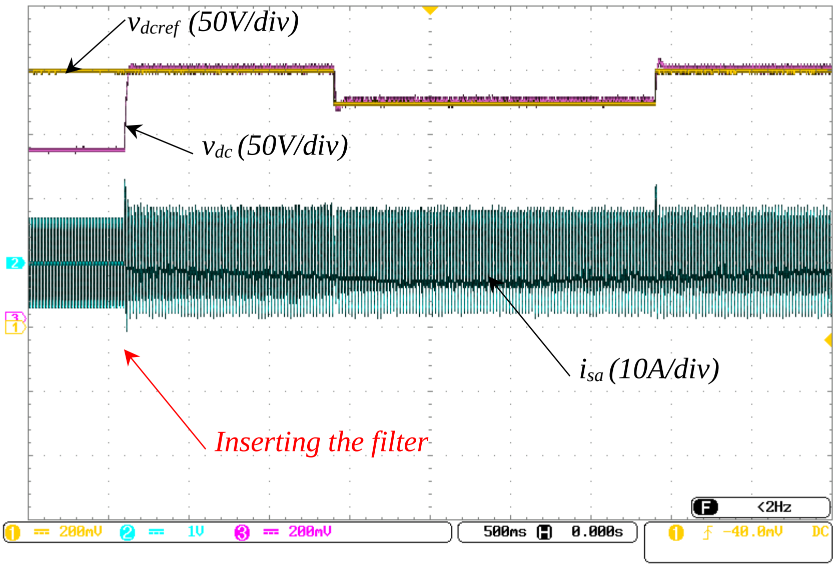

Figure IV.21 : Response of DC bus voltage under double step change of voltage reference based on conventional *(a)* and optimized *(b)* anti-windup PI controller.

The performance of PSO-PI with anti-windup is compared to that of the conventional PI controller, the response of each one under double step change of DC bus voltage from 160V to 140V and vice versa are shown in Figure IV.21. It is noticed that PSO-PI with anti-windup can improve the transient state by dipping overshoot and upper shoot of DC-link voltage as well as providing much-reduced settling time. Therefore, the supply current is not highly affected by DC-link voltage variation after using the anti-windup PI controller. The proposed system was

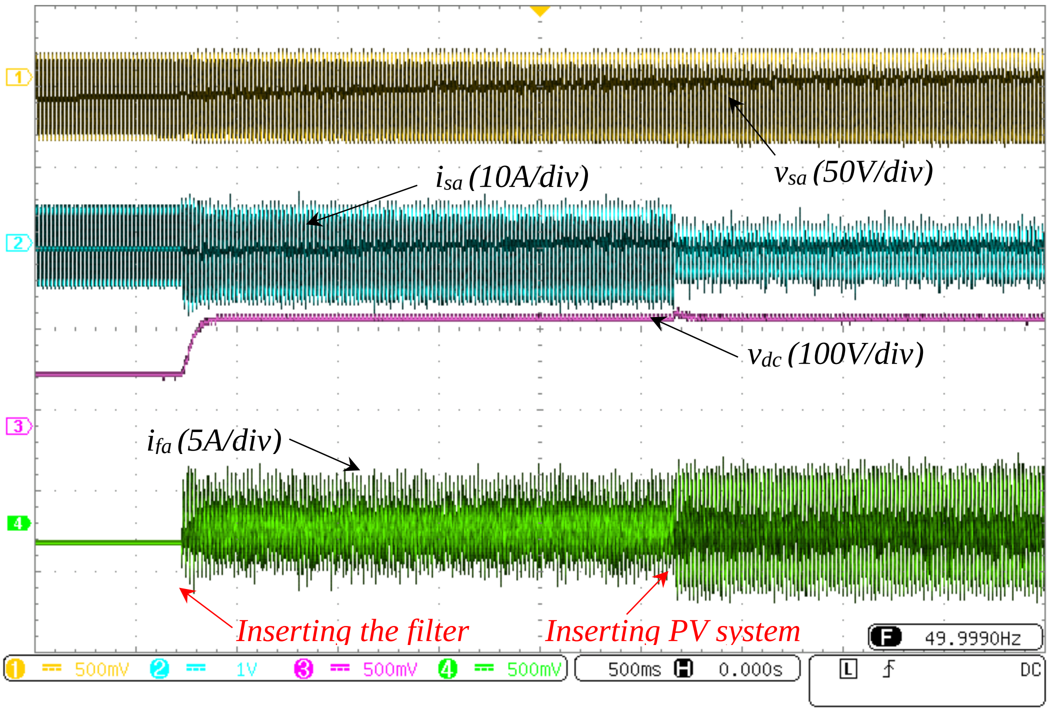

Figure IV.22 : Experimental results of *(v_s)*, source current *(i_s)*, DC bus voltage *(v_{dc})*, filter current *(i_f)* under different operating conditions.

designed to operate as shunt active power filter (SAPF) when the PV system is disconnected (lack of illumination); it performs the power quality improvement by reducing the current harmonics of the source and enhance its power factor but once the PV system is connected (exist of illumination), additional active power is injected into the load/grid. After connecting the PV system, in Figure IV.22, it is noticed that the current provided by the main source is reduced, the injected current is increased, the PV power is different to zero whereas the active power provided by the source is reduced. The experimental tests were done in real time under the following conditions *(T=37 C° and G= 860 W/ m2).* In this test, the fixed tilt ground-mounted PV string provides its maximum available *power (240 W)* to the load and the grid ensures the rest needed power.

The investigated scenarios of the proposed system operation are summarized in Figure IV.22. It shows the results in three different phases; before connecting the inverter (filter) into the grid, after connecting the inverter into the grid (filtering phase), during the operation of the PV system. Before connecting the filter, the load supplied directly by the source that offers the needed active and reactive power simultaneously and harmonic currents. Once the filter is connected, the inverter provides the needed reactive power and the harmonic currents to the load in order to make the source operates with unity power factor and suppress the higher order harmonic components. Then, after connecting the PV system the inverter performs three main functions which are reactive power compensation, active power injection by PV system) as well as source current filtering.

The three phases are clearly demonstrated by the source and injected current waveform, DC bus voltage in addition to active and reactive power waveform.

It is noticed in Figure IV.23 that the injected current after connecting PV system has a different waveform as compared to that obtained in the absence of PV system because it is included harmonic current, reactive current as well as active current provided by PV panels. However, the active current does not exist before connecting PV system.This results is clearly confirmed in Figure IV.24.

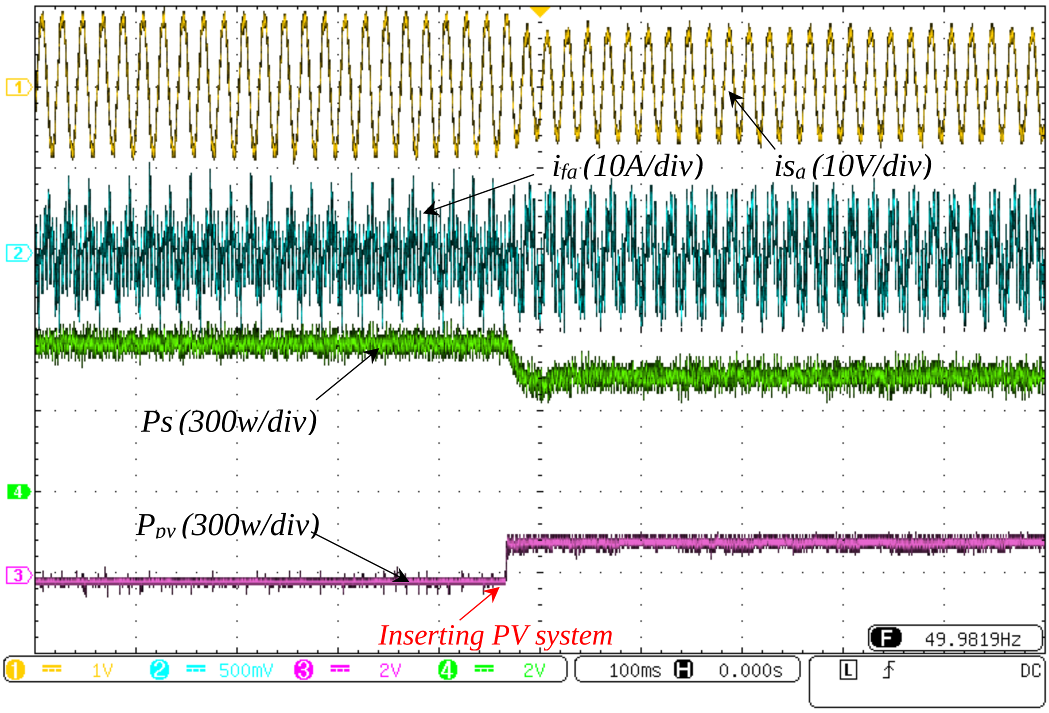

Figure IV.23 : Experimental results of *(v_s)*, source current *(i_s)*, source active power *(p_s)*, PV power *(p_{pv})* during the connection of PV system.

Figure IV.25 shows the spectrum analysis of the main source current when the PV system is connected. It is clearly noticed that higher order harmonics are effectively suppressed and only the 5th and 13th harmonics appear in the spectrum graph with small magnitude, which prove the proficiency of the proposed system in suppressing harmonic currents in addition to PV power injection. The measured $THD_{is} = 6.16$, this results can be improved by using high performance control board that allows achieving lower sampling time.

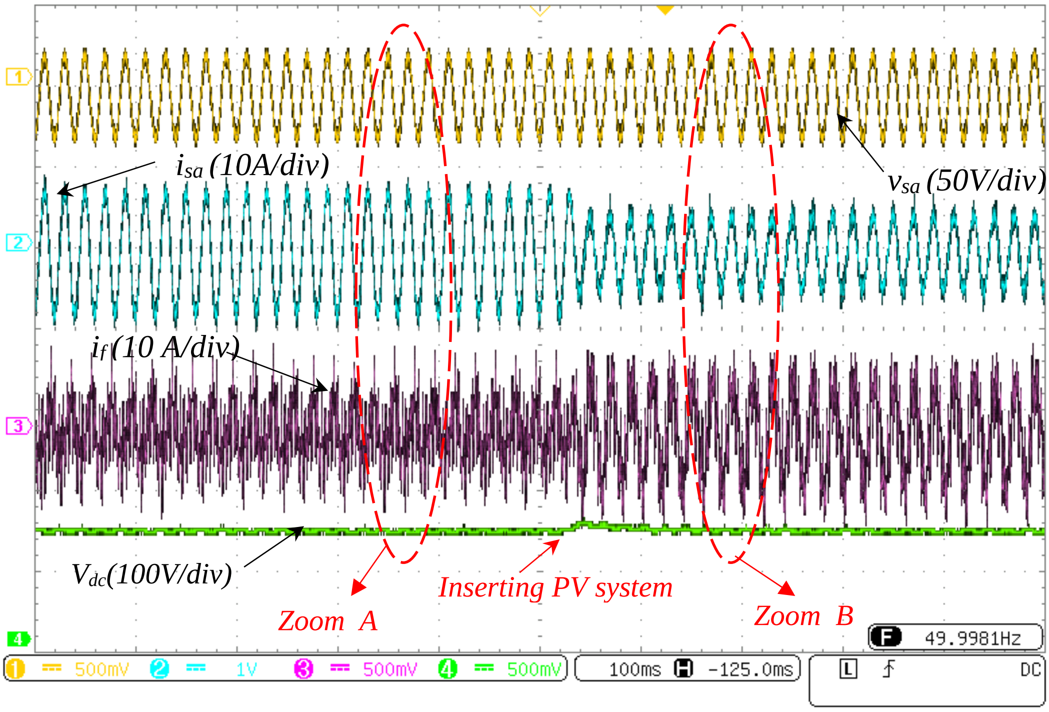

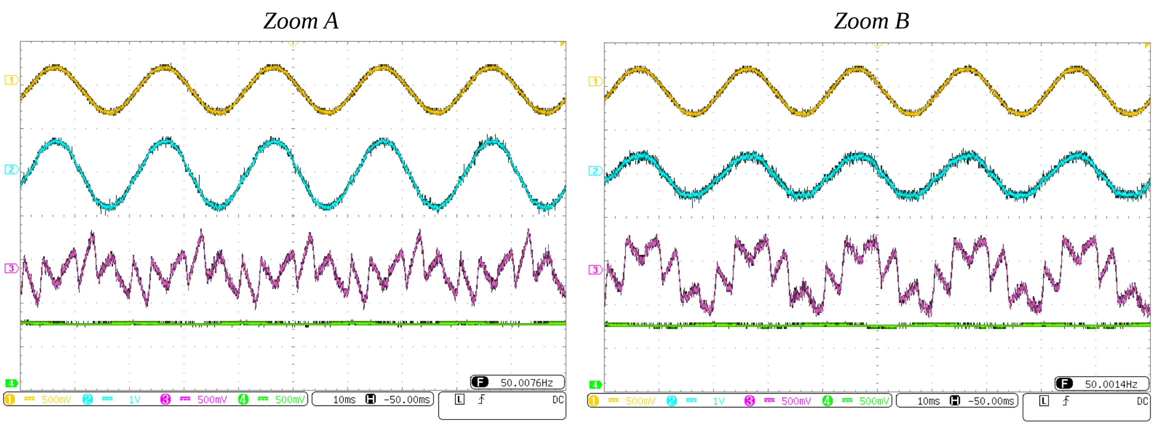

Figure IV. 24 : Experimental results of *(v_s)*, source current *(i_s)*, filter current *(i_f)*, DC bus voltage *(v_{dc})* during the connection of PV system.

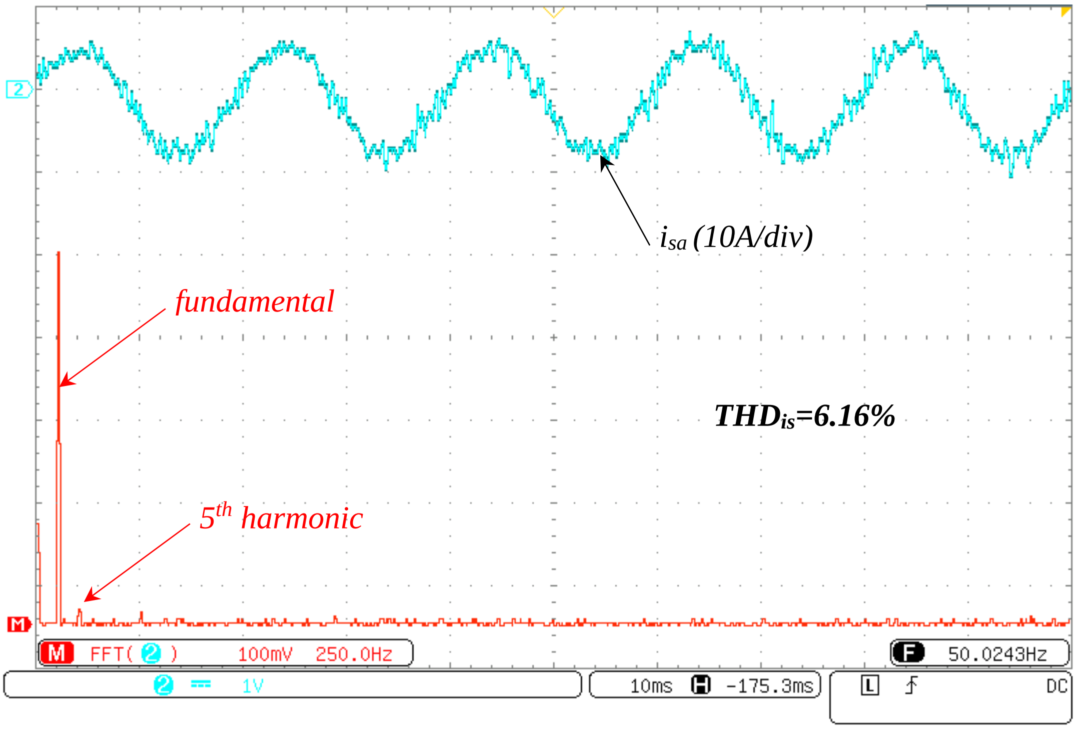

Figure IV. 25 : Experimental FFT analysis of source current after connecting PV system.

IV.7. Conclusion

In this chapter, P-DPV- SVM for double function grid-tied PV system has been designed and validated in an experimental prototype. The proposed control scheme replaces the cost function block of the MPC approach by SVM to operate at fixed and low switching frequency, enhance the performance of the system and to prevent the reliability of its hardware components. One important feature that characterizes this control strategy is the simplicity of implementation; it does not need the coordinate transformation of system variables into rotating reference frame (d–q) as well as current control loops. In addition, it does not need current harmonic extraction stage, which reduces the number of required sensors and minimize the cost and the size of SAPF. likewise decreases the computing time and improve the accuracy. Furthermore, the voltage control vectors are calculated without using linear controllers. The efficiency of the developed SM-MPPT based PSO algorithm has been clearly demonstrated during a sudden change in illumination. Then again, PSO algorithm demonstrates its capability to design optimal anti-windup PI controller that can improve the control of DC side of the inverter. The obtained results in different operating conditions demonstrate the efficiency of the proposed control scheme in terms of harmonic current filtering, power factor correction, DC bus voltage regulation as well as PV power injection.

General Conclusion

In this thesis, we presented our contribution to the study of Shunt active power filter connected to a photovoltaic system (PV). The advantage of this system is the production of electricity (PV) using clean and renewable energy source to with an active power filter to ensure a good power quality.

After a detailed study of the problem of harmonics in the electrical networks, their effects, their origins and the regulations to limit this phenomenon, several types of passive, active and hybrid filters have been studied in order to select the there-phase shunt active filter as an effective device for current harmonics elimination and reactive power compensation.

Three control techniques have been used to control the compensation system, direct power control (DPC) that based on predefined switching table, Finite-control-set (FCS-MPC) . These two control approach provides satisfactory results. However, they operate with variable switching frequency. Predictive direct power control (P-DPC-SVM) is proposed to overcome the variable switching frequency issue. Simulation results have been validated experimentally and confirm the superiority of FCS-MPC against P-DPC-SVM and DPC. However, the difference in performance is not so far.

PI control with anti-windup is the most used in DC bus voltage regulation for shunt active power filter. In this study, we used Particle Swarm Optimization algorithm to optimize its parameters. According to the simulation results obtained, an improvement in the dynamic performance is observed with a short response time and fewer oscillations around the reference voltage even under load variation.

Subsequently, Robust PSO-Sliding mode based Maximum Power Point (MPPT) tracking approaches were developed and validated by the simulation and experimentally. The simulation results show their superiority against conventional P-O algorithm. The choice of the MPPT technique is based on several factors such as speed, stability, cost of implementation, simplicity and robustness.

In addition, we selected P-DPC-SVM technique because of its simplicity, operation with low and fixed switching frequency in addition to low computation requirements. The simulation results show the effectiveness of overall system (SAPF-PV) under different operating conditions such as variable illumination and load variations with good static and dynamic performance. All the simulation results obtained were validated experimentally using a dSPACE-1104 based test bench.

Our perspectives to this study are:

- Implementation of these control algorithms on high-level inverters and new topologies of multi-level inverters.
- Using virtual-flux approach to reduce the cost and improve the efficacy.
- Using different renewable energy sources with power management system.

References

[1] A. Krama, L. Zellouma, B. Rabhi, S.. Refaat, M. Bouzidi, Real-Time Implementation of High Performance Control Scheme for Grid-Tied PV System for Power Quality Enhancement Based on MPPC-SVM Optimized by PSO Algorithm, Energies. 11 (2018) 3516. doi:10.3390/en11123516.

[2] Renewables Global Status Report, Renewable Energy Policy Network for the 21st Centuray (REN21), 2019. https://www.ren21.net/.

[3] M.F. Arman, An ‘ Active ’ Passive -Filter Topology for Low Power DC / AC Inverters (PhD thesis), Brunel University, London, UK, 2011.

[4] D. Ould Abdeslam, Techniques neuromimétiques pour la commande dans les systémes électriques : application au filtrage actif parallèle dans les réseaux _electriques basse tension (PhD thesis), University of Haute-Alsace, France, 2005.

[5] K. Alexander, T.T. Marc, Power Quality in Electrical Systems, McGraw-Hil, 2007.

[6] T. MAHNI, Etude et Conception d’un Filtre Actif Paralléle Triphasé à Quatre Fils en vue de sa Commande par des Méthodes d’Intelligence Arti ficiélle (PhD thesis), University of Biskra, Algeria, 2017.

[7] D.L. rosa Francisco, HARMONICS AND POWER SYSTEMS, CRC Press, Taylor & Francis Group, 2006.

[8] H. Akagi, E.H. Watanabe, M. Aredes, INSTANTANEOUS POWER THEORY AND APPLICATIONS TO POWER CONDITIONING, WILEY-INYERSCIENCE A JOHN WILEY & SONS, INC., PUBLICAYION, 2007.

[9] A. Emadi, N. Abdolhosein, S. Bekiarov, Uninterruptible Power Supplies and Active Filters, CRC Press Web, 2005.

[10] G.R. Rey, L.M. Muneta, POWER QUALITY HARMONICS ANALYSIS AND REAL MEASUREMENTS DATA, InTech, 2011.

[11] liew AH-Choy, Excessive Neutral Currents in Three-phase Fluorescent Lighting Circuits, IEEE Trans. Ind. Appl. 25 (1989) 776–782.

[12] M. Malinowski, Sensorless Control Strategies for Three - Phase PWM Rectifiers (PhD thesis), University of Warsaw, Poland, 2001.

[13] E.C.A. MATUS, ANALYSIS AND DESIGN OF NEW HARMONIC MITIGATION APPROACHES (PhD thesis), Texas A&M University, USA, 2012.

[14] IEEE Recommended Practices and Requirements for Harmonic Control of Electrical Power systems, IEEE Standards. 519-1992, 1993.

[15] C. P. Arnold, R. M. Duke, J. Arrillaga, TRANSIENT STABILITY IMPROVEMENT USING THYRISTOR CONTROLLED QUADRATURE VOLTAGE INJECTION Ys, IEEE Trans. Power Appar. Syst. (1981) 1382–1388.

[16] B. Singh, A. Chandra, K. Al-Haddad, Power Quality Problems and Mitigation Techniques, John Wiley and Sons Ltd, 2015. doi:10.1002/9781118922064.

[17] A. MEHDI TOWLIAT, Integrated Electric Alternators / Active Filters (PhD thesis), Texas A&M University, USA, 2004.

[18] H. Zubi, A Genetic Algorithm Approach for Three- Phase Harmonic Mitigation Filter Design (PhD thesis), University of Bath, UK, 2013.

[19] M. El-Habrouk, A new configuration for shunt active filters (PhD thesis), University of BRUNEL, UK, 1998.

[20] L. Zellouma, B. Rabhi, A. Krama, A. Benaissa, M.F. Benkhoris, Simulation and real time implementation of three phase four wire shunt active power filter based on sliding mode controller, Rev. Roum. Des Sci. Tech. Ser. Electrotech. Energ. 63 (2018) 77–82.

[21] A. Dastfan, Active power filter with minimum components (PhD thesis), University of Wollongong, Australia, 1998.

[22] B. Singh, K. Al-Haddad, A. Chandra, A Review of active filters for power quality improvement, IEEE Trans. Ind. Electron. 46 (1999) 960–971. doi:10.1109/41.793345.

[23] F. Fukuda, M. Yamaji, Design and Characteristics of Active Power Filter Using Current Source Converter, in: IEEE IAS Annu. Meet. Proc., 1990: pp. 965–970.

[24] H. Akagi, Trend in Active Power Line Conditioners, in: IEEE Int. Conf. Ind. Electron. Control. Instrum., 1992: pp. 19–24.

[25] T.M. Gruzs, A Survey of Neutral Current in Three-Phase Computer Power Systems, IEEE Trans. Ind. Appl. Vol (1990) 719–725.

[26] P. Enjeti, W. Shireen, P. Packebush, I. Pitel, Analysis and Design of New Active Power Filter to Cancel Neutral Current Harmonics in Three Phase Four Wire Electric Distribution System, in: IEEE Ind. Appl. Meet., Toronto, Canada, 1993: pp. 939–946.

[27] A. Ghamri, T. Mahni, M.T. Benchouia, K. Srairi, A. Golea, Comparative Study between Different Controllers used in Three-phase Four-wire Shunt Active Filter, Energy Procedia. 74 (2015) 807–816. doi:10.1016/j.egypro.2015.07.816.

[28] H. Fujita, H. Akagi, A Practical Approach to Harmonic Compensation in Power Systems-Series Connection of Passive and Active Filters, IEEE Trans. Ind. Appl. 27 (1991) 1020–1025.

[29] A.H. Varjani, Harmonic control techniques for inverters and adaptive active power filters (PhD thesis), University of Wollongong, Australia, 1998.

[30] W.M. Grady, M.J. Samotyj, A.H. Noyola, Survey of Active Power Line Co.nditioning Methodologies, Ieee Trans. Power Deliv. 5 (1990).

[31] H. Akagi, y Kanazawa, A. NABAE, Instantaneous reactive power compensators comprising switching devices without energy storage components, IEEE Transsactions Ind. Appl. IA-20 (1984) 625–630.

[32] S. Saad, L. Zellouma, Fuzzy Logic Controller for Three-phase Shunt Active Filter Compensating Harmonics and Reactive Power Simultaneously, Electr. Power Syst. Res. 79 (2009) 1337–1341. doi:10.1016/j.epsr.2009.04.003.

[33] S. Bhattacharya, D. Divan, Synchronous frame based controller implementation for a hybrid series active filter system, in: IEEE-IAS Annu. Meet., 1995: pp. 2531–2540.

[34] M.T. Benchouia, I. Ghadbane, A. Golea, K. Srairi, M.E.H. Benbouzid, Implementation of adaptive fuzzy logic and PI controllers to regulate the DC bus voltage of shunt active power filter, Appl. Soft Comput. J. 28 (2015) 125–131. doi:10.1016/j.asoc.2014.10.043.

[35] C.E. Lin, W.F. Su, S.L. Lu, C.L. Chen, C.L. Huang, Operation strategy of hybrid harmonic filter in

demand-side system, in: IEEE-IAS Annu. Meet., 1995: pp. 1862–1866.

[36] S.A. Larrinaga, Predictive Control of the 2L-Vsi and 3L-Npc Vsi Based on Direct Power Control for Mv Grid- Connected Power Applications (PhD thesis), University of Mondragon, Spain, 2007.

[37] A. Bouafia, F. Krim, J.-P. Gaubert, Fuzzy-Logic-Based Switching State Selection for Direct Power Control of Three-Phase PWM Rectifier, IEEE Trans. Ind. Electron. 56 (2009) 1984–1992. doi:10.1109/TIE.2009.2014746.

[38] M.J. M. Malinowski M. P. Kazmierkowski, Simple Direct Power Control of Three-Phase PWM Rectifier Using Space Vector Modulation, In. Proc. EPE-PEMC 2002. 8368 (2002) CD-ROM. doi:10.1080/09398368.2003.11463529.

[39] J. Rodriguez, P. Cortes, PREDICTIVE CONTROL OF POWER CONVERTERS AND ELECTRICAL DRIVES, 2012.

[40] T. Ohnishi, Three phase PWM converter/inverter by means of instantaneous active and reactive power control, in: Proc. IECON '91 1991 Int. Conf. Ind. Electron. Control Instrum., IEEE, 1991: pp. 819–824. doi:10.1109/IECON.1991.239183.

[41] I. Takahashi, T. Noguchi, A New Quick-Response and High-Efficiency Control Strategy of an Induction Motor, IEEE Trans. Ind. Appl. IA-22 (1986) 820–827.

[42] J. Rodriguez, P. Cortés, Predictive Control of Power Converters and Electrical Drives, A John Wiley & Sons, Ltd, 2012.

[43] M. Malinowski, M. Jasin, M.P. Kazmierkowski, Simple Direct Power Control of Three-Phase PWM Rectifier Using Space-Vector, IEEE Trans. Ind. Electron. 51 (2004) 447–454. doi:10.1109/TIE.2004.825278.

[44] J. Rodriguez, M.P. Kazmierkowski, J.R. Espinoza, P. Zanchetta, H. Abu-rub, S. Member, H.A. Young, C.A. Rojas, State of the Art of Finite Control Set Model Predictive Control in Power Electronics, IEEE Trans. Ind. Informatics. 9 (2013) 1003–1016. doi:10.1109/TII.2012.2221469.

[45] S.V. and L.G.F. R. P. Aguilera, D. E. Quevedo, Generalized Predictive Direct Power Control for AC / DC Converters, in: 2013 IEEE ECCE Asia Downunder, Melbourne, VIC, VIC, 2013: pp. 1215–1220.

[46] S. Kouro, M.A. Perez, J. Rodriguez, Model Predictive Control: MPC's Role in the Evolution of Power Electronics, IEEE Ind. Electron. Mag. (2015). doi:10.1109/MIE.2015.2478920.

[47] L. Tarisciotti, A. Formentini, A. Gaeta, M. Degano, P. Zanchetta, R. Rabbeni, M. Pucci, Model Predictive control for Shunt Active Filters with Fixed Switching Frequency, IEEE Trans. Ind. Appl. PP (2016). doi:10.1109/TIA.2016.2606364.

[48] A. Razali, A. Rahman, G. George, N. Rahim, Analysis and Design of New Switching Look-Up Table for Virtual Flux Direct Power Control of Grid Connected Three Phase PWM AC-DC Converter, IEEE Trans. Ind. Appl. 9994 (2014) 1–1. doi:10.1109/TIA.2014.2344503.

[49] M. Cichowlas, PWM Rectifier with Active Filtering, PhD Thesis,. (2004) 1–154.

[50] H. Akagi, A. Nabae, S. Atoh, Control Strategy of Active Power Filters Using Multiple Voltage-Source PWM Converters, Ieee Trans. Ind. Appl. IA-22 (1986) 460–465. doi:10.1109/TIA.1986.4504743.

[51] A. Chaoui, J.-P. Gaubert, F. Krim, Power quality improvement using DPC controlled three-phase shunt active filter, Electr. Power Syst. Res. 80 (2010) 657–666. doi:10.1016/j.epsr.2009.10.020.

[52] A. Krama, L. Zellouma, B. Rabhi, ANTI-WINDUP PROPORTIONAL INTEGRAL STRATEGY FOR

SHUNT ACTIVE POWER FILTER INTERFACED BY PHOTOVOLTAIC SYSTEM USING TECHNIQUE OF DIRECT POWER CONTROL, Rev. Roum. Sci. Techn.– Électrotechn. Énerg. 62 (2017) 252–257.

[53] P. Cortés, M.P. Kazmierkowski, R.M. Kennel, D.E. Quevedo, J. Rodriguez, Predictive control in power electronics and drives, IEEE Trans. Ind. Electron. 55 (2008) 4312–4324. doi:10.1109/TIE.2008.2007480.

[54] P. Antoniewicz, Predictive Control of Three Phase AC/DC Converters (PhD thesis), WARSAW UNIVERSITY OF TECHNOLOGY, Poland, 2009.

[55] L. Zellouma, A. Krama, B. Rabhi, M.F. Benkhoris, M. Bouzidi, A. Benaissa, Design and Experimental Investigation of Predictive Direct Power Control of Three-Phase Shunt Active Filter with Space Vector Modulation using Anti-windup PI Controller Optimized by PSO, Arab. J. Sci. Eng. (2018). doi:10.1007/s13369-018-3611-6.

[56] S. Kouro, P. Cortes, R. Vargas, U. Ammann, J. Rodriguez, Model Predictive Control-A Simple and Powerful Method to Control Power Converters, IEEE Trans. Ind. Electron. 56 (2009) 1826–1838. doi:10.1109/TIE.2008.2008349.

[57] J. Holtz, S. Stadtfeld, A predictive controller for the stator current vector of ac machines fed from a switched voltage source, in: Proc. IPEC, 1983: pp. 1665–1675.

[58] R. Ottersten, J. Svensson, Vector current controlled voltage source converter - Deadbeat control and saturation strategies, IEEE Trans. Power Electron. 17 (2002) 279–285. doi:10.1109/63.988947.

[59] H. Abu-Rub, J. Guzinski, Z. Krzeminskiand, H.A. Toliyat, Predictive current control of voltage source inverters, IEEE Trans. Ind. Electron. 51 (n.d.) 585–593.

[60] P. Antoniewicz, M.P. Kazmierkowski, Virtual-flux-based predictive direct power control of AC/DC converters with online inductance estimation, IEEE Trans. Ind. Electron. 55 (2008) 4381–4390. doi:10.1109/TIE.2008.2007519.

[61] E. F. Camacho, C. Bordons, Model Predictive Control, Springer-Verlag, 1999.

[62] D.E. Quevedo, R.P. Aguilera, A.P. Marcelo, Model Predictive Control of an AFE Rectifier With Dynamic References, IEEE Trans. Power Electron. 27 (2012) 3128–3136. doi:10.1109/TPEL.2011.2179672.

[63] P. Cortés, J. Rodríguez, P. Antoniewicz, M. Kazmierkowski, Direct Power Control of an AFE Using Predictive Control, IEEE Trans. Power Electron. 23 (2008) 2516–2523.

[64] S. Ouchen, A. Betka, S. Abdeddaim, A. Menadi, Fuzzy-predictive direct power control implementation of a grid connected photovoltaic system, associated with an active power filter, Energy Convers. Manag. 122 (2016) 515–525. doi:10.1016/j.enconman.2016.06.018.

[65] B. Boukezata, J.P. Gaubert, A. Chaoui, M. Hachemi, Predictive current control in multifunctional grid connected inverter interfaced by PV system, Sol. Energy. 139 (2016) 130–141. doi:10.1016/j.solener.2016.09.029.

[66] B. Kahia, A. Bouafia, M. Abdelrahem, Z. Zhang, A. Chaoui, A. Krama, R. Kennel, A predictive direct power control strategy for three-level npc rectifier, in: 2017 5th Int. Conf. Electr. Eng. - Boumerdes, ICEE-B 2017, 2017. doi:10.1109/ICEE-B.2017.8192128.

[67] A. Laib, F. Krim, B. Talbi, A. Kihal, H. Feroura, Improved control of three phase dual-stage grid-connected PV system based on a predictive control strategy, Control Eng. Appl. Informatics. 20 (2018) 12–23.

[68] S. Aurtenechea, M. A. Rodríguez, E. Oyarbide, J.R. Torrealday, Predictive Direct Power Control - A New Control Strategy for DC/AC Converters, in: IEEE Ind. Electron. IECON 2006 - 32nd Annu. Conf., 2006: pp. 1661–1666.

[69] S. Aurtenechea, M. a Rodríguez, E. Oyarbide, J.R. Torrealday, Predictive Control Strategy for DC/AC Converters Based on Direct Power Control, IEEE Trans. Ind. Electron. 54 (2007) 1261–1271. doi:10.1109/TIE.2007.893162.

[70] A. Bouafia, J.-P. Gaubert, F. Krim, Predictive Direct Power Control of Three-Phase Pulsewidth Modulation (PWM) Rectifier Using Space-Vector Modulation (SVM), IEEE Trans. POWER Electron. 25 (2010) 228–236. doi:10.1109/TPEL.2009.2028731.

[71] B. Arif, Real-time grid parameter estimation methods using model based predictive control for grid-connected converters, University of Nottingham, UK, 2015.

[72] T. Geyer, MODEL PREDICTIVE CONTROL OF HIGH POWER CONVERTERS AND INDUSTRIAL DRIVES, John Wiley & Sons, Ltd, 2017.

[73] B. Wu, M. Narimani, HIGH-POWER CONVERTERS AND AC DRIVES, John Wiley & Sons, Inc., Hoboken, New Jersey, 2017.

[74] W. Xiao, Photovoltaic Power System, John Wiley & Sons Ltd, 2017. doi:10.1002/9781119280408.

[75] H.S. Goh, The Effect of Grid Operating Conditionson the Harmonic Performance of Grid-Connected PV Inverters (PhD thesis), Newcastle University, UK, 2001.

[76] E. Karatepe, M. Boztepe, M. Colak, Neural network based solar cell model, Energy Convers. Manag. 47 (2006) 1159–1178. doi:10.1016/j.enconman.2005.07.007.

[77] G. Bhuvaneswari, R. Annamalai, Development of a solar cell model in MATLAB for PV based generation system, Proc. - 2011 Annu. IEEE India Conf. Eng. Sustain. Solut. INDICON-2011. (2011). doi:10.1109/INDCON.2011.6139509.

[78] M.G. Villalva, J.R. Gazoli, E.R. Filho, Comprehensive Approach to Modeling and Simulation of Photovoltaic Arrays, IEEE Trans. POWER Electron. 24 (2009) 1198–1208.

[79] F.H.B. Berba, Minimisation of Output DC Current Component in Grid-Connected Inverters for Solar Power Applications (PhD thesis), University of Newcastle, UK, 2012.

[80] A. Goetzberger V.U. Hoffmann, Photovoltaic Solar Energy Generation, Springer-Verlag Berlin Heidelberg, 2005. doi:10.1109/9.412626.

[81] K.S. Nathan, A Novel DC-DC Converter for Photovoltaic Applications Kumaran (PhD thesis), University of Cambridge, UK, 2018.

[82] M.A.S. Masoum, H. Dehbonei, E. Fuchs, Theoretical and Experimental Analyses of Photovoltaic Systems With Voltage- and Current-Based Maximum Power-Point Tracking, IEEE Trans. Energy Convers. 17 (2002) 514–522.

[83] Y. Levron, D. Clement, B. Choi, C. Olalla, D. Maksimovic, Control of Submodule Integrated Converters in the Isolated-Port Differential Power-Processing Photovoltaic Architecture, IEEE J. Emerg. Sel. Top. Power Electron. 2 (2014) 821–832.

[84] J. Bing, Advances in Commercial Applications of Photovoltaic Technology in North America, in: 2009 Updat. Power Energy Soc. Gen. Meet., 2010: pp. 1–5.

[85] Y. Yang, K.A. Kim, F. Blaabjerg, A. Sangwongwanich, Advances in Grid-Connected Photovoltaic Power

Conversion Systems, Elsevier Ltd, 2019.

[86] Y. Yang, F. Blaabjerg, Overview of single-phase grid-connected photovoltaic sys- tems, Electr. Power Compon. Syst. 43 (2015) 1352–1363.

[87] S. Kouro, J.. Leon, D. Vinnikov, L.G. Franquelo, Grid-connected photovoltaic systems: An overview of recent research and emerging PV converter technology, IEEE Ind. Electron. Mag. 9 (2015) 47–61.

[88] B. Lindgren, Topology For Decentralised Solar Inverters With a Low Voltage AC Bus, in: 8th Eur. Conf. Power Electron. Appl., Lausanne, Switzerland, 1999: pp. 1–10.

[89] A.I. Bratcu, I. Munteanu, S. Bacha, D. Picault, B. Raison, Cascaded DC-DC Converter Photovoltaic Systems: Power Optimization Issues, IEEE Trans. Ind. Electron. 58 (2011) 403–411.

[90] H. Haeberlin, Evolution of inverters for grid connected systems from 1989 to 2000, in: 17th Eur. Photovolt. Sol. Energy Conf., 2001.

[91] T. Esram, P. Chapman, Comparison of Photovoltaic Array Maximum Power Point Tracking Techniques, Energy Conversion, IEEE Trans. Energy Convers. 22 (2007) 439 449.

[92] S.K. Dash, D. Verma, Comparative Analysis of Maximum Power Point (MPP) Tracking Techniques for Solar PV Application using MATLAB Simulink, IEEE Int. Conf. Recent Adv. Innov. Engineeering. (2014) 1–7.

[93] R. Bradai, R. Boukenoui, A. Kheldoun, H. Salhi, M. Ghanes, J.P. Barbot, A. Mellit, Experimental assessment of new fast MPPT algorithm for PV systems under non-uniform irradiance conditions, Appl. Energy. 199 (2017) 416–429. doi:10.1016/j.apenergy.2017.05.045.

[94] P. Sivakumar, A. Abdul Kader, Y. Kaliavaradhan, M. Arutchelvi, Analysis and enhancement of PV efficiency with incremental conductance MPPT technique under non-linear loading conditions, Renew. Energy. 81 (2015) 543–550. doi:10.1016/j.renene.2015.03.062.

[95] B. Talbi, F. Krim, T. Rekioua, S. Mekhilef, A. Laib, A. Belaout, A high-performance control scheme for photovoltaic pumping system under sudden irradiance and load changes, Sol. Energy. 159 (2018) 353–368. doi:10.1016/j.solener.2017.11.009.

[96] S.A. Rizzo, G. Scelba, ANN based MPPT method for rapidly variable shading conditions, Appl. Energy. 145 (2015) 124–132. doi:10.1016/j.apenergy.2015.01.077.

[97] A. Menadi, S. Abdeddaim, A. Betka, M.T. Benchouia, Real Time Implementation of A Fuzzy Logic Based Mppt Controller for Grid Connected Photovoltaic System, ISA Trans. 5 (2015).

[98] B. Castillo-Toledo, R. Castro-Linares, On robust regulation via sliding mode for nonlinear systems, Syst. Control Lett. 24 (1995) 361–371. doi:10.1016/0167-6911(94)00039-X.

[99] A. Krama, L. Zellouma, B. Rabhi, A. Laib, Fuzzy Logic Controller for Improving DC Side of PV Connected Shunt Active Filter Based on MPPT Sliding Mode Control, in: Int. Conf. Artif. Intell. Renew. Energ. Syst., 2018: pp. 224–235. doi:10.1007/978-3-319-73192-6_23.

[100] Y. Levron, D. Shmilovitz, D.S. Yoash Levron, Maximum Power Point Tracking Employing Sliding Mode Control, IEEE Trans. Circuits Syst. I Regul. Pap. 60 (2013) 724–732. doi:10.1109/TCSI.2012.2215760.

[101] L. Zellouma, B. Rabhi, A. Krama, A. Benaissa, M.F. Benkhoris, Simulation and real time implementation of three phase four wire shunt active power filter based on sliding mode controller, Rev. Roum. Des Sci. Tech. Ser. Electrotech. Energ. 63 (2018) 77–82.

[102] R. Eberhart, J. Kennedy, A new optimizer using particle swarm theory, in: Proc. Sixth Int. Symp. Micro

Mach. Hum. Sci., 1995: pp. 39–43. doi:10.1109/MHS.1995.494215.

[103] F. vandenBergh, A.P. Engelbrecht, A Cooperative Approach to Particle Swarm Optimization, IEEE Trans. Evol. Comput. 8 (2004) 225–239. doi:10.1109/TEVC.2004.826069.

[104] J. Sun, C. Lai, X. Wu, Particle Swarm Optimization: Classical and Quantum Perspectives, 2012. doi:10.1017/CBO9781107415324.004.

[105] Y. Shi, R. Eberhart, A modified particle swarm optimizer, 1998 IEEE Int. Conf. Evol. Comput. Proceedings. IEEE World Congr. Comput. Intell. (Cat. No.98TH8360). (1998) 69–73. doi:10.1109/ICEC.1998.699146.

[106] Y. Bekakra, D. Ben Attous, Optimal tuning of PI controller using PSO optimization for indirect power control for DFIG based wind turbine with MPPT, Int. J. Syst. Assur. Eng. Manag. 5 (2014) 219–229. doi:10.1007/s13198-013-0150-0.

[107] H. Lee, J. Lee, Design of iterative sliding mode observer for sensorless PMSM control, IEEE Trans. Control Syst. Technol. 21 (2013) 1394–1399. doi:10.1109/TCST.2012.2199493.

[108] A. Saadi, M. Becherif, H.S. Ramadan, Hydrogen production horizon using solar energy in Biskra, Algeria, Int. J. Hydrogen Energy. 41 (2016) 21899–21912. doi:10.1016/j.ijhydene.2016.08.224.

[109] J.Zhang, H. Cho, R. Luck, P.J. Mago, Integrated photovoltaic and battery energy storage (PV-BES) systems: An analysis of existing financial incentive policies in the US, Appl. Energy. 212 (2018) 895–908.

Appendix

Table A.1: Power circuit parameters

Source	***Vs***	*65 V*
	F	*50 Hz*
	Rs	*0.45 Ω*
	Ls	*0.25 mH*
Load	***Lc***	*1 mH*
	Rc	*0.6 Ω*
	Rl	*11 Ω*
SAPF	***Rf***	*0.9 Ω*
	Lf	*4 mH*
	C1	*1100 µF*
Boost	***L***	*5 mH*
	C2	*560 µF*

Table A.2: Main parameters of PSO Algorithm

Number of particles in a swarm	*50*
Max number of iteration $k_{\max}$	40
Acceleration coefficients c_1, c_2	2
Inertia coefficients $\beta_{\min}, \beta_{\max}$	0.9, 0.6

Table A.3: Optimized and calculated gains.

	Optimized gains	***Calculated gains***
DC bus controller	***Kp=0.176, Ki=6.714, Ga =456.17***	***Kp=0.1, Ki=6.12, Ga=1000*(chosen manually)**
SMC gain	***K= 0.074***	----------

Table A.4: The main parameters of the used PV module.

Parameters of the PV module ALPV85-125M-36	
Maximum power P_{max}	85 W (+/- 5%)
Maximum power point Voltage (V_{mpp})	17.36 V
Open circuit voltage (V_{oc})	22.38 V
Maximum power point Current (I_{mpp})	4.95 A
Short circuit current (I_{oc})	5.48 A

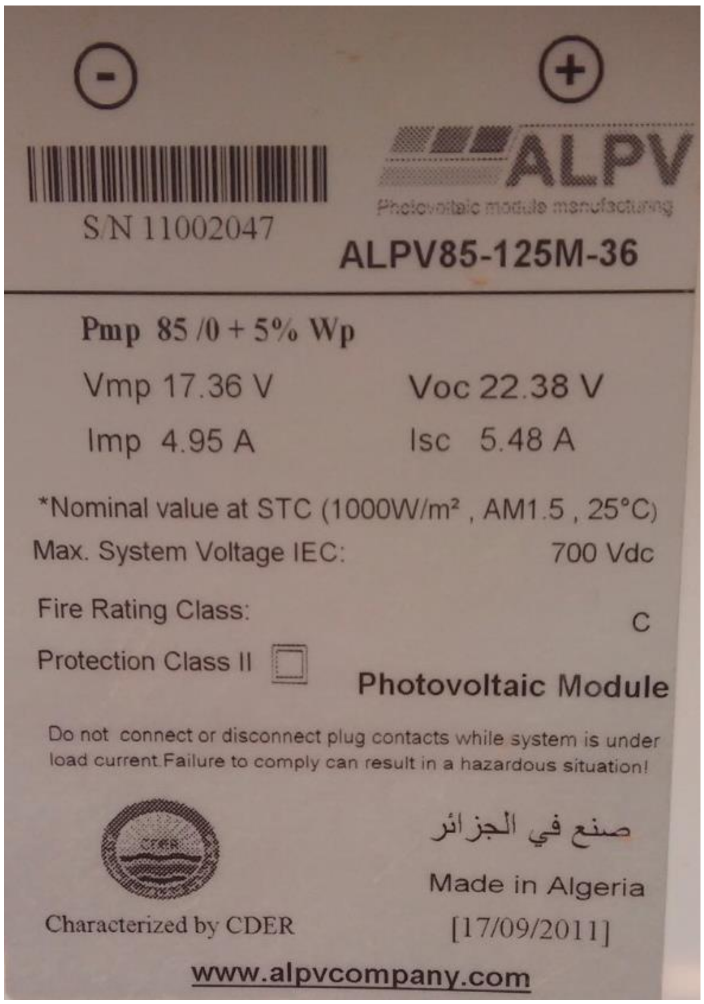

Figure A.1: Solar panel specifications

Abstract

This study is concerned with the power quality issues in the distribution network. One of the major problems facing power electronics technology nowadays is protecting the power distribution system from the harmful effects of current harmonics generated by nonlinear loads connected to the grid. On the other hand, the use of renewable energies is more than necessary; it is a global strategic issue and it would be a tool against global warming.

This research proposes a high-performance control scheme for a double function grid-tied double stage PV system. It is based on predictive direct power control with space vector modulation (P-DPC-SVM). This strategy uses a discrete model of the system based on time domain to generate the average voltage vector, at each sampling period, with the aim of canceling the errors between the estimated active and reactive power values and their references. Also, it imposes the sinusoidal waveform of the current at the grid side, which allows active power filtering without harmonic currents identification phase. The latter attempts to reduce the size and the cost of the system as well as providing better performance. In addition, it can be implemented in a low-cost control platform due to its simplicity. The performance of P-DPC-SVM is compared with Direct power control and Finite-control-set Model predictive control.

A double stage PV system is selected due to its flexibility in control, unlike the single-stage strategy. Sliding mode control based particle swarm optimization (PSO) is used to track the maximum power of the PV system. It offers high accuracy and good robustness. Concerning the DC bus voltage of the inverter, the anti-windup PI controller is tuned offline using a particle swarm optimization algorithm to deliver optimal performance in DC bus voltage regulation. All the studied control approaches are investigated in simulation using Matlab/Simulink and validated in an experimental test bench based on dSPACE 1104.

Keywords: Shunt Active Power Filter, Photovoltaic, Sliding Mode, Particle Swarm Optimization, Predictive.

Résumé

Cette étude concerne les problèmes de qualité de l’énergie dans le réseau de distribution. L’un des problèmes majeurs auxquels l’électronique de puissance est actuellement confrontée est la protection du système de distribution d’énergie contre les effets néfastes des harmoniques de courant générés par des charges non linéaires connectées au réseau. D'autre part, l'utilisation des énergies renouvelables est plus que nécessaire ; il s’agit d’un enjeu stratégique global et d’un outil de lutte contre le réchauffement climatique.

Cette recherche propose un schéma de commande hautes performances pour un système photovoltaïque à double étage connecté au réseau. Il repose sur le contrôle prédictif de la puissance directe avec modulation de largeur d’impulsion vectoriel (P-DPC-SVM). Cette stratégie utilise un modèle discret du système basé sur le domaine temporel pour générer le vecteur de tension moyenne, à chaque période d'échantillonnage, dans le but d'annuler les erreurs entre les valeurs de puissance active et réactive estimées et leurs références. De plus, il impose la forme d'onde sinusoïdale du courant côté réseau, ce qui permet un filtrage de puissance active sans phase d'identification des courants harmoniques. Ce dernier tente de réduire la taille et le coût du système tout en améliorant les performances. De plus, il peut être implémenté dans une plate-forme de contrôle à faible coût en raison de sa simplicité. Les performances de P-DPC-SVM sont comparées à celles du contrôle direct de la puissance et du contrôle prédictif par modèle fini.

Un système photovoltaïque à double étage est sélectionné en raison de sa flexibilité de contrôle, contrairement à la stratégie à un étage. L’algorithme de mode glissant basée sur l'optimisation de l'essaim de particules (PSO) le est utilisée pour suivre la puissance maximale du système photovoltaïque. Il offre une grande précision et une bonne robustesse. En ce qui concerne la tension de bus continu du l’onduleur, le régulateur PI avec anti-emballement est réglé hors ligne à l’aide d’un algorithme d’optimisation de l’essaim de particules afin d’optimiser le performance de régulation de la tension du bus continu. Toutes les approches de contrôle sont vérifiées en simulation avec Matlab / Simulink et validées sur un banc d’essai expérimental basé sur dSPACE 1104.

Mots clés : Filtre active parallèle de puissance, Photovoltaïque, Mode glissant, Optimisation des essaims de particules, Prédictif.

ملخص

تهتم هذه الدراسة بقضايا جودة الطاقة في شبكة التوزيع. تتمثل إحدى المشكلات الرئيسية التي تواجه تكنولوجيا إلكترونيات الطاقة في الوقت الحاضر في حماية نظام توزيع الطاقة من الآثار الضارة للتوافقيات الحالية الناتجة عن الأحمال غير الخطية المتصلة بالشبكة. من ناحية أخرى ، فإن استخدام الطاقات المتجددة أصبح مطلب جد ملح ؛ إنها قضية إستراتيجية عالمية وستكون أداة ضد الاحتباس الحراري

يقترح هذا البحث نظام تحكم عالي الأداء لنظام مزدوج المرحلة مرتبط بشبكة مزدوجة. يعتمد على التحكم المباشر في القدرة التنبؤية مع تشكيل ناقل الفضاء . تستخدم هذه الاستراتيجية نموذجًا مفصلاً للنظام استنادًا إلى المجال الزمني لتوليد متجه الجهد المتوسط ، في كل فترة أخذ العينات ، بهدف إلغاء الأخطاء بين قيم القدرة النشطة والمفاعلة المقدرة ومراجعها. أيضا ، فإنه يفرض الشكل الموجي الجيبية للتيار في جانب الشبكة ، والذي يسمح بترشيح القدرة النشط دون مرحلة تحديد التيارات التوافقي. يحاول الأخير تقليل حجم وتكلفة النظام بالإضافة إلى توفير أداء أفضل. بالإضافة إلى ذلك ، يمكن تنفيذه في منصة تحكم منخفضة التكلفة بسبب بساطته. تم القيام بمقارنة أداء جميع أساليب التحكم المدروسة في الأطروحة.

يتم اختيار نظام مزدوج المرحلة للتحكم في طاقة الألواح الشمسية بسبب مرونته في التحكم ، على عكس استراتيجية المرحلة الواحدة. يتم استخدام تحسين انزلاق سرب الجسيمات القائم على التحكم في الوضع المنزلق لتتبع الطاقة القصوى لنظام الطاقة الضوئية. إنه يوفر دقة عالية ومتانة جيدة. فيما يتعلق بجهد ناقل التيار المباشر في العاكس ، يتم ضبط وحدة التحكم في وضع عدم الاتصال باستخدام خوارزمية تحسين سرب الجسيمات لتقديم أداء أفضل في تنظيم الجهد. يتم فحص جميع مناهج التحكم المدروسة في المحاكاة باستخدام برنامج ماطلاب والتحقق من صحتها في اختبار تجريبي .

الكلمات الرئيسية: تحويل النشط مرشح الطاقة ، الضوئية ، وضع انزلاق ، الجسيمات سرب الأمثل ، التنبؤية

يقترح هذا البحث نظام تحكم عالي الأداء لنظام

.الكلمات الرئيسية: تحويل النشط مرشح الطاقة ، الضوئية ، وضع انزلاق ، الجسيمات سرب الأمثل ، التنبؤية